UNIVERSITAT POLITÈCNICA DE CATALUNYA
BARCELONATECH
Departament d'Enginyeria Electrònica

"ENERGY MANAGEMENT STRATEGIES BASED ON FUZZY LOGIC CONTROL FOR GRID-TIED DOMESTIC ELECTRO-THERMAL MICROGRID"

PhD dissertation submitted for obtaining the Doctoral degree from the Universitat Politècnica de Catalunya, in the PhD program in Electronics Engineering

Diego Gustavo Arcos Avilés

Advisors: *Francisco Juan Guinjoan Gispert (UPC)*

Luis María Marroyo Palomo (UPNa)

June 2016

This work has been partially supported by the grant No. 2013-AR2Q4081, Secretaría Nacional de Educación Superior, Ciencia, Tecnología e Innovación SENESCYT and the Instituto de Fomento al Talento Humano of the Government of Ecuador.

Part of this work has been carried out at the Laboratories of the Universidad Pública de Navarra

To Ale and Gabriel

ACKNOWLEDGMENTS

I would like to express my gratitude to my advisors Francesc Guinjoan and Luis Marroyo, for the motivation, enthusiasm, guidance, knowledge, support, and friendship throughout my time as a PhD. student.

I would like to thank the Public University of Navarre and the INGEPER research group for hosting me during the experimental validation period. Especially thank to Julio Pascual for his patience and guidance.

I would also like to thank my parents Caty and Chelo for their support and unconditional love during this difficult period of my life.

Finally, I would like to thank the Secretaría Nacional de Educación Superior, Ciencia, Tecnología e Innovación (SENESCYT) and the Instituto de Fomento al Talento Humano of the Government of Ecuador by the scholarship No. 2013-AR2Q4081 from “Programa de becas para Docentes Universitarios”, which helped me for finishing my doctoral studies.

ABSTRACT

The environmental and economic benefits related to the reduction of both carbon dioxide emission and transmission losses have made distributed renewable generation systems became a competitive solution for future power systems. In this context, Microgrids (MG) are considered as the key building blocks of smart grids and have aroused great attention in the last decade for their potential and the impact they may have in the coming future. The MG concept has captured great attention in the last years since it can be considered one of the most suitable alternatives for integration of distributed generation units in the utility grid. However, this integration involves some challenges to deal with especially when penetration of Renewable Energy Sources (RES) into the distribution network is increased. Therefore, an effective Energy Management System (EMS) is required to ensure optimal energy utilization within the MG, consequently, facilitating both the grid integration and operator control. In this regard, the EMS strategy design depends on the application, MG power architecture, and the power management capability of the MG elements.

This dissertation research focuses on the design of different EMS strategies based on Fuzzy Logic Control (FLC) for a residential grid-connected electro-thermal MG including renewable power generation (i.e. photovoltaic and wind turbine generators) and storage capability (i.e. battery bank and water storage tank). The main goal of the FLC-based EMS strategies is to minimize the grid power fluctuations while keeping the battery State-of-Charge (SOC) within secure limits. In order to accomplish this goal, the controller design parameters, such as membership functions and rule-base, of the FLC-based EMS strategies, are adjusted to optimize a pre-defined set of quality criteria of the MG behavior.

The analysis and design of the FLC-based EMS strategies for electrical and electro-thermal MG power architectures are developed considering two different scenarios. A first scenario where the MG power forecasting is not provided and a second scenario where the forecast of generation power and load demand are considered. A comparison with the different EMS strategies is presented in simulation level, whereas the features of the enhanced FLC-based EMS strategies are experimentally tested on a real residential microgrid implemented at the Public University of Pamplona.

RESUMEN

Este estudio presenta el diseño de diferentes estrategias de gestión energética basadas en un controlador difuso para una microrred electro-térmica residencial conectada a la red eléctrica compuesta por generadores de energía renovable (solar y eólico) y elementos de almacenamiento de energía (banco de baterías y tanque de almacenamiento de agua). El objetivo principal de las estrategias de gestión es reducir los picos y fluctuaciones de potencia en el perfil de potencia intercambiado con la red eléctrica y preservar la vida útil del sistema de almacenamiento.

Se presenta una revisión del estado del arte de estudios anteriores que buscan este objetivo. Se muestra el análisis de dos arquitecturas de microrred. La primera arquitectura consiste en una microrred eléctrica compuesta fuentes de energía renovables, sistema de almacenamiento de energía y el consumo eléctrico de una vivienda. La segunda arquitectura consiste en una microrred electro-térmica que contiene los elementos de la microrred eléctrica e incluye adicionalmente generadores térmicos y el consumo térmico de la vivienda.

Con el objetivo de medir la eficiencia de las diferentes estrategias de gestión, se presenta un conjunto de criterios de evaluación que analizan la calidad del perfil de potencia intercambiado con la red eléctrica obtenido mediante las diferentes estrategias de gestión energética. Estos criterios de calidad son utilizados adicionalmente para la optimización de parámetros de los controladores difusos, lo cual se realiza mediante un proceso de aprendizaje fuera de línea que considera los datos históricos del comportamiento de la microrred.

La comparación entre las diferentes estrategias de gestión energética se realiza mediante simulación, utilizando los datos reales de generación y consumo adquiridos en la Universidad Pública de Navarra durante el período comprendido entre Julio 2013 y Julio 2014. El diseño de las estrategias de gestión energética para la arquitectura de microrred eléctrica supone dos posibles escenarios, el primer escenario no considera la previsión de consumo y generación de la microrred, y el segundo escenario si considera esta previsión.

Las prestaciones de las estrategias basadas en control difuso para cada uno de estos escenarios son validadas experimentalmente en condiciones reales en la microrred de la Universidad Pública de Navarra. Finalmente, se presenta el análisis de las estrategias de gestión basadas en control difuso empleadas a la arquitectura de microrred electro-térmica. La comparación, mediante simulación, con otras estrategias de gestión aplicadas a la misma arquitectura ha demostrado el correcto desempeño de las estrategias desarrolladas basadas en control difuso.

CONTENTS

FIGURE INDEX

TABLE INDEX

NOMENCLATURE

Constants

A	WT rotor swept area
DOD	Maximum battery Depth of Discharge
ΔT	Integration period
f_i, f_f	Initial and final frequency limits for computing PPV criterion
G_{STC}	Incident irradiance under STC
γ	Power temperature coefficient
k	Maximum power assigned by the controller output of the fuzzy ERoC strategy
k_B	Maximum power assigned by the controller output of the fuzzy NPT strategy
k_e	Proportional gain of the battery control loop
k_T	Thermal conductivity of the water storage tank
L	Length of the water storage tank
M	Number of samples in one day
M_3	Number of samples in 3-hours
M_{12}	Number of samples in 12-hours
m	Molar mass of the air
N	Number of samples in a year
p	Atmospheric pressure
P_e	Maximum forecast error
P_{STC}	Output power of PV array under STC
R	Universal gas constant
R_1	Inner radius of the water storage tank
R_2	Outer radius of the water storage tank
ρ	Air density
SOC_{MIN}	Minimum battery SOC allowed
SOC_{MAX}	Maximum battery SOC allowed
SOC_{REF}	Battery SOC reference value
SOC_{R1}	Threshold which allows the power injection from storage state of charge
T_{EXT}	Ambient temperature where the water storage tank is located
T_s	Sampling period
T_{STC}	Temperature under STC
T_W	Timing window for one day
T_{week}	Sampling period of one week

V	Volume of the water storage tank
Z	WT hub-height
Z_{REF}	Height at the measured data
Z_0	Roughness index of the terrain

Variables

C_{BAT}	Rated battery capacity
C_P	Specific heat capacity of water
$C_{p,WT}$	Power coefficient of the WT
ΔE_i	Energy evolution of a power variable P_i
ΔSOC	Battery SOC variation during T_s
ΔT_{WD}	Water temperature variation during T_s
e	Battery capacity status respect to its half-rated capacity.
η	Battery efficiency
η_C, η_D	Battery charge, discharge efficiencies
E_{saved}	Annual electric energy saved through the electro-thermal MG strategies
$E_{WH,E}$	Annual electric energy consumed by the EWH
E_{WH}^{G}	Annual energy supplied by the mains to the EWH
E_{WH}^{B}	Annual energy supplied by the ESS to the EWH
$G(\beta,\alpha)$	Incident irradiance on an inclined surface
n, (n-1)	Current and previous samples
P_A^- , P_A^+	Minimum and maximum value of the MG net power trend
P_{AVG}	Average net power profile
$\dot{P}_{AVG}$	Microgrid energy rate-of-change over time
$\dot{P}_{AVG,MAX}$	Maximum value of $\dot{P}_{AVG}$
$\dot{P}_{AVG,MIN}$	Minimum value of $\dot{P}_{AVG}$
P_{BAT}	Battery power
$P_{BAT,FLC}$	Low-frequency component of the battery power
P_{BAT}^{MG}	Battery power resulting from the EMS strategy
P_{CTR}	Average net power of the MG through a CMA filter
P_{DC}	Yearly grid power profile average value
P_E	Forecast error
P_E^{3H}	Power forecast error of the previous 3-hours
P_{FLC}	Output power of the FLC for the fuzzy ERoC and the fuzzy EMS-FC strategies
$P_{G,LF}$	Low-frequency component of P_G

$P_{G,HF}$	High-frequency component of P_G
P_{GEN}	Renewable power generation
$P_{GEN,FC}$	Power generation forecast
P_{GRID}	Grid power
$P_{GRID,MAX}$	Positive grid power peak
$P_{GRID,MIN}$	Negative grid power peak
$P_{GRID,f}$	Grid power harmonic at frequency f
$\dot{P}_{GRID}$	Grid power profile ramp-rate
P_{IN}	Input power
P_{LG}	MG net power
$P_{LG,FC}$	Forecast of the MG net power
$P_{LG,LF}$	Low-frequency component of P_{LG}
$P_{LG,HF}$	High-frequency component of P_{LG}
$P_{LG,MAX}$	Maximum fluctuation of P_{LG}
$P_{LG,MIN}$	Minimum fluctuation of P_{LG}
P_{LG}^{-12H}	Average value of the MG net power of the previous 12-hours
$P_{LG,FC}^{+12H}$	Average value of the MG net power forecast for the nest 12-hours
P_{LOAD}	Load power demand
$P_{LOAD,FC}$	Load demand forecast
$P_{LOSS,T}$	Thermal conduction power losses
P_N, P_P	Minimum and maximum power assigned by the controller output of the fuzzy EMS-FC strategy
P_{OUT}	Output power
P_{PV}	Photovoltaic power
$P_{PV,FC}$	Photovoltaic power forecast
$P_{SC,T}$	Solar thermal collector power
P_{SOC}	Battery power used to keep the battery SOC centered close to the 75% of the rated battery capacity
$P_{WH,E}$	Electric power consumed by the EWH
P_{WH}^{B}	Power supplied by the battery to the EWH
P_{WT}	Wind power
$P_{WT,FC}$	Wind turbine power forecast
Q_{DHW}	Domestic hot water consumption
$Q_{LOSS,T}$	Rate of energy loss from the storage tank
Q_{SC}	Rate of energy collected from the solar thermal collectors

$Q_{ST,T}$	Capacity of the water storage tank
$Q_{WH,T}$	Rate of energy transferred from the EWH
ρ_W	Density of water
SOC	Battery State-of-Charge
SOC_{AVG}	Average value of the battery SOC
T_a	Ambient temperature
T_C	PV cell temperature
T_{WD}	Temperature in the water storage tank
$v_{(Z)}$	Wind speed at the WT hub-height
$v_{(Z_{REF})}$	Wind speed at Z_{REF} height
X1, X2, X3	Parameters of a triangular membership function

ACRONYMS

APD	Average Power Derivative
BESS	Battery Energy Storage System
CMA	Central Moving Average
DER	Distributed Energy Resources
DF	Derivative and Filter block
DG	Distributed Generation
DHW	Domestic Hot Water
DOD	Depth of Discharge
DR	Demand Response
DSM	Demand Side Management
EMS	Energy Management System
EMS-FC	Energy Management System strategy based on MG Power Forecasting
ERoC	Energy Rate-of-Change
ESS	Energy Storage System
EWH	Electric Water Heater
FLC	Fuzzy Logic Control
GHG	Greenhouse Gasses
IEA	International Energy Agency
HRES	Hybrid Renewable Energy System
HVAC	Heating, Ventilation and Air Conditioning
LPF	Low-Pass Filter
MF	Membership Function
MG	Microgrid
MPC	Model Predictive Control
MPD	Maximum Power Derivative
NB	Negative Big
NI-PXI	National Instruments PCI eXtensions for Instrumentation
NM	Negative Medium
NOCT	Nominal Operating Cell Temperature
NPT	Net Power Trend
NS	Negative Small
NSS	Negative Smallest
NWP	Numerical Weather Prediction
OECD	Organisation for Economic Co-operation and Development

PB	Positive Big
PCC	Point of Common Coupling
PM	Positive Medium
PPV	Power Profile Variability
PS	Positive Small
PSS	Positive Smallest
PV	Photovoltaic
PVR	Power Variation Range
RES	Renewable Energy Sources
SMA	Simple Moving Average
SOC	State-of-Charge
STC	Standard Test Conditions
TPES	Total Primary Energy Supply
UPNa	Public University of Navarre
WT	Wind Turbine
ZE	Zero

Chapter 1
Introduction and objectives

1.1. Introduction

The growing demand of energy, derived from worldwide economic growth and development, has caused the increase of energy in the last 40 years, as it can be seen in Fig. 1.1. Moreover, as shown in Fig. 1.2, according to the International Energy Agency (IEA), the world Total Primary Energy Supply (TPES) has increased form 6100 Mtoe (i.e. million tons of oil equivalent) in the year 1973 to 13541 Mtoe in the year 2013 [1], which represents an increase of 122% in this period.

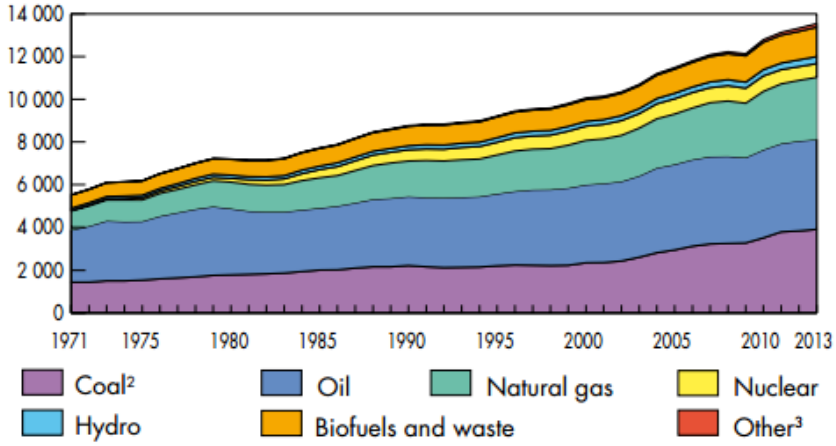

Fig. 1.1. World total primary energy supply from 1971 to 2013 by fuel (Mtoe), [1] © OECD/IEA, 2015

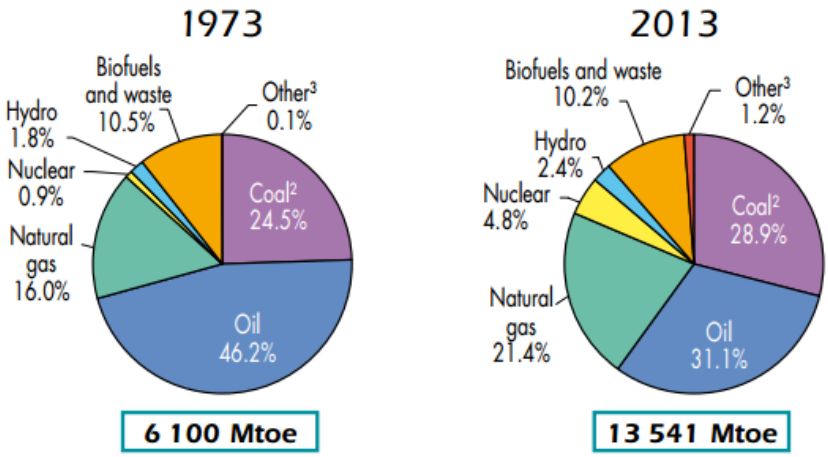

Fig. 1.2. 1973 and 2013 fuel shares of TPES, [1] © OECD/IEA, 2015

In addition, the increasing demand of energy has led to the increase of the use of fossil fuels accounting the 82% of the global TPES in the year 2013 [2], which has caused the global concern, due to the increased greenhouse gases (GHG) resulting from this combustion (i.e.

carbon dioxide CO_2). According to IEA the use of energy represents by far the largest source of GHG emissions [2]. Therefore, countries all over the world are implementing targets for GHG emission reduction, improved energy efficiency, and increased clean energy production [3].

As a result of these initiatives, the use of Renewable Energy Sources (RES) has increased in the last decades, being Photovoltaic (PV) and Wind power the kind of RES that has had the greatest growth with average annual rates of 46.6% and 24.8%, respectively, since the year 1990 [4], as shown in Fig. 1.3. In this regard, the IEA reports that the Organisation for Economic Co-operation and Development (OECD) countries account for most of the world production and growth of PV and wind energy [4].

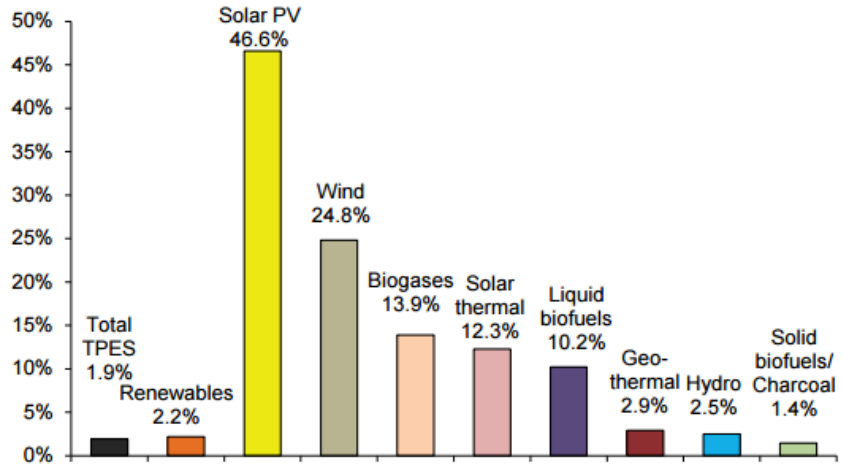

Fig. 1.3. Annual growth rates of world renewable supply from 1990 to 2013, [4] © OECD/IEA, 2015

In this concern, the benefits that RES (e.g. photovoltaic, wind turbines…) have exhibited in the last years, such as reducing the fuel consumption and the GHG emissions [5], have contributed with the Distributed Generation (DG) systems to become a competitive solution for the future power systems (i.e. Smart Grids) [6], since they can produce electrical power with less environmental impacts, they are easy to install, and they are highly efficient with increased reliability [7], [8]. However, the adaptation of the utility grid to integrate them in a distributed, efficient and reliable manner without excessive investment still remains a challenge [9].

The Microgrid (MG) concept is a quite appealing alternative for overcoming the challenges of integrating Distributed Energy Resources (DER) units, including RES, into power systems [10], [11]. In this context, MGs are emerging as an integral feature of the upcoming power systems shaped by the various smart grid initiatives [12].

The concept of MG was first defined in the literature in [13] and [14] as the cluster of micro-sources, loads and storage systems operating as a single controllable system that can respond to central control signals. However, this concept has been discussed by several authors

[3], [11], [15]–[17]. At the present, the MG concept follows a similar philosophy that of smart grid one and their research will benefit the smart grid technology development [18].

In general, MGs are defined as low-voltage distribution network comprising loads, DG units and Energy Storage System (ESS) (e.g. batteries, flywheels, ultra-capacitors…), that are connected to the mains at a single Point of Common Coupling (PCC) [15], [19], and that include an Energy Management System (EMS) associated, which is responsible for the reliable, secure and economic operation of the MG [10], [20]. MGs are capable to operate in both grid-connected and stand-alone modes [14], [16]. According to [21], in grid-connected mode, the MG adjusts power balance of supply and demand by purchasing or selling power to the main grid in order to maximize operational benefits [22], [23]. Conversely, in stand-alone mode, where the MG is separated from the distribution network, the MG is in charge of keeping a reliable power supply to customers [24].

The EMS is in charge of controlling the power fluxes among the MG elements to reach a set of predefined objectives such as minimizing the MG operating costs [25], [26] or maximizing the revenues according to DG' bids and electricity market price [21]. Additionally, the EMS design should take into account the MG power architecture and, in particular, the power management capability of the elements within the MG (i.e. which sources, loads and storage elements can be controlled). Once the power architecture and the predefined objectives are known, the EMS design can be undertaken by applying different methods [8], [10], [12], [20], [27]–[30].

In this regard, there is a wide variety of works handling different scenarios in terms of power architectures, objectives and methods. For instance in [31] an EMS strategy is designed by using local prediction and local forecasting as well as Stochastic Dynamic Programming (SDP) to control and extend the lifetime of an ESS included in a grid-connected MG with diesel an renewable generation. Moreover, in [32] the design of the EMS strategy focuses on controlling through a predictive control technique the ESS to compensate the hourly deviations of a forecasted energy plan in a grid-connected MG.

Other studies consider scenarios with more degrees of freedom where the EMS drives different storage elements (e.g. batteries, fuel cells…), controllable loads (e.g. electrical load management, heat pumps…) or a combination of both as in [22], [33]–[37], to carry out Demand Side Management (DSM) and Demand Response (DR) strategies. The control methods used in this case are usually sophisticated as Model Predictive Control (MPC) and, include both generation and demand forecasting as in [38], [39].

In addition, Fuzzy Logic Control (FLC) has also been applied to the design of EMS for both stand-alone and grid-connected modes. For instance, [40]–[42] presents a fuzzy-based EMS

applied to stand-alone MG, whereas [43] presents an EMS with fuzzy control for a DC MG, where the FLC is designed for both prioritizing selling additional electricity generated by Renewable Energy Sources (RES) and maintaining the battery State of Charge (SOC) above 50% to extend its life. Moreover, [44] presents an EMS where the FLC considers the evolution of the prices during one day, the energy demand, the production and the time of the day in order to ensure an affordable grid.

It can be noticed form the literature that smoothing the power exchanged with the grid is generally not addressed as the main objective of the EMS strategy, since most of the studies focus on the economic achievement of the MG. However, new regulations for grid-connected systems with RES [45] require the control of the ramp-rates of the power generation and the quality support of the mains [46]. Thus, smoothing the grid power profile becomes an additional challenge for the EMS.

This new challenge, i.e., smoothing the grid power profile, can be considered a suitable solution in a residential MG scenario facilitating the grid operators control and consequently the penetration of RES into the distribution network. In addition, the grid power profile control allows residential consumers generate their own energy causing the minimization of the amount of energy consumed from the utility grid, thus, reducing their electricity bill [47]. In this concern, the studies developed in [36], [37], [48]–[57] focus on minimizing the power peaks and fluctuations of the power exchanged with the grid.

The first approach to smooth the power profile exchanged with the grid is performed by the Simple Moving Average (SMA) strategy [49]. This strategy uses a Low Pass Filter (LPF) to separate the low- and high-frequency components of the grid power profile via a simple moving average filter with a window size of one day [36]. Thus, the high-frequency component is handled by the ESS and the low-frequency component is exchanged with the grid. However, this strategy does not consider the state-of-Charge (SOC) of the ESS, causing the operation of the ESS outside secure limits compromising its lifetime.

Alternatively, [50] suggests an EMS strategy design based on an heuristic knowledge of the desired behavior of the MG, where the amount of power assigned to the grid and to the storage system is computed by means of heuristically adjustable analytical expressions involving the power balance between consumption and generation as well as the battery SOC as main variables. This strategy reduces the fluctuations of the power exchange with the grid with respect the SMA strategy. However, it leads to a highly fluctuating grid power profile.

This heuristic knowledge suggests the use of FLC for the design of the EMS strategy in a residential grid-connected scenario. In this regard, fuzzy logic provides a formal methodology

for representing, manipulating, computing, and implementing a human's heuristic knowledge about how to control a system [58], [59]. In addition, it is a powerful control technique capable of dealing with the imprecisions and nonlinearity of complex systems, that can be based on experience of the user about the system behavior rather than the mathematical model of the system as in the traditional control theory [60], [61].

In this concern, considering the same inputs variables as in [50], the author presented in [51] an EMS strategy based on FLC, which includes the design of a two-input one-output FLC and 25-rules, which slightly improves the battery SOC and the grid power profile obtained in [50]. This study presented a detailed description for the design of the Membership Functions (MF) and rule-base, which parameters such as number of MFs per input, mapping, and dynamic range were adjusted to optimize a set of quality criteria of the MG behavior through an off-line learning-process simulation [54].

Furthermore, using the same design methodology, a new EMS based on FLC is presented in [52], this design improves the results obtained in [51] through the inclusion of supplementary information into the FLC. This new design was considering the MG Net Power Trend (NPT) as an additional input of the FLC, resulting in a 50-rules FLC. Even though the results evidence a low-frequency grid power profile with minimum fluctuations, the new input increases the controller complexity [54].

Therefore, with the aim of improving the aforementioned designs as well as simplifying the FLC complexity (i.e. to reduce the controller inputs number and its rule-base), an enhanced EMS strategy based on FLC of two inputs, one output and 25 rules is presented by the author in [53] and an extended version including experimental validation results is presented in [54]. The key factor of the improved design is to consider the MG Energy Rate-of-Change (ERoC) as a FLC input in order to anticipate the system behavior. This design allows quick reaction of the EMS against the MG energy changes in order to set the battery SOC close to the 75% of the rated battery capacity and smoothing the grid power profile.

As aforementioned, the increase of both number of controllable elements within the MG and the information handled by the EMS strategy leads to the increase of the available degrees of freedom for the MG control, which facilitates the improvement of the grid power profile [50]. For instance, [37] develops a DR coordination control algorithm that uses controllable resources and ESS to compensate power fluctuations produced by RES to provide tie-line services.

In addition, [50] presents an EMS strategy for an electro-thermal MG comprising of RES, ESS and thermal elements such as solar thermal collectors and Electric Water Heater (EWH). Moreover, following the same procedure than [51], the author presents in [55], [56] a

fuzzy-based EMS strategy for an electro-thermal MG, where results slightly improve to those presented in [50]. Furthermore, an improved strategy for that seen in [50], [51] is designed in [36] which improves significantly the power profile exchanged with the grid by the use of both DSM and a variable battery SOC with the purpose of compensating seasonal fluctuations of the MG net power. Finally, to directly address the problems produced by previous strategies, [57] presents an enhanced EMS strategy, which uses a Central Moving Average (CMA) filter, the cumulative forecast error, and the battery SOC to minimize the fluctuation in the grid power profile.

This dissertation presents the analysis, design, and comparison of the research work carried out by the author and partly referred in the publications cited above for smoothing the power profile exchanged with the grid of a residential grid-connected MG. Moreover, presents an enhanced EMS design based on FLC and microgrid power forecasting for conducting the same objective. In addition, this dissertation presents the experimental results achieved by the fuzzy-based EMS strategies, which were obtained in the MG installed at the Public University of Navarre (UPNa). Finally, presents the analysis and design of the improved fuzzy EMS strategies applied to an electro-thermal MG scenario.

1.2. Dissertation aim and objectives

1.2.1. Aim

The aim of this research is the design of energy management strategies based on Fuzzy Logic Control for smoothing the grid power profile of a residential grid-connected microgrid including renewable energy sources, energy storage system, and electrical and thermal load demand.

1.2.2. Objectives

The following objectives have been defined in order to achieve the aim cited above:

- Definition of a set of quality criteria for quantifying the improvement of the grid power profile achieved through an EMS strategy.
- Inclusion of the information related with the power fluctuations within the MG into the EMS strategy.
- Analysis of the effect of using generation and demand forecasts on the power profile exchanged with the grid.
- Simulation comparison according to the defined quality criteria of the grid power profile resulting from the fuzzy-based EMS designed strategies.

- Experimental validation in a real MG of several fuzzy-based EMS designed strategies.
- Analysis of the extension of the FLC EMS strategies to an electro-thermal MG scenario.

1.3. Dissertation outline

This dissertation research work is organized as follows:

Chapter 2 describes the residential microgrid architectures under study. It also presents the complete description the elements of the MG installed at UPNa. In addition, it presents the mathematical models of the main elements of the MG such as RES and ESS. Finally, it includes the recorded data of power generation and load demand for the year under analysis.

Chapter 3 presents on the one hand the problem formulation to solve and defines a set of energy management quality criteria, which are used to quantify the improvement of an EMS strategy. On the other hand it presents the analysis and design of Net Power Trend-based (NPT) and Energy Rate of Change (ERoC) FLC-based strategies. Subsequently, the chapter includes a simulation comparison among the features of SMA, NPT and ERoC strategies. The experimental validation of the improved fuzzy-based EMS ERoC strategy is presented at the end of this chapter.

Chapter 4 presents the analysis and design of an enhanced fuzzy-based EMS strategy based on MG power forecasting (i.e. fuzzy EMS-FC). It describes the forecasting method used to estimate the power generation and load demand, which are based on weather forecasting and persistence method, respectively. It also presents the simulation results and comparison with the EMS strategies described in Chapter 3. Finally, the chapter concludes with the experimental validation of the fuzzy-based EMS strategy based on MG power forecasting.

Chapter 5 presents the design extension of the fuzzy EMS strategies applied to an electro-thermal MG scenario. Simulation results and comparison of the fuzzy ERoC and fuzzy EMS-FC strategies in an electro-thermal MG are included at the end of the chapter.

Finally, Chapter 6 summarizes the main conclusions of this study. It also suggests possible future lines to pursue this research.

Chapter 2
Residential grid-connected microgrid description

This Chapter describes the electrical and electro-thermal microgrids of a residential grid-connected MG under study installed at UPNa. This description includes both, the architectures and the information of each physical element of the microgrid, which will be further used in the experimental validations of the several of the EMS strategies designed in Chapter 3 and 4.

In addition, this Chapter presents the mathematical models of renewable generators and ESS which are respectively used to calculate the power generation forecast and the state-of-charge of the storage elements resulting from the EMS.

Finally, the Chapter presents the records of MG power generation and load demand for the year under study, which were measured and recorded at UPNa. These data will be used to compare the different energy management strategies described in Chapters 3 and 4.

2.1. Electric and Electro-thermal microgrid configuration

2.1.1. Electric microgrid description

The first architecture under study is a residential grid-connected MG [52], [54], [53], [62], [63], [51], [50], [57], which includes an Hybrid Renewable Energy System (HRES), a domestic demand and an ESS. The MG configuration is shown in Fig. 2.1 and includes the following elements:

- An HRES, which includes a Photovoltaic Generator (PV) of 6 kWp and a small Wind Turbine (WT) of 6 kW.
- An ESS, which consists of a lead-acid battery bank with a rated capacity of 72 kWh.
- A domestic load demand, which involves typical electrical loads (e.g. electrical appliances, lighting…) with a rated power of 7 kW.

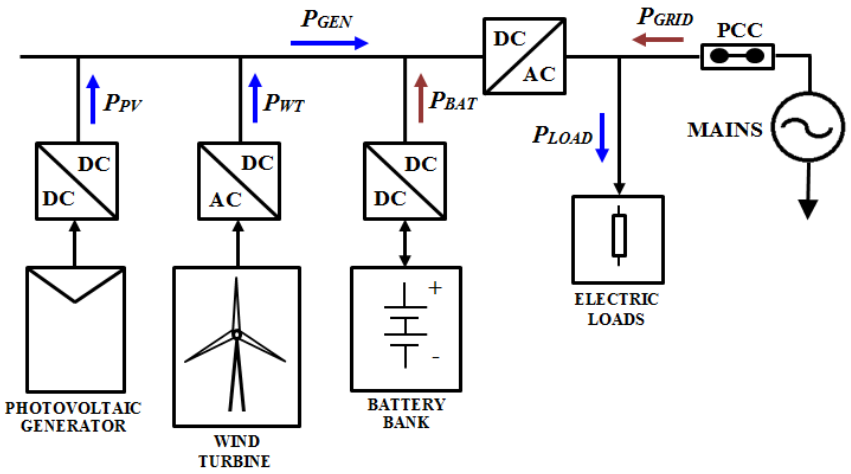

Fig. 2.1. First architecture, residential grid-connected microgrid

From Fig. 2.1, on the supply side, P_{PV} and P_{WT} represent the photovoltaic and wind power generation, respectively, P_{BAT} represents the power delivered/absorbed by the battery, and P_{GRID} represents the power delivered/injected by/to the mains. On the demand side, P_{LOAD} stands for the load power demand required by the electric loads.

Note that the power variables involved in Fig. 2.1 are considered positive when the power flows according to the direction of the corresponding arrows. Therefore, the power generated by both renewable generators, P_{PV} and P_{WT}, and the power consumed by the electric loads, P_{LOAD}, are always positive. Additionally, P_{BAT} is considered positive when the battery injects power to the MG (i.e. discharging process) and it is considered negative when the battery absorbs power from the MG (i.e. charging process). Finally, P_{GRID} is considered positive when the grid delivers power to the MG and it is negative when the grid absorbs power from the MG. A complete description of the elements belonging to the MG is presented in section 2.2.

Given the configuration shown in Fig. 2.1, the power exchanged with the mains, P_{GRID}, could be defined as follows:

$$P_{GRID} = P_{LOAD} - P_{GEN} - P_{BAT}, \tag{2.1}$$

$$P_{GEN} = P_{PV} + P_{WT}, \tag{2.2}$$

being P_{GEN} the total renewable power generation in the MG.

In addition, defining the MG net power (i.e. P_{LG}) as the difference between consumption and generation power, the grid power profile for the first architecture expressed in (2.1) can be rewritten as:

$$P_{LG} = P_{LOAD} - P_{GEN}, \tag{2.3}$$

$$P_{GRID} = P_{LG} - P_{BAT}. \tag{2.4}$$

2.1.2. Electro-thermal microgrid description

The second architecture under study is a residential grid-connected electro-thermal MG [50], [55], [56], [36], which comprises the elements described in the first architecture and includes a Domestic Hot Water (DHW) system consisting of an Electric Water Heater (EWH) of 2 kW, a flat plate solar thermal collector array of 2 kW, and a thermal storage system represented by a water storage tank with a capacity of 800 liters. The electro-thermal MG configuration is shown in Fig. 2.2.

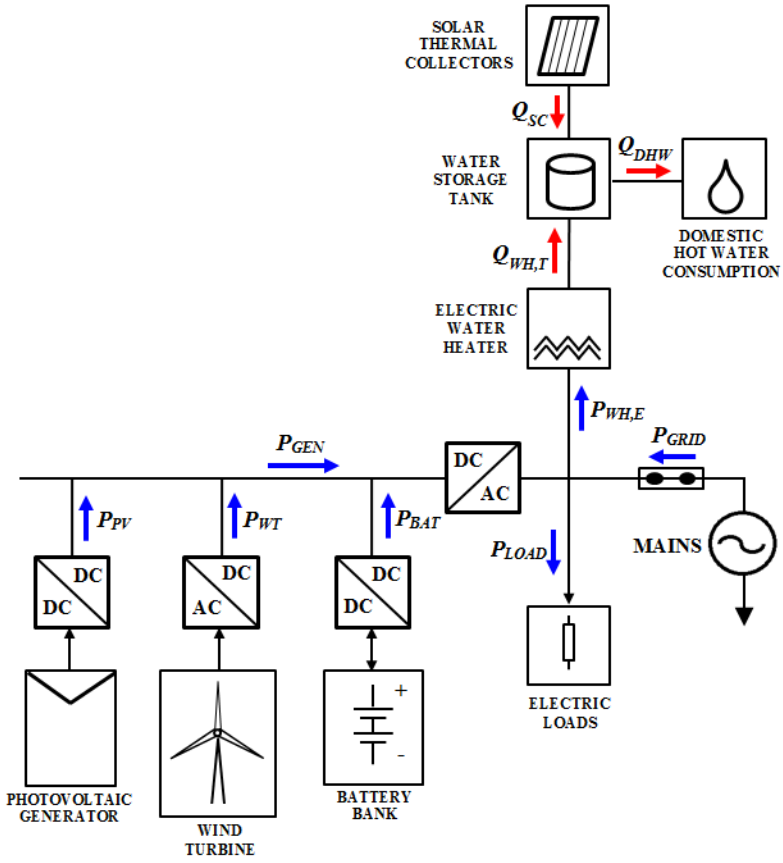

Fig. 2.2. Second architecture, residential grid-connected electro-thermal microgrid

where $P_{WH,E}$ is the power required by the EWH to maintain the water temperature in the storage tank between 45 °C and 65 °C, $Q_{WH,T}$ is the rate of energy transferred from the EWH, Q_{SC} is the rate of energy collected from the solar thermal collectors, and Q_{DHW} is the domestic hot water consumption.

Similarly to the first architecture, the power variables involved in Fig. 2.2 are considered positive when the power flows according to the direction of the corresponding arrows. Note that the analysis of an electro-thermal MG implies the analysis of all thermal variables involved in the process of water heating to supply the DHW demand. Therefore, besides the thermal variables depicted in Fig. 2.2 (i.e. $Q_{WH,T}$, Q_{SC}, and Q_{DHW}) the complete analysis should consider the thermal losses, $Q_{LOSS,T}$. The description of the thermal variables used in this architecture is presented in section 2.3.

Finally, according to the configuration shown in Fig. 2.2, the power exchanged with the mains, P_{GRID}, and the MG net power for the second architecture are defined as follows:

$$P_{GRID} = P_{LOAD} - P_{GEN} - P_{BAT} + P_{WH,E}, \tag{2.5}$$

$$P_{LG} = P_{LOAD} - P_{GEN} + P_{WH,E}, \tag{2.6}$$

$$P_{GRID} = P_{LG} - P_{BAT}. \tag{2.7}$$

2.2. UPNa microgrid configuration

The configuration of the UPNa MG is shown in Fig. 2.3 and includes a renewable generation system, a programmable load, an energy storage system, a power converter, a weather station, and a supervisory and control station [54], [57], [36], [46]. Each component is described below:

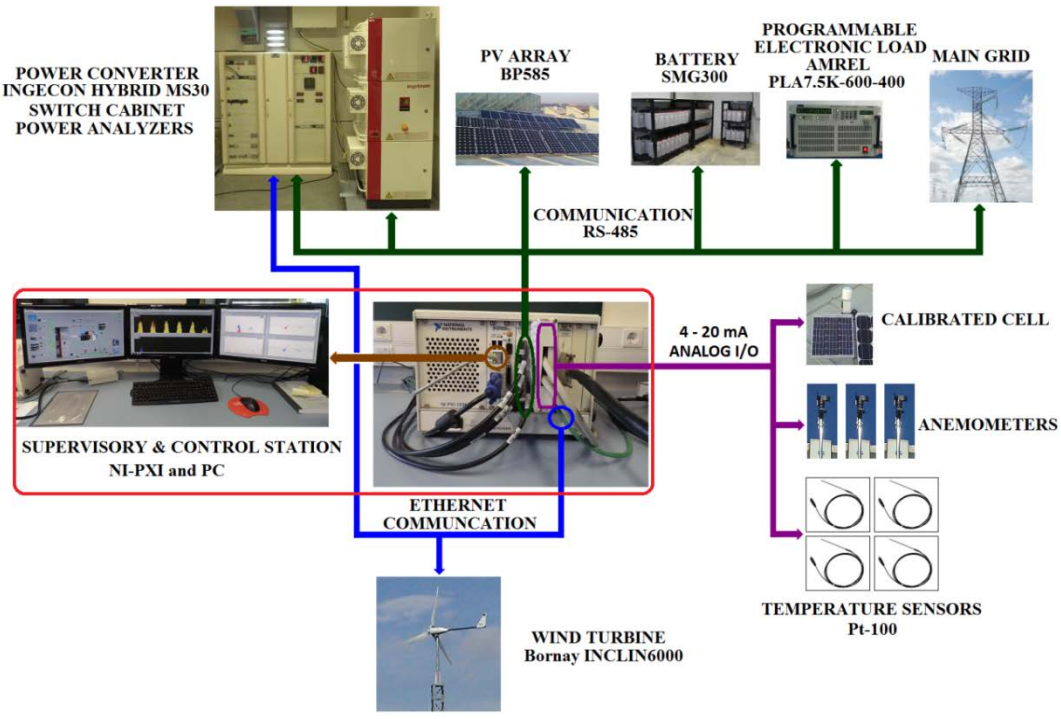

Fig. 2.3. UPNa microgrid configuration, component description and bus connections, © 2016, IEEE

2.2.1. Renewable generation system

The RES consists of a photovoltaic and wind generators shown in Fig. 2.4. The photovoltaic generator is composed by 48 BP585 [64] solar panels coupled in four strings of 12 panels connected in series. It has a rated power of 4080 W, and is mounted facing south and tilted 30º on the roof of the Renewable Energy Laboratory at UPNa.

The wind generator used in the MG at UPNa is a Bornay INCLIN6000 [65] small wind turbine with a rated power of 6 kW located next to the UPNa Renewable Energy Laboratory.

Fig. 2.4. Photovoltaic generator and wind turbine at UPNa

2.2.2. Programmable load

The load demand profile is physically emulated through an electronic load AMREL PLA7.5K-600-400 [66], which uses the sequence of load consumption provided in real time by the simulation station. This electronic load is physically connected to the supervisory and control station through the RS-485 communication bus. The programmable load and the simulation station are shown in Fig. 2.5.

Fig. 2.5. Programmable load AMREL PLA7.5K-600-400 and simulation station

2.2.3. Energy storage system

The ESS includes 120 FIAMM SMG300 [67] stationary lead-acid cells connected in series, as shown in Fig. 2.6. Each cell has a rated voltage of 2 V and a C_{10} capacity of 300 Ah resulting in a total capacity of 72 kWh.

Fig. 2.6. Lead-acid battery bank

2.2.4. Power converter and switch cabinet

The MG at UPNa uses a modified INGECON® HYBRID MS30 [68] power converter, shown in Fig. 2.7, which includes a wind turbine power conversion module, a battery charger and photovoltaic power conversion module, and an inverter module. The switch cabinet includes the interconnection relays used for the critical loads and for connection to the grid, and the power analyzers used for monitoring the main electrical variables (e.g. voltage, current, and frequency) of the renewable generators, the load, the inverter output, the battery and the mains.

Fig. 2.7. Hybrid power converter INGECON® HYBRID MS30 and switch cabinet which includes the control relays, power analyzers and digital indicators.

2.2.5. Weather station

The weather station is used to measure the environmental conditions of the different elements of the MG. The weather station is distributed along the MG and is composed by an irradiance calibrated cell shown in Fig. 2.8(a), three anemometer, as the one shown in Fig. 2.8(b), two of them located at the wind turbine and the other one located next to the photovoltaic array, four Pt-100 sensors, as shown in Fig. 2.8(c), used for measuring the outdoor, the PV panel, the battery and the battery room temperatures [54].

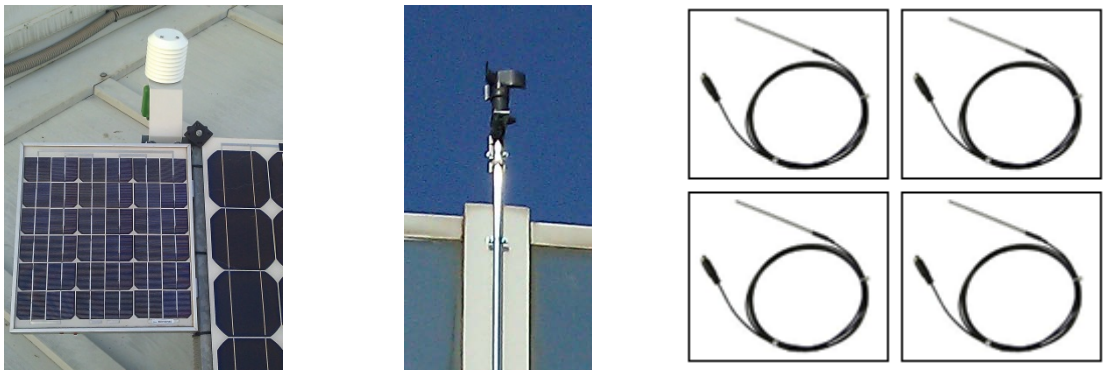

(a) (b) (c)

Fig. 2.8. Components of the weather station (a) irradiance calibrated cell, (b) anemometer, and (c) Pt-100 temperature sensors.

2.2.6. Supervisory and control station

The supervisory and control station includes the National Instruments PCI eXtensions for Instrumentation (NI-PXI) [69], and a general purpose PC.

The NI-PXI, shown in Fig. 2.9(a), uses four modules to control and acquire data, in real time (i.e. every second), from the power analyzers of each element of the MG. The modules used by the NI-PXI are the following: NI PXI-8102 Embedded Controller, NI PXI-8433/4 Serial Interface (RS-485 Communication), NI PXI-8231 Gigabit Ethernet Interface, and NI PXI-6238 Analog I/O data acquisition board [54].

The general purpose PC is used as the MG user interface and to display the historic data of the variables acquired through the NI-PXI as shown in Fig. 2.9(b), (c) and (d).

(a) (b)

(c) (d)

Fig. 2.9. Supervisory and control station (a) NI-PXI frontal view, (b) monitoring and control station, (c) user interface, and (d) historic data acquired.

2.3. Microgrid components models

2.3.1. Photovoltaic model

Photovoltaic energy is based on the direct conversion of light into electricity. This process consists in the use of different materials, which absorb photons of light to generate electron charges [70], [71].

Irradiance is defined as the density of power radiation from the sun incident on the surface. It is given in W/m^2. Despite the solar radiation density at the outer atmosphere is 1373 kW/m^2 only a peak density of 1000 W/m^2 is the final incident sunlight on the earth surface, which is known as standard irradiance (G_{STC}). Irradiation or insolation is defined as the solar radiation energy received on a given surface area in a given time (i.e. the time integral of the irradiance) [70]. It is given in Wh/m^2. Both definitions are shown in Fig. 2.10.

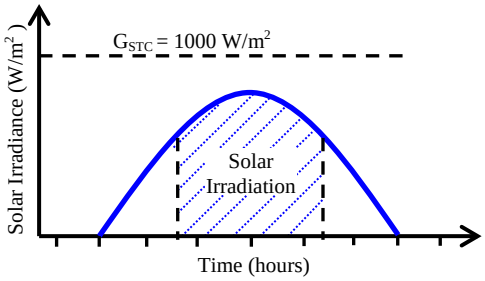

Fig. 2.10. Solar irradiance and solar irradiation

The basic element of a photovoltaic system is the solar cell, which consists of a PN junction molded in a semiconductor material. The solar cells convert the sunlight energy in DC current. The typical semiconductor used to build PV cells is Silicon (Si). There are numerous types of solar material cells, for instance, monocrystalline silicon, polycrystalline cells, thin films and organic cells, whose give different efficiencies and has different cost.

A PV module consists of several solar cells circuits sealed in an environmentally protective laminate. A PV panel includes one or more PV modules, connected in series and/or in parallel, grouped together on a common support structure. A PV array is a complete power generation system comprising some number of PV modules and panels as shown in Fig. 2.11.

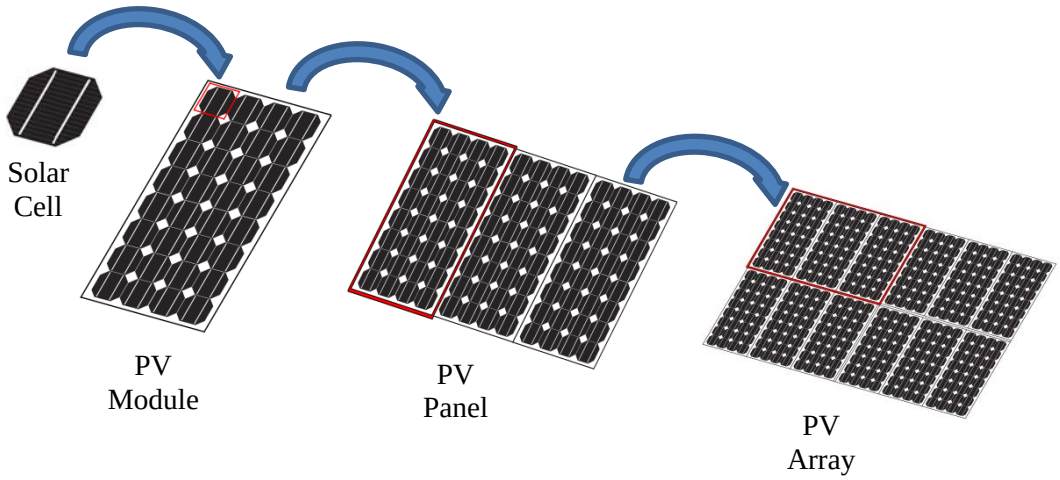

Fig. 2.11. Solar cell, PV module, PV panel and PV array

In this concern, the power supplied by a PV generator depends on different variables including the type of material, temperature and solar radiation incident on the surface of the modules. The output power of the PV array can be expressed as follows [71]–[73]:

$$P_{PV} = P_{STC} \frac{G(\beta,\alpha)}{G_{STC}} \left[1+\gamma\left(T_C - T_{STC}\right)\right], \tag{2.8}$$

where P_{STC} is the output power of the PV array under Standard Test Conditions (STC), $G(\beta,\alpha)$ is the incident irradiance in the plane of the panels, G_{STC} is incident irradiance under STC, γ is the power temperature coefficient, T_{STC} is the temperature under STC, and T_C is the cell temperature in ºC, which can be evaluated using as follows [71], [74]:

$$T_C = (T_a - 273) + \frac{G(\beta,\alpha)}{800} \cdot (NOCT - 20), \tag{2.9}$$

where T_a is the ambient temperature in K, and *NOCT* is the Nominal Operating Cell Temperature in °C.

Note that the values of P_{STC}, γ and *NOCT* are provided by the panel manufacturer. In contrast, the local observatories usually provide the weather report of incident solar irradiance on a horizontal plane G_0. Thus, in order to obtain the photovoltaic power generation by means of (2.8) and (2.9) it is necessary to transform the solar irradiance on a horizontal plane, G_0, into the solar irradiance on an tilted surface, $G(\beta,\alpha)$. In his regard, the process described in [75] can be used to perform this transformation.

2.3.2. Wind turbine model

The energy available in wind is essentially the kinetic energy of large masses of air moving over the earth's surface [76]. The kinetic energy is transformed by the blades of the wind turbine into mechanical or electrical energy, depending on the end use. Therefore, for electrical applications the output power of a wind turbine can be estimated as follows [77], [78]:

$$P_{WT} = \frac{1}{2} \cdot \rho \cdot A \cdot C_{p,WT} \cdot v_{(Z)}^3, \tag{2.10}$$

where P_{WT} is the output power of the wind turbine, ρ is the air density, $v_{(Z)}$ is the wind speed at the wind turbine hub-height, A is the rotor swept area and, $C_{P,WT}$ is the power coefficient of the wind turbine. Note that A and $C_{P,WT}$ are provided by the WT manufacturer.

Equation (2.10) evidences that the available power of a wind turbine could be affected by the wind speed, which is most prominent given its cubic relationship with the power, the rotor swept area, the power coefficient of the wind turbine and the air density. In this regard, factors such as the temperature and the atmospheric pressure affect the air density. Therefore, the air density ρ can be written as [76]:

$$\rho = \frac{m \cdot p}{T_a \cdot R}, \tag{2.11}$$

where m is the molar mass of the air, p is the atmospheric pressure and, R is the universal gas constant.

Moreover, wind speeds provided by the local observatories are usually measured at a height of 10 m above the ground. Therefore, the measured wind speed has to be extrapolated to the wind turbine hub-height, thus, wind turbines usually operate at a hub-height greater than 10 m. For this purpose, the relationship for the frictional terrain resistances, the height of the measured data and the wind turbine hub-height is expressed as follows [76], [78], [79]:

$$v_{(Z)} = v_{(Z_{REF})} \cdot \frac{\ln\left(Z/Z_0\right)}{\ln\left(Z_{REF}/Z_0\right)}, \tag{2.12}$$

where $v_{(ZREF)}$ is the wind speed at Z_{REF} height, Z_{REF} is the height at the measured data, Z is the turbine hub-height, and Z_0 is the roughness index of the terrain [80].

2.3.3. Battery bank model

The ESS is one of the principal components to be considered for a successful operation of the MG. The ESS is used to balance out the irregularities and to improve the grid power quality. The ESS acts as a buffer or back-up storing the energy that can then be used to provide electricity during the period of high demand [71], [12].

The Battery Energy Storage System (BEES) stores energy as a charge in electrochemical cells, where the desired capacity and voltage can be achieved through the connection of them in series or parallel or both [71]. In this context, lead-acid batteries are eminently suitable for medium- and large-scale energy storage operations, because they offer an acceptable combination of performance parameters at a cost that is substantially below of those of an alternative system [81].

Typically lead-acid batteries have columbic (Ah) efficiencies around 85% and energy (Wh) efficiencies of around 70% over most of the SOC range, and they exhibit a self-discharge of between 1% and 5% per month at a temperature of 20 °C. The practical operational life of lead-acid battery depends on the Depth of Discharge (DOD) range and temperature to which is exposed. In addition, the batteries operation over a reduced range of DOD generally leads to a longer cycle-life than service over a wide range [81].

The battery SOC gives the estimation about the amount of energy stored in the BESS with respect to the rated battery capacity. In this concern, the current battery SOC can be estimated as follows [52], [54], [53], [62], [63], [51], [82]:

$$SOC(n) = SOC(n-1) - \Delta SOC(n), \tag{2.13}$$

where the indices n and (n-1) represent the current and the previous samples, respectively, and ΔSOC refers to the battery SOC variation during the sampling period T_s.

Moreover, ΔSOC can be estimated using the general definition of energy evolution ΔE_i of a power variable P_i during a period time ΔT. Therefore, for sampled variables and assuming equal integration and sampling periods (i.e. $\Delta T = T_s$), ΔSOC can be estimated as follows [54]:

$$\Delta E_i(t) = \int_{t}^{t+\Delta T} P_i(\tau) d\tau, \tag{2.14}$$

$$\Delta SOC(n) = \frac{\eta}{C_{BAT}} \int_{(n-1)T_s}^{nT_s} P_{BAT}(\tau) d\tau = \frac{\eta}{C_{BAT}} \cdot P_{BAT}(n-1) \cdot T_s, \tag{2.15}$$

where C_{BAT} is the rated battery capacity, and η is the battery efficiency. In general, the efficiency of the ESS considers different efficiencies for charging and discharging processes [54], [53], [83]. Therefore η is expressed as follows:

$$\eta = \begin{cases} 1/\eta_D, & \forall P_{BAT} > 0 \\ \eta_C, & \forall P_{BAT} < 0 \end{cases}, \tag{2.16}$$

where η_D and η_C are the battery discharge and charge efficiencies, respectively.

The block diagram of the battery SOC estimator is shown in Fig. 2.12 [54], [53], [62], [63].

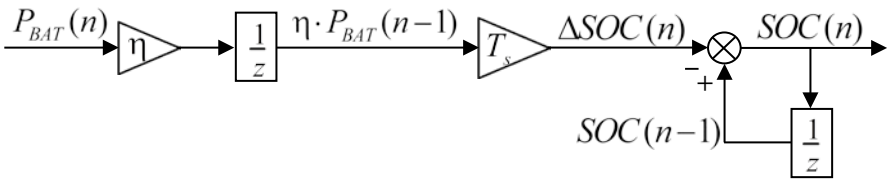

Fig. 2.12. Battery SOC estimator block diagram

In addition, the available battery bank capacity must not be less than the minimum allowable capacity, SOC_{MIN}, and must not be higher than the maximum allowable capacity, SOC_{MAX}, [62], [63], [72], [82], [84]. Thus, the limitations for the SOC of lead-acid battery can be expressed as follows:

$$SOC_{MIN} \le SOC(n) \le SOC_{MAX}, \tag{2.17}$$

$$SOC_{MIN} = (1 - DOD) \cdot SOC_{MAX}. \tag{2.18}$$

This study considers a maximum DOD of 50% in order to not compromise the ESS lifetime [85].

2.3.4. Solar thermal collectors model

The solar thermal collector is a special type kind of heat exchanger that transforms solar radiant energy into heat, which is transfer to a fluid (i.e. usually air, water or oil) flowing through the collector [86], [87]. The advantages of flat-plate collectors are that they are inexpensive to manufacture, they collect booth beam and diffuse radiation, and they are permanently fixed in a position [86].

Since the solar collector array is not physically available in the MG at UPNa, its operation has been simulated by combining the meteorological data obtained through the MG weather station with the actual characteristics of the solar thermal collector DIUM-CL4 and assuming that the solar thermal collector array is facing south and tilted 30° as the PV array. In this regard, the rate of useful energy collected from a solar thermal collector, Q_{SC}, derived from the technical characteristics sheet of the solar collector is expressed as follows [55], [46]:

$$Q_{SC} = \frac{G(\beta,\alpha)}{G_{STC}}\Big[-2\cdot10^{-9}\cdot\left(T_{WD}-T_a\right)^6+6\cdot10^{-7}\cdot\left(T_{WD}-T_a\right)^5-7\cdot10^{-5}\cdot\left(T_{WD}-T_a\right)^4+\ldots \\ \ldots+0,003\cdot\left(T_{WD}-T_a\right)^3-0,07\cdot\left(T_{WD}-T_a\right)^2-8,6968\cdot\left(T_{WD}-T_a\right)+1735,5\Big] \quad (2.19)$$

being T_{WD} the fluid temperature.

2.3.5. Thermal storage and water storage tank temperature

Thermal storage is one of the main parts of a solar heating, cooling, and power generating system, since it has several functions. For instance, it improves the use of collected solar energy by providing thermal capacitance to alleviate the solar availability and load mismatch, and improve the system response to sudden peak loads or loss of solar input [87].

The solar energy is usually stored in liquids, being water the most frequently used as a storage medium, due to is inexpensive and non-toxic [87]. In addition, this fluid can be used in residential MG scenarios, where the DHW demand is required.

In the second architecture under study, the control of the temperature of the fluid should be the appropriate, in order to satisfy the user requirements. Therefore, the model of water temperature in the storage tank should consider the rate of energy produced by the solar thermal collectors, Q_{SC}, the capacity of the water storage tank, Q_{SC}, the rate of energy transferred from the EWH, $Q_{WH,T}$, and the rate of energy loss of the storage tank as mentioned in Chapter 2.1.2.

In this regard, the rate of energy loss of the storage tank can be expressed as follows [87], [88]:

$$Q_{LOSS,T}(n) = \frac{2\pi \cdot L \cdot k_T}{\ln\left(R_1/R_2\right)} \cdot \left(T_{WD} - T_{EXT}\right), \tag{2.20}$$

where L is the water storage tank length (i.e. L = 2.14 m), k_T is the thermal conductivity of the water storage tank, which is $2.4 \cdot 10^{-6}$ kW/m·°C for a polyurethane insolation, R_1 is the inner radius of the storage tank (i.e. R_1 = 0.375 m), R_2 is the outer radius of the storage tank (i.e. R_2 = 0.475 m considering an insolation thickness of 0.1 m) [46], and T_{EXT} is the temperature of the environment where the storage tank is located (i.e. T_{EXT} = 25°C).

Moreover, the capacity of the water storage tank can be expressed as [87], [89], [90]:

$$Q_{ST,T}(n) = \rho_W \cdot C_P \cdot V \cdot \Delta T_{WD}(n), \tag{2.21}$$

where ρ_W is the density of water (i.e. ρ_W = 985.65 kg/m^3), C_P is the specific heat capacity of water (i.e. C_P = 4.18 kJ/kg·°C), V is the water storage tank volume (i.e. V = 0.8 m^3), and ΔT_{WD} is the water temperature variation during the sampling period T_s, which is defined as follows:

$$\Delta T_{WD}(n) = \frac{dT_{WD}}{dt} = \frac{T_{WD}(n) - T_{WD}(n-1)}{T_s}, \tag{2.22}$$

where T_{WD} (n) is the new tank temperature after time interval T_s and T_{WD} (n-1) is the water temperature before the time interval T_s.

In this concern, the energy balance of the water storage tank is given by:

$$\left(\rho_W \cdot C_P \cdot V\right) \cdot \left(\frac{T_{WD}(n) - T_{WD}(n-1)}{T_s}\right) = Q_{SC} + Q_{WH,T} - Q_{LOSS,T} - Q_{DHW}. \tag{2.23}$$

Consequently, the new temperature of the water in the storage tank could be expressed as follows:

$$T_{WD}(n) = T_{WD}(n-1) + \frac{T_s}{\rho_W \cdot C_P \cdot V} \cdot \left[Q_{WH,T}(n) + Q_{SC,T}(n) - Q_{DHW}(n) - Q_{LOSS,T}(n)\right]. \tag{2.24}$$

Note that the last expression assumes that the heat losses are constant in the period T_s.

2.4. Generation and demand profiles

2.4.1. Photovoltaic generation

As mentioned in section 2.1, this study considers a PV generator of 6 kW located at the city of Pamplona-Spain (42°49'06"N 1°38'39"O) facing south and tilted 30°. The PV generation profile is obtained by means of measuring the output power from PV array every 15 minutes (i.e. T_s = 900 s) at the UPNa microgrid. Furthermore, for simulation purposes a scaling factor of 5/3 is considered for PV power generation, due to the PV generator at UPNa has a peak power of 3.6 kWp [46]. The power generation produced by the PV array during the year under study ranging from July 2013 to July 2014 is presented in Fig. 2.13.

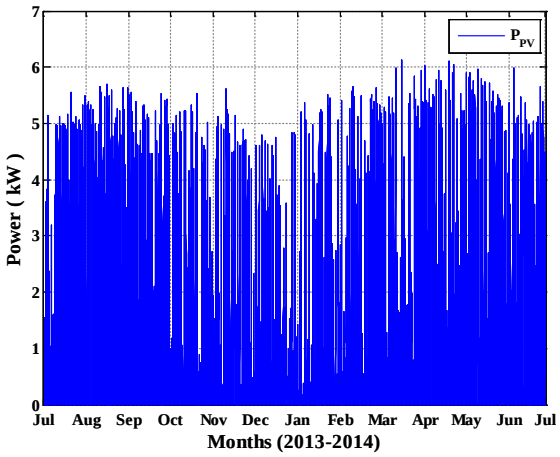

Fig. 2.13. Photovoltaic power measured at UPNa microgrid

2.4.2. Wind turbine generation

This study considers a small WT of 6 kW located at UPNa microgrid. As well as the PV generator, the generation profile of the WT, shown in Fig. 2.14, is obtained by means of measuring the output power of the WT every 15 minutes during the year under study.

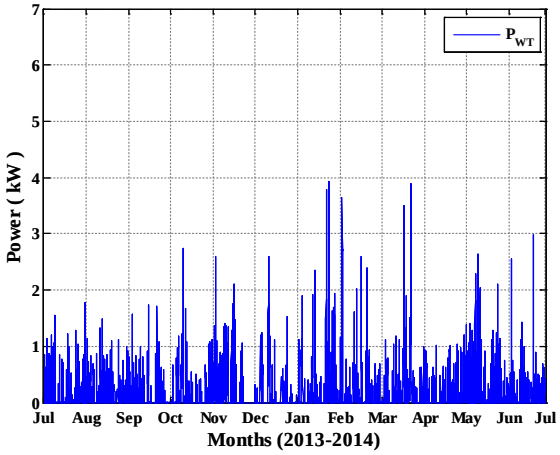

Fig. 2.14. Wind turbine power measured at UPNa microgrid

2.4.3. Thermal generation

The thermal generation of the residential MG is produced by a flat-plate solar collector with a rated power of 2 kW. The thermal generation profile, shown in Fig. 2.15, is simulated taking into account the meteorological data provided by the weather station of the MG at UPNa and considering that the solar collectors are installed with the same orientation and inclination than the PV array [46]. Similarly to PV and WT generators, the sampling period used to obtain the thermal generation profile is 15 minutes.

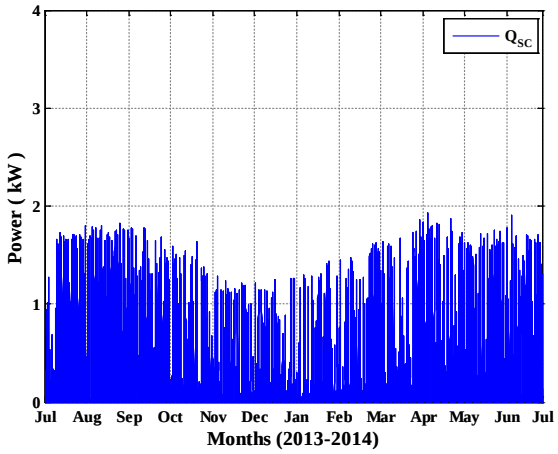

Fig. 2.15. Rate of energy collected from the solar thermal collectors

2.4.4. Electric load power demand

The electrical load shown in Fig. 2.1 contemplates typical domestic loads (e.g. electrical appliances, lighting) and a Heating, Ventilation and Air Conditioning (HVAC) system comprising of a heating pump and the EWH, where the EWH supplies the thermal energy to cover the DHW consumption of the house. In this regard, two possible scenarios are considered in this study.

The first scenario considers the first MG architecture and takes into account the load demand profile of the domestic loads excluding the EWH consumption. The load demand profile shown in Fig. 2.16(a) is obtained by means of measuring the output power of the load every 15 minutes during a year under study [50].

The second scenario considers the second MG architecture and takes into account the load demand profile of the domestic loads including the EWH consumption (i.e. DHW consumption). In this scenario, the EWH operates as a passive load and it will beyond the control of the energy management strategy. In this context, the EWH consumption was obtained through a hysteresis control in order to keep mater temperature in the storage tank between 45 °C and 65 °C [46]. The load demand profile in this scenario is shown in Fig. 2.16(b).

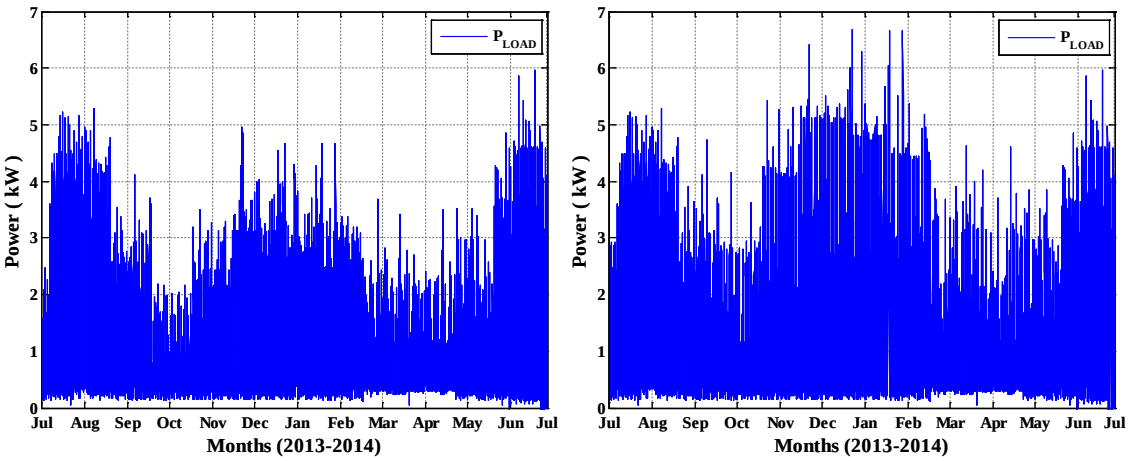

(a) (b)

Fig. 2.16. Electric load demand profile (a) excluding the EWH consumption, and (b) including the EWH consumption

2.4.5. Thermal load demand

The thermal load demand (i.e. DHW) consumption profile is taken from [50], where the data was obtained by simulation assuming that the daily DHW demand is the same for each day during the year under study, as shown in Fig. 2.17.

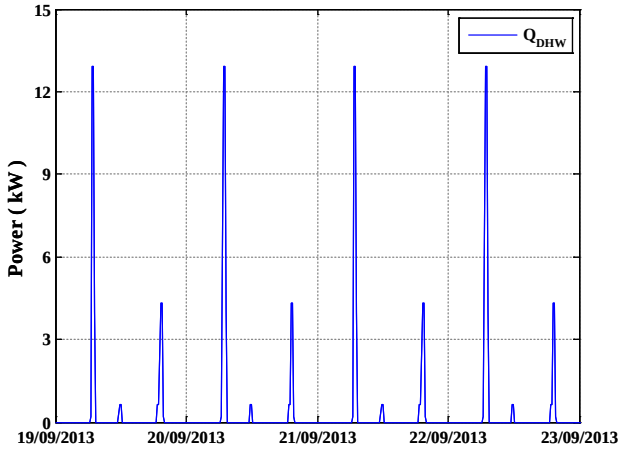

Fig. 2.17. Domestic hot water demand

Chapter 3

FLC-based Energy management strategies for a residential grid-connected electric microgrid

This chapter presents the analysis and comparison of different energy management strategies, which have been developed with the purpose of smoothing the power profile exchanged with the grid. In order to help the comparison process, the Chapter begins by stating the problem and presenting a set of quality criteria to quantitatively evaluate the degree of grid power profile "smoothnes" resulting from the different energy management strategies.

Then, the analysis and design of two previous approaches seeking the same goal are evaluated (i.e. SMA and fuzzy NPT strategies). From the conclusions of the behavior of these strategies, a complete design of an improved fuzzy EMS strategy based on a FLC and the MG Energy Rate-of-Change (ERoC) over time is presented in this Chapter. The new design includes the description of the optimization procedure developed in order to adjust all the parameters involved in the FLC design.

The behavior of all these previous strategies is compared by means of Matlab® numerical simulation taking into account the real data recorded from July 2013 to July 2014 on the microgrid available at the UPNa described in Chapter 2.

Finally, the experimental results of the improved fuzzy EMS strategy based on MG ERoC are presented at the end of the Chapter in order to confirm the feasibility of the strategy.

3.1. Problem formulation, quality criteria and baseline values

3.1.1. Problem formulation

In a residential MG scenario, where RES can be easily integrated and allow residential consumers to generate their own energy, the grid power profile control facilitates reducing both the electricity bill and the mains overload [47]. However, this integration could bring certain challenges to handle when penetration of RES into the distribution network increases, due to the stochastic nature of solar and wind generation as well as the load demand which may cause significant fluctuations in the grid power profile [37].

This behavior can be seen in Fig. 3.1, which shows the grid power profile when the MG includes neither an ESS nor an energy management strategy [53], [57], [36]. In a MG without ESS (i.e. $P_{BAT} = 0$), the utility grid should compensate all fluctuations produced by the RES and

the load demand. Hence, under this condition according to (2.4) the grid power profile is expressed as:

$$P_{GRID} = P_{LG}. \tag{3.1}$$

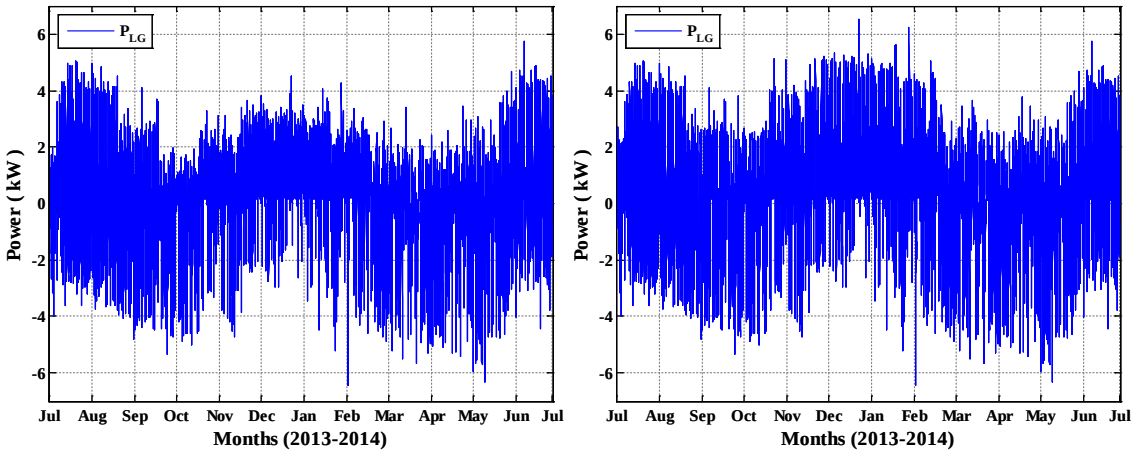

(a) (b)

Fig. 3.1. Net power profile (a) excluding the EWH consumption, and (b) including the EWH consumption

As it can be seen, the power exchanged with the grid is highly fluctuating with significant power peaks, which causes the mains overload and affects the user since it will need to contract a higher power in order to satisfy the load demand power peaks. Therefore, the integration of an ESS (e.g. batteries, flywheels, ultra-capacitors…) and an efficient energy management strategy are required in order to minimize the overload in the distribution lines and to improve the system stability and its performance [91], [11].

In this regard, the ESS is used for balancing the power demand with generation as well as to store energy during high generation periods to be used in the future to supply electricity during a period of high demand. However, the ESS cannot compensate all fluctuations produced by the RES (i.e. daily and seasonal fluctuations); since it would require a huge amount of storage capability, thus, it would be unsuitable for a residential MG scenario. Note that the BESS used in this study is sized to attenuate up to daily fluctuations. Therefore, the EMS strategies are focused on reducing the daily fluctuations produced in the MG.

In addition, the EMS strategies should try to manage the power produced by both RES and the ESS in order to minimize the power injected/absorbed to/from the grid while keeping the ESS between secure limits. Moreover, the EMS strategies should satisfy the battery constraints at any time in order to preserve the battery lifetime. Therefore, in situations where the renewable power generation is not enough to supply the load demand and the amount of energy stored in the battery is very low (i.e. $SOC = SOC_{MIN}$), the EMS strategies should cut off the power delivered by the battery to avoid deep discharges below secure limit and to preserve its lifetime.

Consequently, in such situations, the mains should supply the remaining power to satisfy the load demand causing an undesirable fluctuation in the grid power profile. The same principle should be considered when the battery is reaching its maximum charge to not overcharge the storage system (i.e. $SOC = SOC_{MAX}$). Note that in residential MG scenarios reducing the grid power profile becomes the main goal at the moment of designing the energy management strategy, thus, facilitating the grid operators control, and the penetration of RES into the distribution network.

In this concern, the main goal of the EMS strategy is the suitable control of the power delivered/injected by the mains in order to smooth the power exchanged with the grid (i.e. minimizing grid power fluctuations and power peaks) while keeping the battery SOC between secure limits.

In order to numerically compute the degree of achievement of the aforementioned goal, a set of quality criteria is defined to compare the behavior of the grid power profile accomplished by the different EMS strategies that are described in this study.

3.1.2. Energy management quality criteria

The energy management quality criteria are defined in order to assess and compare the grid power profile behavior of an EMS strategy. In this regard, a better performance of an energy management strategy is considered when the resulting values of the quality criteria are minimized. On the basis of the evaluation criteria that have been defined in [52], [54], [53], [51], [50], [57], [55], [36], [46], this study considers a set of six quality criteria, which are considered the most representative of those presented in previous studies. These quality criteria are described next.

3.1.2.1. Positive grid power peak

The positive grid power peak, $P_{GRID,MAX}$, is defined as the maximum power delivered by the mains during one year.

$$P_{GRID,MAX} = \max\left(P_{GRID}\right). \tag{3.2}$$

3.1.2.2. Negative grid power peak

The negative grid power peak, $P_{GRID,MIN}$, is defined as the maximum power fed into the mains during one year.

$$P_{GRID,MIN} = \min\left(P_{GRID}\right). \tag{3.3}$$

3.1.2.3. Power Variation Range

The Power Variation Range (PVR) criterion quantifies the effectiveness of an energy management strategy. It is defined as follows:

$$PVR = \frac{P_{GRID,MAX} - P_{GRID,MIN}}{P_{LG,MAX} - P_{LG,MIN}}, \tag{3.4}$$

where $P_{LG,MAX}$ and $P_{LG,MIN}$ are the maximum and minimum fluctuations of the MG net power.

3.1.2.4. Maximum Power Derivative

The Maximum Power Derivative (MPD) represents the maximum rate-of-change (i.e. the slope of two consecutive samples, being the sampling period T_s = 900 s) of the grid power profile in the year under study. The MPD criterion is expressed in W/h and it is defined as the maximum absolute value of the grid power slopes during one year, as follows [54]:

$$MPD = \max\left(\left|\dot{P}_{GRID}\right|\right), \tag{3.5}$$

$$\dot{P}_{GRID}(n) = \frac{P_{GRID}(n) - P_{GRID}(n-1)}{T_s}, \tag{3.6}$$

where $\dot{P}_{GRID}$ is the grid power profile ramp-rate over a year and T_s is the sampling period.

3.1.2.5. Average Power Derivative

The Average Power Derivative (APD) criterion is defined as the absolute value, expressed in W/h, of the annual average value of the slopes of two consecutive samples of the grid power profile. It is defined as follows [54]:

$$APD = \frac{1}{N}\sum_{n=1}^{N}\left|\dot{P}_{GRID}(n)\right|, \tag{3.7}$$

being N the number of samples in one year.

3.1.2.6. Power Profile Variability

The Power Profile Variability (PPV) measures the steadiness of the grid power profile. It is defined as follows:

$$PPV = \frac{\sqrt{\sum_{f=f_i}^{f_f} P_{GRID,f}^2}}{P_{DC}}, \tag{3.8}$$

$$P_{DC} = \frac{1}{N}\sum_{n=1}^{N} P_{GRID}(n), \tag{3.9}$$

where $P_{GRID,f}$ is grid power harmonic at frequency f, fi and f_f are the initial and final frequencies, respectively, and P_{DC} is the yearly grid power average value.

Note that this criterion only evaluates frequencies with variations periods of one week or less (i.e. T_{week} = 7 days), since the energy management strategy seeks to compensate daily variations. Additionally, the maximum frequency of half of the sampling frequency (i.e. Nyquist frequency) is considered. Therefore, given the sampling period of 15 minutes, fi and f_f are computed as:

$$f_i = \frac{1}{T_{week}} = \frac{1}{7 \cdot 24 \cdot 3600} = 1.65 \times 10^{-6} \text{ Hz} \tag{3.10}$$

$$f_f = \frac{f_s}{2} = \frac{1/T_s}{2} = \frac{1/900}{2} = 5.56 \times 10^{-4} \text{ Hz} \tag{3.11}$$

3.1.3. Reference values for comparison purposes

In order to compare the behavior of different energy management strategies, it is necessary to establish a set of reference values, which are used as the baseline of comparison for the energy management strategies. The reference values are obtained by means of computing the quality criteria for the grid power profile corresponding to a MG which includes neither ESS nor an energy management strategy. The results are summarized in Table 3-1.

Table 3-1 Evaluation quality criteria values (baseline values)

EMS Strategy	$P_{G,MAX}$ (kW)	$P_{G,MIN}$ (kW)	*PVR*	*MPD* (W/h)	*APD* (W/h)	*PPV*
No EMS & ESS excluding the EWH consumption	5.75	-6.45	1.00	18468	1121	13.3
No EMS & ESS Including the EWH consumption	6.53	-6.45	1.00	18468	1221	5.99

Additionally, Fig. 3.2 shows the corresponding grid power profile ramp-rates. As it will be evidenced in the following Chapters, the grid power profile ramp-rates are minimized by the energy management strategy.

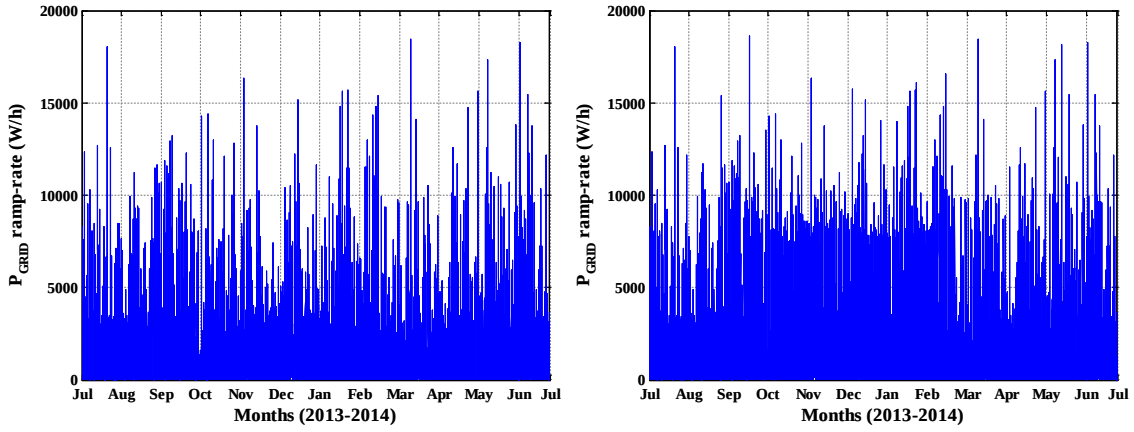

Fig. 3.2. Grid power profile ramp-rates for a MG when $P_{GRID} = P_{LG}$ (a) excluding the EWH consumption, and (b) including the EWH consumption

3.2. Simple Moving Average Strategy

3.2.1. Introduction

An easy way to reduce the power fluctuations in the grid power profile is to apply a low-pass filter to the MG net power profile [92], [49] in order to obtain an average grid power profile (i.e. low-frequency grid power). A first approach to achieve this goal is the Simple Moving Average (SMA) strategy, which uses a simple moving average filter with a window size of 24-hours to remove the high-frequency component of the MG net power .

3.2.2. SMA control design

The SMA strategy is described in [53], [57], [36]. However, for the sake of completeness and for comparison purposes this strategy is resumed below.

As mentioned above, in order to smoothing the grid power profile, the SMA strategy uses a simple moving average filter to separate the low- and high-frequencies of the MG net power. Thus, the high-frequency component is exchanged with the battery, and the low-frequency component is exchanged with the grid according to the following expressions:

$$P_{LG,LF}(n) = P_{AVG}(n) = \frac{1}{M}\sum_{k=1}^{M} P_{LG}(n-k), \tag{3.12}$$

$$P_{LG,HF}(n) = P_{LG}(n) - P_{LG,HF}(n), \tag{3.13}$$

$$P_{BAT}(n) = P_{LG,HF}(n), \tag{3.14}$$

$$P_{GRID}(n) = P_{LG,LF}(n), \tag{3.15}$$

where M is the number of samples in one day (i.e. window size), $P_{LG,LF}$ and $P_{LG,HF}$ are the low- and high-frequency components of the MG net power P_{LG}. Note that in this strategy P_{AVG} is the average value of the last 24-hours of the MG net power. Additionally, if $P_{BAT} < 0$, $P_{LG,HF}$ is absorbed the battery, if $P_{BAT} > 0$, $P_{LG,HF}$ is delivered by the battery, if $P_{GRID} < 0$, $P_{LG,LF}$ is injected to the grid, and if $P_{GRID} > 0$, $P_{LG,LF}$ is delivered by the grid.

The block diagram of SMA strategy is shown in Fig. 3.3 and includes a LPF used to obtain the low-frequency component of P_{LG} according to (3.12) and the battery SOC estimator presented in Fig. 2.12, which is used to estimate the current battery SOC according to the battery bank model described in Chapter 2.3.3.

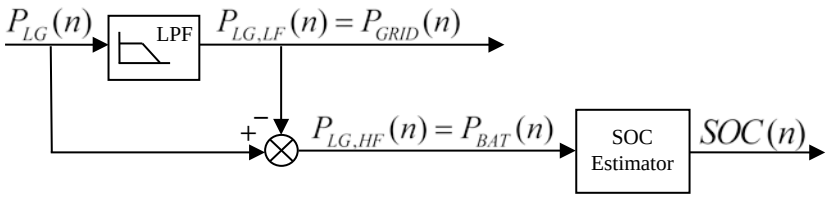

Fig. 3.3. Simple moving average strategy (SMA) block diagram

3.2.3. Simulation results and comparison

The simulation results for the SMA strategy excluding the EWH consumption are shown in Fig. 3.4. As it can be seen, the grid power profile shown in Fig. 3.4(a), has strong power fluctuations, since the SMA strategy leads the battery to reach the secure limits during several time intervals, thus, the SOC constraints are breached (i.e. $SOC < SOC_{MIN}$ or $SOC > SOC_{MAX}$), as shown in Fig. 3.4(b). As a result of the grid power fluctuations, the power exchanged with the grid exhibits high ramp-rates as depicted in Fig. 3.4(c).

The behavior of SMA strategy is further reflected through the analysis of the resulting values of the quality criteria defined in section 3.1.2. These results are summarized in Table 3-2. As it can be appreciated, the SMA strategy minimizes the quality criteria values with respect to the baseline ones. For instance, the positive and negative grid power peaks are reduced in 18.09% and 64.79%, respectively. In addition, *PVR*, *APD* and *PPV* criteria are significantly reduced in 42.00%, 96.04% and 81.13%, respectively. However, the power peaks in the grid power profile leads to the reduction of the *MPD* criterion of only 30.48%.

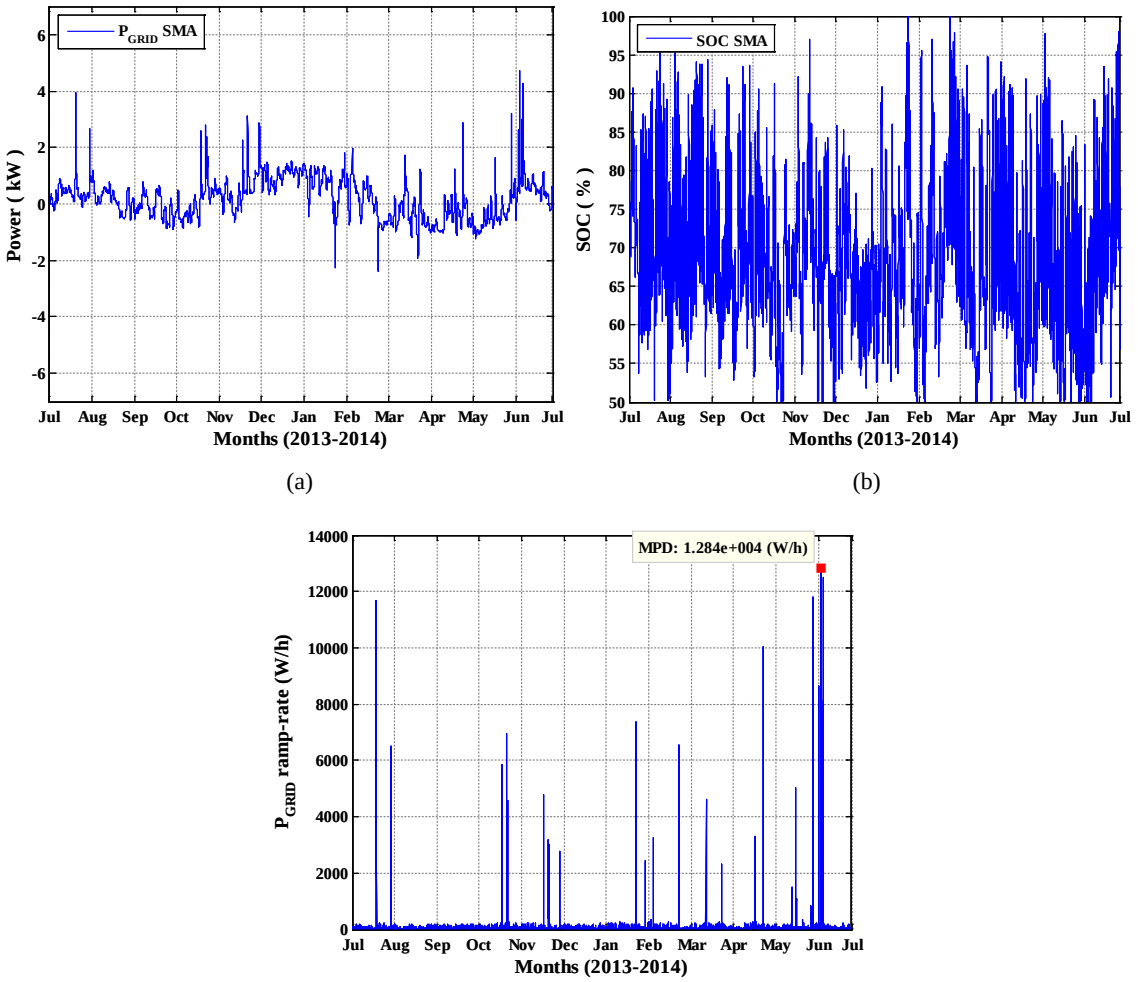

Fig. 3.4. Simulation results of the SMA strategy excluding the EWH consumption (a) grid power profile, (b) battery SOC, and (c) grid power profile ramp-rates

Table 3-2 Quality criteria comparison between SMA strategy and baseline values excluding the EWH consumption

EMS Strategy	$P_{G,MAX}$ (kW)	$P_{G,MIN}$ (kW)	*PVR*	*MPD* (W/h)	*APD* (W/h)	*PPV*
No EMS & ESS excluding the EWH consumption	5.75	-6.45	1.00	18468	1121	13.3
SMA strategy	4.71	-2.40	0.58	12839	44.42	2.51

Note that the SMA strategy exhibit a suitable behavior as long as no abrupt changes affect the MG net power from one day to the next one. However, in a real environment, the stochastic nature of the renewable energy sources and the load may significantly change the MG net power from one day to another. Consequently, the SMA strategy is not adequate under these conditions.

Similarly, the same drawbacks are present when performing the simulation of the SMA strategy including the EWH consumption. As it can be seen in Fig. 3.5(a) and (b), the increase of the load demand leads to the increase the time intervals where the battery SOC reaches the secure

limits. Consequently, the fluctuations and power peaks in the grid power profile and the grid power profile ramp-rates increase as shown in Fig. 3.5(c). Finally, Table 3-3 summarizes the resulting values of the quality criteria through the SMA strategy including the EWH consumption.

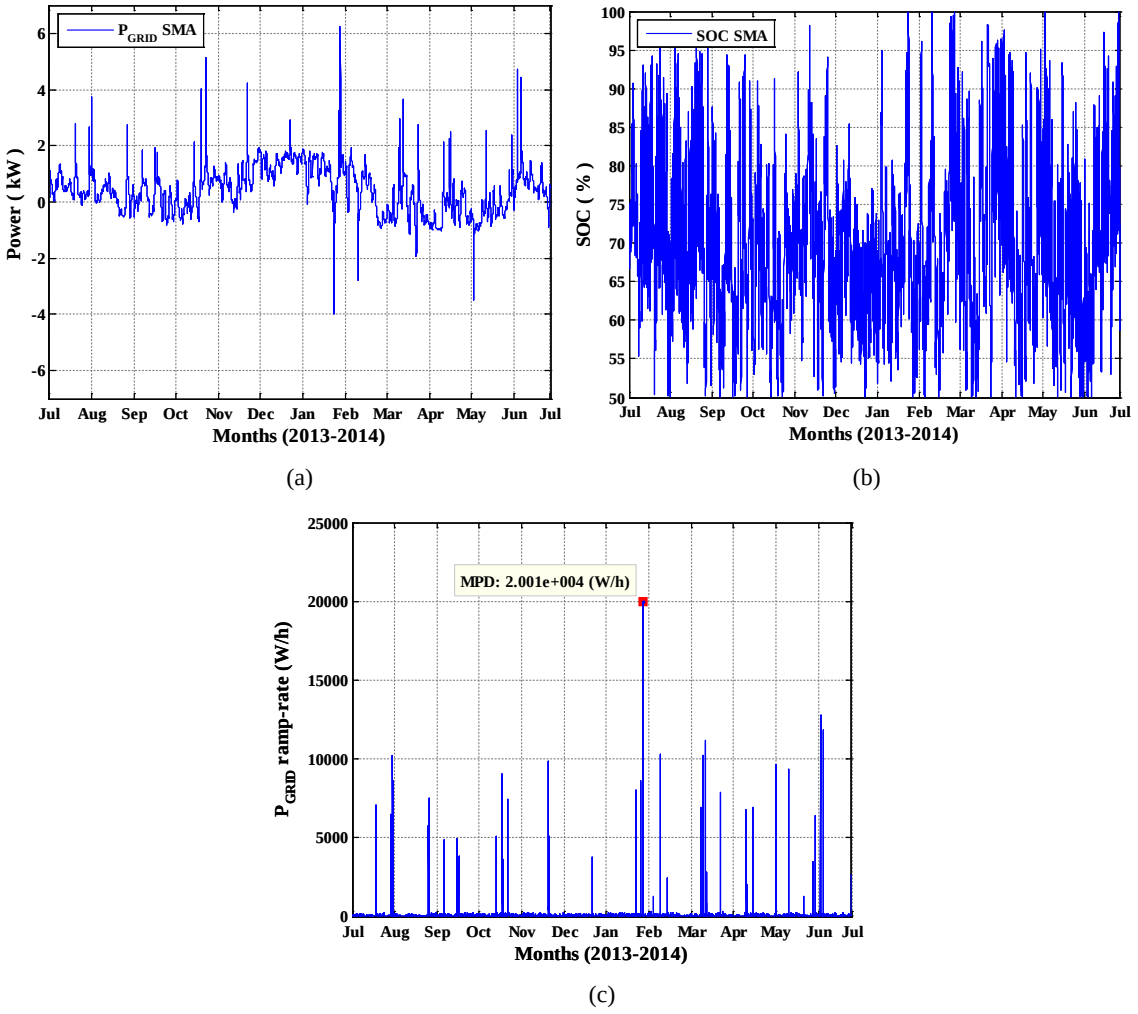

Fig. 3.5. Simulation results of the SMA strategy including the EWH consumption (a) grid power profile, (b) battery SOC, and (c) grid power profile ramp-rates.

Table 3-3 Quality criteria comparison between SMA strategy and the baseline values including the EWH consumption

EMS Strategy	$P_{G,MAX}$ (kW)	$P_{G,MIN}$ (kW)	*PVR*	*MPD* (W/h)	*APD* (W/h)	*PPV*
No EMS & ESS including the EWH consumption	6.53	-6.45	1.00	18468	1221	5.99
SMA strategy	6.25	-3.98	0.79	20006	57.41	1.23

3.3. Fuzzy energy management strategy based on MG Net Power Trend (NPT)

3.3.1. Introduction

A first approach to solve the drawbacks of the SMA strategy was developed and presented in [52]. This approach was designed with the aim of improving the performance of the battery energy management strategy of a grid connected MG presented in [51] by means of including the information about the Net Power Trend (NPT) of the MG into the FLC. According to the information provided by the MG net power trend, this approach increases/decreases the power delivered/absorbed by the battery in order to smooth the grid power profile. The control strategy and the FLC design are presented in the next paragraphs.

3.3.2. Control strategy and FLC design

The fuzzy NPT approach focuses on the direct control of the power delivered/absorbed by the battery with the purpose of minimizing the fluctuations in the grid power profile. This approach uses the MG NPT to quantify the trend of the net power fluctuations in the MG (i.e. consumption and generation trend). In this regard, P_{AVG} is considered as the trend of the MG net power and is defined by (3.12) as one-day average of the MG net power.

The block diagram of this approach is illustrated in Fig. 3.6 [52], [54] and includes a LPF used for smoothing the grid power, a battery SOC estimator shown in Fig. 2.12, and a Mamdani-based FLC [58] of three inputs $P_{LG}(n)$, $P_{AVG}(n)$, $e(n)$, one output $P_{BAT}(n)$, and 25-rules.

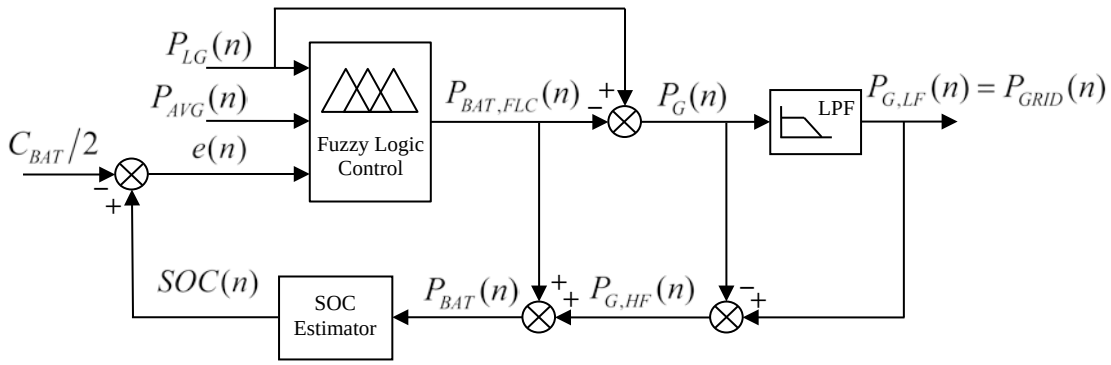

Fig. 3.6. Block diagram of the fuzzy energy management strategy based on MG NPT

In Fig. 3.6, $e(n)$ represents for the battery capacity status respect to its half-rated capacity, i.e.:

$$e(n) = SOC(n) - C_{BAT}/2. \tag{3.16}$$

Note that the FLC provides the desired evolution of the low-frequency battery power $P_{BAT,FLC}$. Therefore, assuming that the battery follows this power evolution, the corresponding grid power profile would be given by [54]:

$$P_G(n) = P_{LG}(n) - P_{BAT,FLC}(n). \tag{3.17}$$

However, $P_G(n)$ also includes the high-frequency components of $P_{LG}(n)$, which can be removed by means of a LPF as suggested in [93]. This results in smoothing the grid power which now is given by [54]:

$$P_{GRID}(n) = P_{G,LF}(n), \tag{3.18}$$

where $P_{G,LF}$ is the low-frequency content of $P_G(n)$. As a consequence, the power handled by the battery is expressed as follows:

$$P_{BAT}(n) = P_{BAT,FLC}(n) + P_{G,HF}(n), \tag{3.19}$$

$$P_{G,HF}(n) = P_G(n) - P_{GRID}(n), \tag{3.20}$$

where $P_{G,HF}$ the high-frequency content of $P_G(n)$.

Regarding the FLC design, the adjustment of all parameters involved in the FLC, for instance, number of Membership Functions (MF), type, mapping and rule-base, is performed following the process described in [51], which will be further detailed in section 3.4.4. The main goal of this process is to find the FLC parameters which minimize the quality criteria defined in section 3.1.2.

In short, for each controller input, $P_{LG}(n)$, $SOC(n)$, 5 triangular MFs are defined. These MFs correspond to five fuzzy sets noted as NB, NS, ZE, PS and PB, where B represents “Big”, S “Small”, ZE “Zero”, P “Positive” and N “Negative”, as shown in Fig. 3.7(a) and Fig. 3.7(b). In addition, 2 trapezoidal MFs are defined for the input $P_{AVG}(n)$, which correspond to two fuzzy sets noted as NB and PB, as shown in Fig. 3.7(c). The MFs for the controller inputs are distributed along the variation range defined for each input variable expressed as follows:

$$P_{LG,MIN} \le P_{LG}(n) \le P_{LG,MAX}, \tag{3.21}$$

$$-C_{BAT}/2 \le e(n) \le C_{BAT}/2, \tag{3.22}$$

$$P_A^- \le P_{AVG}(n) \le P_A^+, \tag{3.23}$$

where P_A^- and P_A^+ are the maximum and minimum value of the MG net power trend.

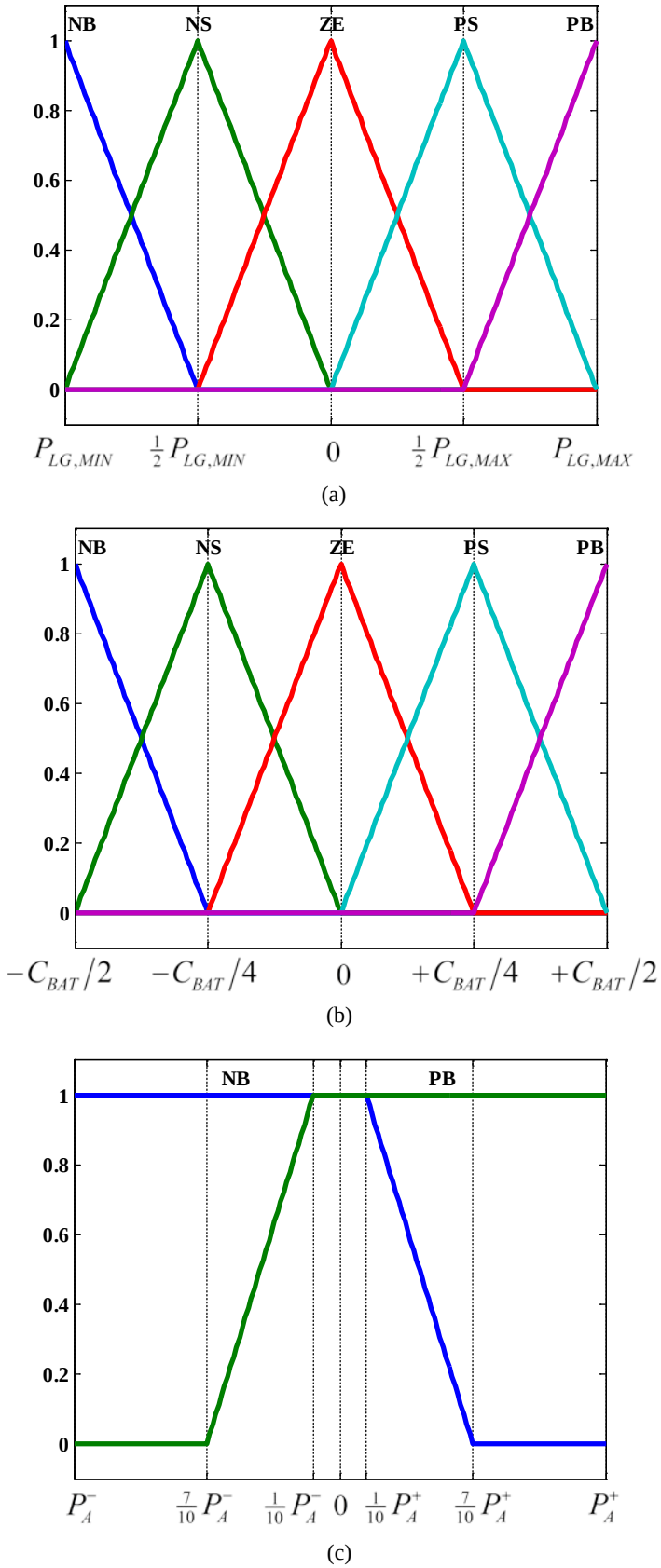

Fig. 3.7. Membership functions for the FLC inputs of the fuzzy NPT strategy (a) MFs for the input $P_{LG}(n)$, (b) MFs for the input $SOC(n)$, and (c) MFs for the input $P_{AVG}(n)$, © 2014, IEEE

Note that the input P_{AVG} uses the MF "NB" to indicate that the MG exhibits a generation trend. On the contrary, it uses the MF "PB" to indicate a consumption trend.

The assignment of the MFs for the inputs variables allows the definition of at most 50 MFs for the output variable. Therefore, after applying the optimization procedure [51], 7 trapezoidal MFs are defined for the controller output $P_{BAT,FLC}$ (n), as shown in Fig. 3.8. These MFs are associated with seven fuzzy sets noted as NB, NM, NS, ZE, PS, PM and PB, where besides of N, P, B, S and ZE previously defined, M represents "Medium". The output MFs are distributed along the variation range defined by:

$$-k_B \leq P_{BAT,FLC}(n) \leq k_B, \tag{3.24}$$

being k_B the maximum power assigned at the controller output $P_{BAT,FLC}$.

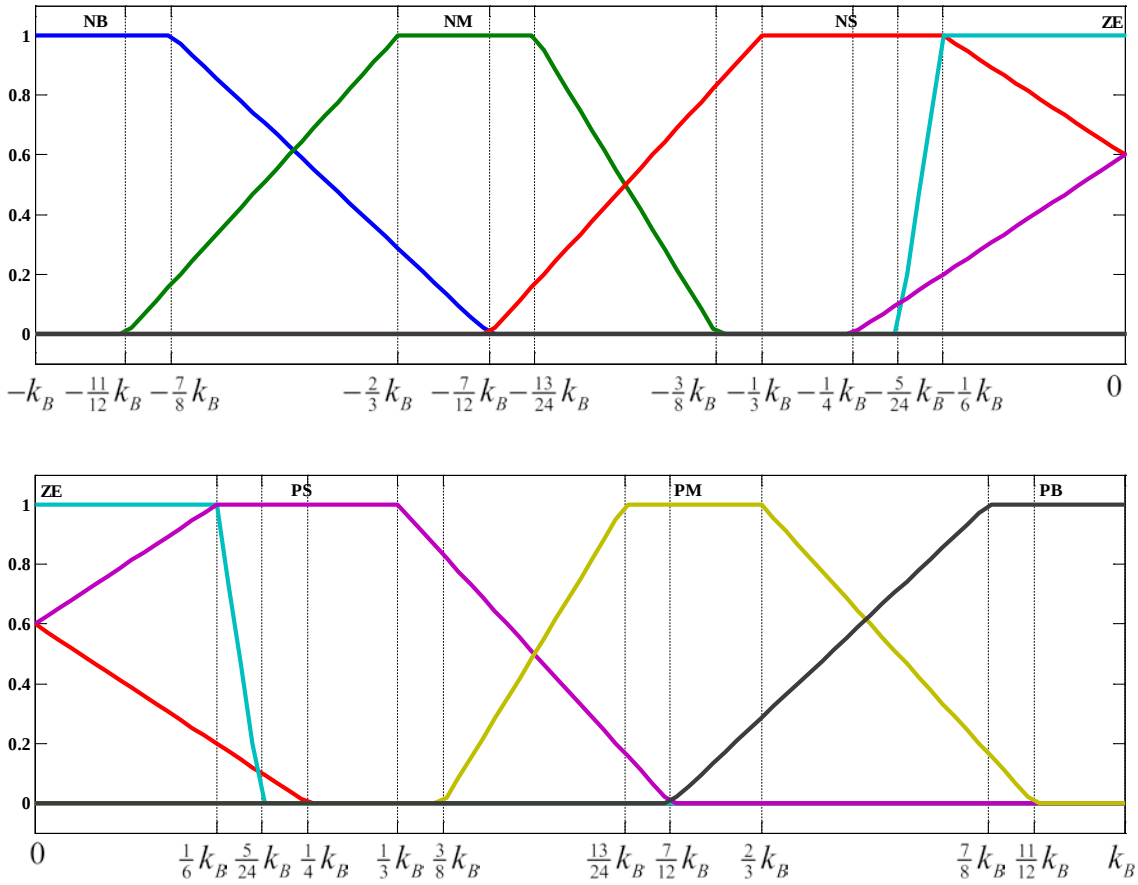

Fig. 3.8. MFs for the FLC output of the fuzzy NPT strategy, © 2014, IEEE

Finally, according to the MFs of the inputs and the output, the FLC rule-base is composed by 50-rules which establish the control policy of the output P_{BAT}. The rule-base is set taking into account the control polices described in [52], [51]. In short, the controller rule-base assigns 25-rules when the MG exhibits a consumption trend and other 25-rules for generation trend. For

instance, one of the rules is formulated as: "IF the MG net power $P_{LG}(n)$ is slightly negative [i.e. $P_{LG}(n) < 0$, there is more generation than consumption] AND the battery is slightly charged [i.e. $e(n) > 0$, or equivalently $SOC(n) > C_{BAT}/2$] AND the MG exhibits high consumption trend [i.e. $P_{AVG}(n) >> 0$] THEN strongly charge the battery for covering this consumption trend in a near future [i.e. $P_{BAT,FLC}(n) << 0$]".

IF P_{LG} **IS** NS **AND** e **IS** PS **AND** P_{AVG} **IS** PB **THEN** $P_{BAT,FLC}$ **IS NB**

As for the inputs and output MFs, the FLC rule-base is optimized following the procedure detailed in [51] with the purpose of minimizing the quality criteria defined in section 3.1.2. The resulting rule-base is presented in Table 3-4.

Table 3-4 FLC rule-base for the fuzzy NPT strategy

$P_{BAT,FLC}(n)$		$P_{LG}(n)$				
		NB	**NS**	**ZE**	**PS**	**PB**
$e(n)$	**NB**	NB / NB	NS / NB	NB / NB	NB / NM	NB / NB
	NS	PM / NS	NB / NM	ZE / NS	NS / PM	PS / NM
	ZE	NM / NB	PS / ZE	ZE / ZE	NS / PM	NS / NS
	PS	PS / NS	PS / NB	PM / ZE	PM / ZE	PM / NB
	PB	PB / PB	PB / PB	PB / PB	PB / PB	PB / PB
$P_{AVG}(n)$	**NB** / PB					

3.3.3. Simulation results and comparison

The simulation results of the fuzzy NPT strategy excluding the EWH consumption are shown in Fig. 3.9. As it can be seen in Fig. 3.9(a), this approach achieves a reduction of the grid power fluctuations and power peaks. However, the grid power profile still exhibits some power peaks, since the SOC of battery occasionally reaches the secure limits, as shown in Fig. 3.9(b). Although, these time intervals are reduced with respect to the SMA strategy, which leads to a minimum reduction of the ramp-rates in the grid power profile as it can be seen in Fig. 3.9(c) and Fig. 3.9 (d).

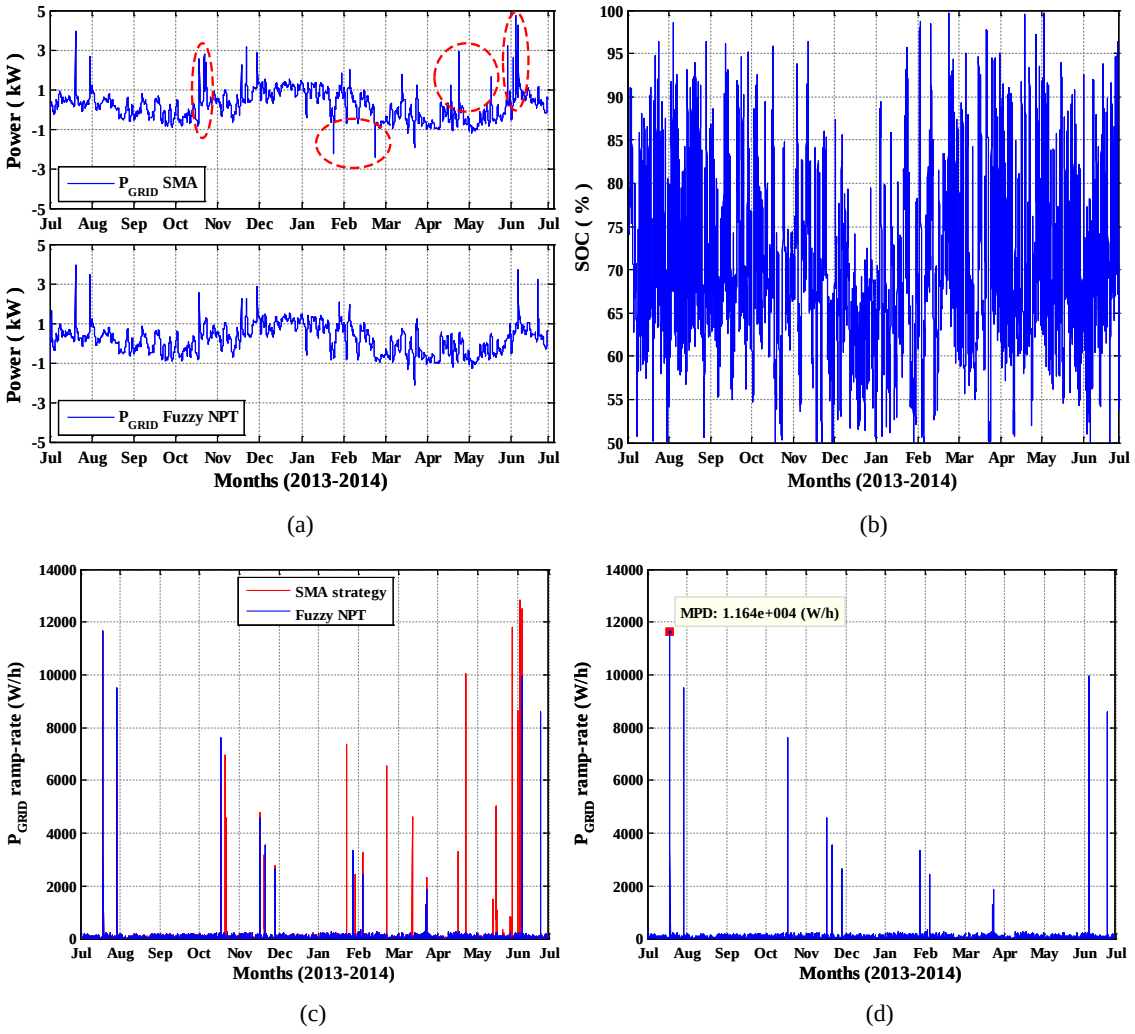

Fig. 3.9. Simulation results of the fuzzy NPT strategy excluding the EWH consumption (a) grid power profile, (b) battery SOC, (c) grid power profile ramp-rates comparison, and (d) maximum grid power profile ramp-rate.

Despite the aforementioned drawbacks, the fuzzy NPT strategy improves the behavior with respect to the SMA strategy, this being verified through the analysis of the resulting values of the quality criteria defined in section 3.1.2. The results are summarized in Table 3-5. In short, the $P_{G,MAX}$, $P_{G,MIN}$, *PVR*, *MPD* and *APD* criteria are reduced in 16.56%, 11.67%, 15.52%, 9.34% and 19.74%, respectively. On the contrary, *PPV* criterion is slightly increased in 3.98%. Note that the value of the *MPD* criterion is high due to the power peaks in the grid power profile.

Table 3-5 Quality criteria comparison for the fuzzy NPT strategy, the SMA strategy and the baseline values excluding the EWH consumption

EMS Strategy	$P_{G,MAX}$ (kW)	$P_{G,MIN}$ (kW)	*PVR*	*MPD* (W/h)	*APD* (W/h)	*PPV*
No EMS & ESS excluding the EWH consumption	5.75	-6.45	1.00	18468	1121	13.3
SMA strategy	4.71	-2.40	0.58	12839	44.42	2.51
Fuzzy EMS based on MG net power trend	3.93	-2.12	0.49	11640	35.65	2.61

Finally, for comparison purposes, the analysis of the fuzzy NPT strategy is carried out including the EWH consumption. The simulation results are shown in Fig. 3.10, where it can be seen that some strong the fluctuations in the grid power are removed with respect to SMA strategy. Consequently, the grid power profile ramp-rates are reduced with respect to the SMA strategy, as confirmed in Table 3-6 through the reduction of the values of the quality criteria.

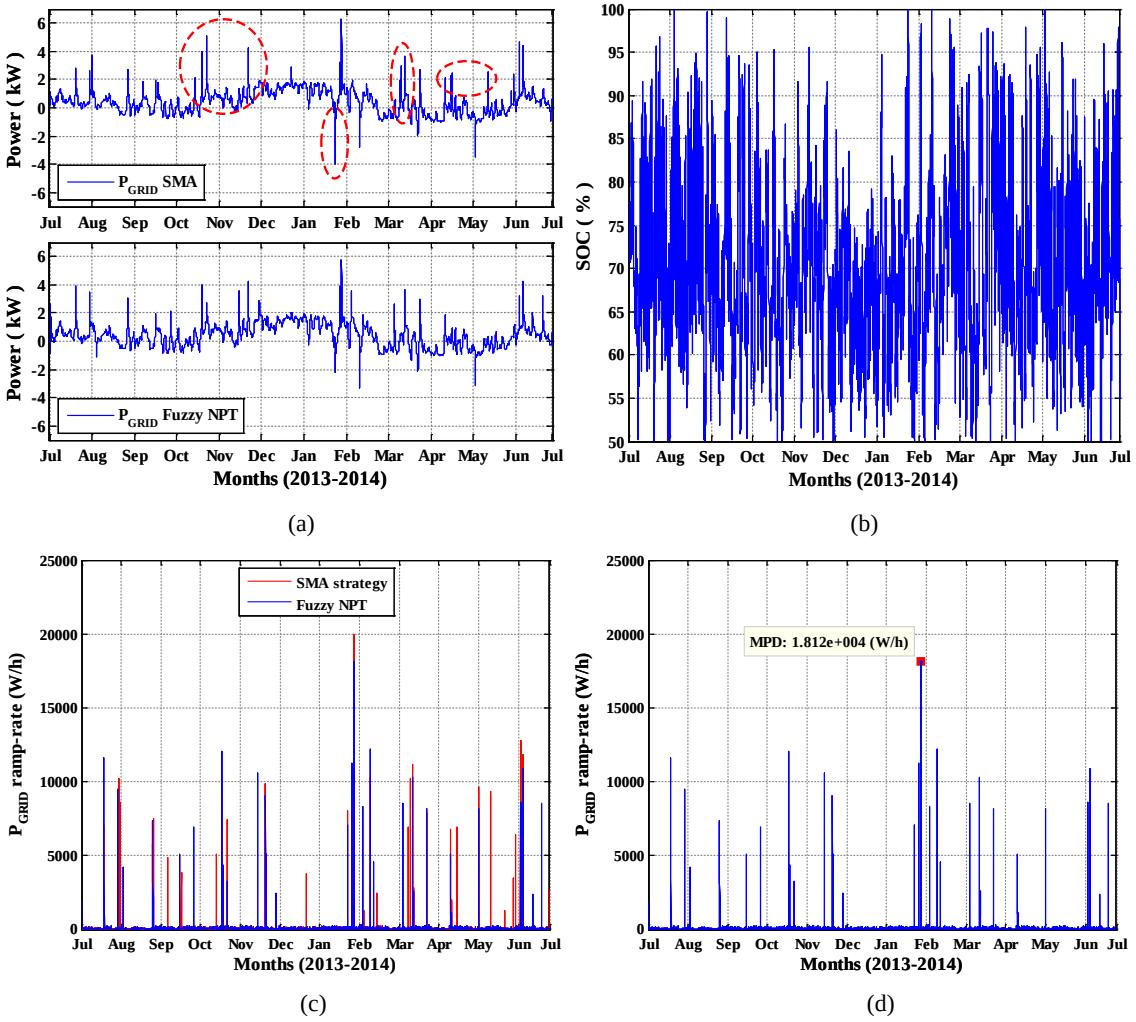

Fig. 3.10. Simulation results of the fuzzy NPT strategy including the EWH consumption (a) grid power profile, (b) battery SOC, (c) grid power profile ramp-rates comparison, and (d) maximum grid power profile ramp-rate.

Table 3-6 Quality criteria comparison for the fuzzy NPT strategy, the SMA strategy and the baseline values including the EWH consumption

EMS Strategy	$P_{G,MAX}$ (kW)	$P_{G,MIN}$ (kW)	*PVR*	*MPD* (W/h)	*APD* (W/h)	*PPV*
No EMS & ESS including the EWH consumption	6.53	-6.45	1.00	18468	1221	5.99
SMA strategy	6.25	-3.98	0.79	20006	57.41	1.23
Fuzzy EMS based on MG net power trend	5.80	-3.28	0.70	18119	50.81	1.31

From the simulation results, it can be concluded that the information provided through the MG net power trend is not the most appropriate to identify the fluctuations in the MG net power. In addition, the use of a new variable at the FLC input results in the increase of the fuzzy controller rule-base (i.e. fifty rules), which increases the controller complexity. In this regard, given the benefits exposed by using a FLC for the EMS design, a new energy management strategy based on FLC is described in the next section with the objective of improving the performance and simplifying the FLC complexity of the EMS strategies described so far.

3.4. Fuzzy energy management strategy based on MG energy Rate-of-Change

3.4.1. Introduction

An improved fuzzy-based design is presented in this section with the aim of minimizing the power peaks and fluctuations in the grid power profile while keeping the battery SOC evolution within secure limits as well as reducing the FLC complexity. This design was presented in [53] and an extended version including experimental validation results was described in [54]. The new fuzzy-based design uses the MG Energy Rate-of-Change (ERoC) over time to quantify the magnitude of the energy changes in the MG; according to this value and the battery SOC, the new EMS design increases, decreases or maintains the power delivered/absorbed by the mains in order to concurrently satisfy the load power demand and the battery constraints defined in Chapter 2.3.3.

3.4.2. Control strategy

The improved fuzzy EMS based on MG ERoC suggests calculating the grid power as the sum of the average net power of the MG, P_{AVG} (n) defined in (3.12) and an additional component, P_{FLC} (n), used to modify the power exchanged with the grid to keep the battery SOC within secure limits at any time. Thus, the grid power profile is defined as [54], [53]:

$$P_{GRID}(n) = P_{AVG}(n) + P_{FLC}(n). \tag{3.25}$$

where P_{FLC} (n) is computing by means of a FLC that uses the battery SOC, SOC (n), and the MG ERoC over time , $\dot{P}_{AVG}$ (n), as inputs variables.

In this regard, the FLC uses the battery SOC, SOC (n), as an input to check its value at any time in order to satisfy the battery constraints established in Chapter 2.3.3 and to preserve the battery life. In addition, the FLC uses $\dot{P}_{AVG}$ (n) as another input to obtain the information of the magnitude of the MG energy change of two consecutive samples (i.e. the slopes produced by

two consecutive samples). In this approach $\dot{P}_{AVG}(n)$ is defined as first backward difference as follows [94]:

$$\dot{P}_{AVG}(n) = \left[P_{AVG}(n) - P_{AVG}(n-1)\right] / T_s \tag{3.26}$$

For instance, Fig. 3.11 shows the MG energy change in two consecutive samples [54] where according to (3.26) a positive slope (e.g. m1, m4, m5, m6 and m8) means a MG energy change due to a reduction of the renewable power generation or an increase of the load demand. On the contrary, a negative slope (e.g. m2, m3 and m7) corresponds to a MG energy change due to an increase of the renewable power generation or a decrease in the load demand.

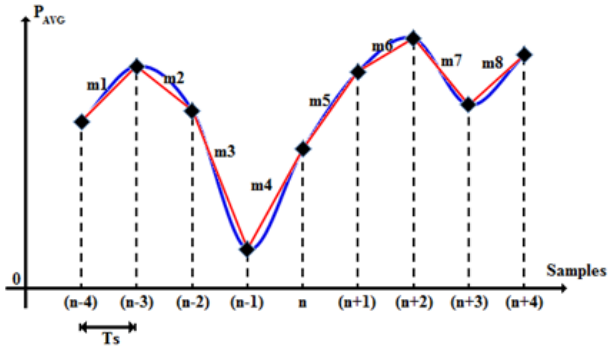

Fig. 3.11. Slopes by two consecutive samples (red solid line) of the average net power profile (blue solid line).

It should be noted that $\dot{P}_{AVG}(n)$ can be understood as the local prediction of the battery SOC future behavior if the grid power is not modified. Therefore, from the information of the $SOC(n)$ and $\dot{P}_{AVG}(n)$ the FLC will modify its output, $P_{FLC}(n)$, to increase, decrease or maintain the power delivered/absorbed by the mains, according to (3.25), to concurrently satisfy the load power demand and to keep the battery SOC within secure limits. In this way, the output of the FLC allows the interaction between the MG and the mains. A complete description of this interaction is presented in Table 3-7 [54].

The block diagram of the fuzzy ERoC strategy is shown in Fig. 3.12 and includes the following blocks:

1. A Low-Pass filter block (LPF), used for computing the average net power of the MG according to (3.12),
2. A digital Derivative and Filter block (DF), used for concurrently obtaining $\dot{P}_{AVG}(n)$, according to (3.26), and limiting the high-frequency gain and noise associated with the derivative term [95],
3. A battery SOC Estimator block, used to estimate the SOC of the battery according to (2.4) and the battery model described in Chapter 2.3.3, and

4. A Fuzzy Logic Controller block (FLC), used for computing the second component, $P_{FLC}(n)$, of the grid power profile defined in (3.25). The design of this block is described in the following section.

Table 3-7 Impact of the FLC output on the grid power profile, © 2016, IEEE

Condition	Grid power	Description
If $P_{AVG} \geq 0$ and $P_{FLC} > 0$	$\Rightarrow P_{GRID} > 0$	P_{FLC} increases the power delivered by the mains
	If $P_{AVG} > \lvert P_{FLC} \rvert \Rightarrow P_{GRID} > 0$	P_{FLC} decreases the power delivered by the mains
If $P_{AVG} \geq 0$ and $P_{FLC} < 0$	If $P_{AVG} < \lvert P_{FLC} \rvert \Rightarrow P_{GRID} < 0$	P_{FLC} increases the power absorbed by the mains
	If $P_{AVG} = \lvert P_{FLC} \rvert \Rightarrow P_{GRID} = 0$	P_{FLC} indicates that use extra power from the mains is not necessary
	If $\lvert P_{AVG} \rvert > P_{FLC} \Rightarrow P_{GRID} < 0$	P_{FLC} decreases the power absorbed by the mains
If $P_{AVG} < 0$ and $P_{FLC} > 0$	If $\lvert P_{AVG} \rvert < P_{FLC} \Rightarrow P_{GRID} > 0$	P_{FLC} increases the power delivered by the mains
	If $\lvert P_{AVG} \rvert = P_{FLC} \Rightarrow P_{GRID} = 0$	P_{FLC} indicates that use extra power from the mains is not necessary
If $P_{AVG} < 0$ and $P_{FLC} < 0$	$\Rightarrow P_{GRID} < 0$	P_{FLC} increases the power absorbed by the mains
If $P_{AVG} \geq 0$ and $P_{FLC} = 0$	$P_{GRID} = P_{AVG} \Rightarrow P_{GRID} \geq 0$	P_{FLC} maintains the power delivered by the mains according to P_{AVG}
If $P_{AVG} < 0$ and $P_{FLC} = 0$	$P_{GRID} = P_{AVG} \Rightarrow P_{GRID} < 0$	P_{FLC} maintains the power absorbed by the mains according to P_{AVG}

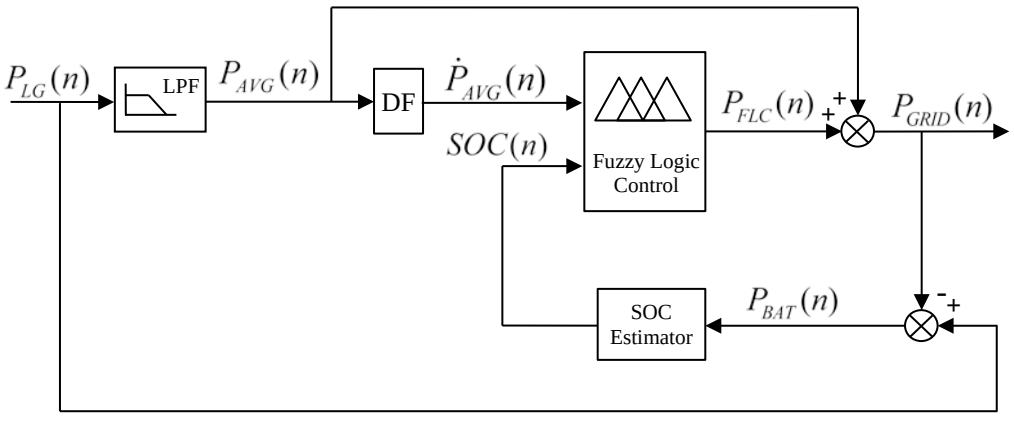

Fig. 3.12. Fuzzy ERoC strategy block diagram, © 2016, IEEE

3.4.3. Fuzzy logic controller design

The FLC block assumes a Mamdani-based inference and defuzzyfication of Centre of Gravity [58] with two-inputs, $SOC(n)$ and $\dot{P}_{AVG}(n)$, and one-output $P_{FLC}(n)$. The variation range of each variable is expressed as follows [54]:

$$SOC_{MIN} \leq SOC(n) \leq SOC_{MAX}, \tag{3.27}$$

$$\dot{P}_{AVG,MIN} \leq \dot{P}_{AVG}(n) \leq \dot{P}_{AVG,MAX}, \tag{3.28}$$

$$-k \leq P_{FLC}(n) \leq k, \tag{3.29}$$

where SOC_{MIN} and SOC_{MAX} are the boundaries of the battery SOC defined in Chapter 2.3.3, $\dot{P}_{AVG,MIN}$ and $\dot{P}_{AVG,MAX}$ are the maximum and minimum variation of the derivative term, respectively, and k is the maximum power assigned by the controller output, which from the optimization process k is defined as $k = \pm 1$ kW. In addition, $\dot{P}_{AVG,MAX}$ and $\dot{P}_{AVG,MIN}$ are expressed in W/s and have been calculated using the approximation developed in [96] assuming a time window T_W of one day, as follows [54]:

$$\dot{P}_{AVG,MAX} = (9/10) \cdot (P_{LOAD}/T_W) \tag{3.30}$$

$$\dot{P}_{AVG,MIN} = -(9/10) \cdot (P_{WT}/T_W) \tag{3.31}$$

Regarding the FLC design, the adjustment of all parameters involved in the FLC (e.g. number of MFs per input, type, mapping, rule-base), was performed by an off-line optimization process using the real recorded data of the renewable power generation and the load demand described in Chapter 2.4 with the objective of minimizing the energy management quality criteria defined in section 3.1.2. The optimization procedure consists in the next steps [51], [54]:

Step 1. Initial setting of the FLC parameters

a. Initial assignment of the MFs for the inputs and outputs variables: number, type and mapping.

b. Initial FLC rule-base setting.

Step 2. Adjustment of the inputs and outputs MFs.

Step 3. Optimization of the initial FLC rule-base

For better understanding and completeness of the study, the optimization procedure presented in [51] is described in the next paragraphs.

3.4.4. Fuzzy controller optimization process

The optimization process consists on the definition of all parameters involved in the FLC design, for instance, number of MFs, type, mapping and rule-base. This process is developed in three steps which are described below:

STEP 1: Initial setting of the FLC parameters:

This step involves the initial FLC design through the assignment of an arbitrary number of MFs to the inputs and output of the FLC. In addition this step sets the initial rule-base, which is built according to the linguistic knowledge about the desired behavior of the MG.

Initially, five triangular MFs, uniformly distributed, are assigned to the FLC inputs $\dot{P}_{AVG}$ (n) and SOC (n). According to (3.27) - (3.31), these MFs are distributed along the variation range defined for each variable and correspond to five fuzzy sets noted as NB, NS, ZE, PS and PB where B represents “BIG”, S “Small”, ZE “Zero”, P “Positive” and N “Negative”. The initial MFs for both input variables are shown in Fig. 3.13 and Fig. 3.14.

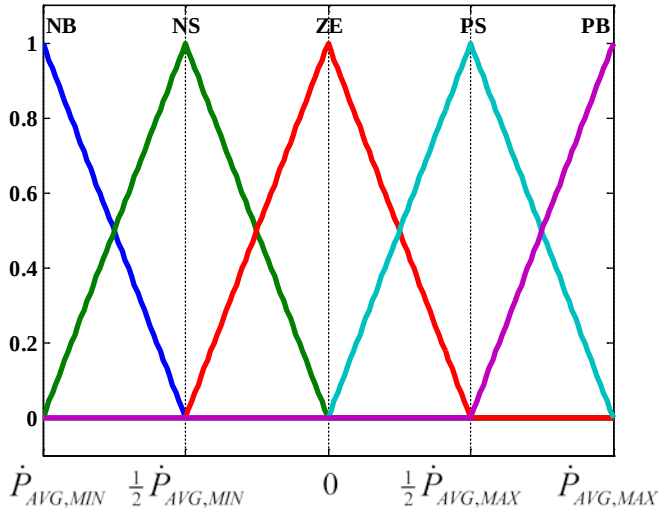

Fig. 3.13. Initial MFs for the FLC input variable $\dot{P}_{AVG}$

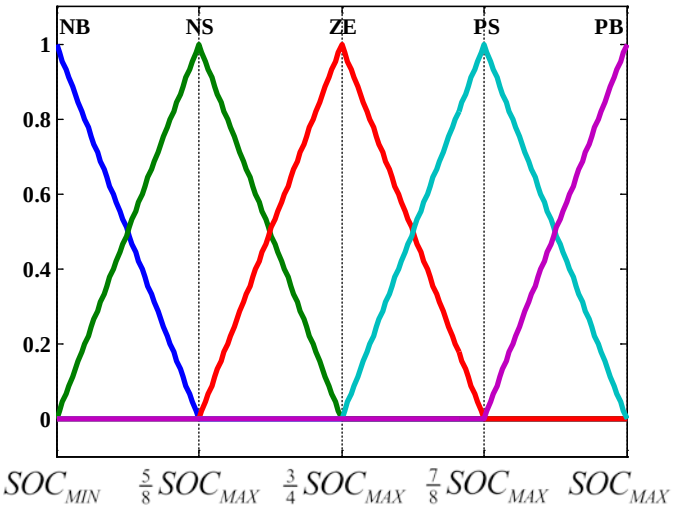

Fig. 3.14. Initial MFs for the FLC input variable battery SOC

The initial assumption of 5 MFs per input leads to the definition of a FLC rule-base up to 25-rules. Hence, allowing the definition of at most 25 MFs for the output variable.

As aforementioned, this step also defines the initial rule-base for the FLC. The initial rule-base is built taking into account the linguistic knowledge about the MG behavior considering the following assumptions:

- Input $\dot{P}_{AVG}$ (n):
  - A "Negative" MF (i.e. NB and NS) denotes a decrease in the MG consumption-generation balance (i.e. "B" specifies a big energy change and "S" specifies a small energy change), which is associated with an increase of the power generation or a decrease of the load demand.
  - A "Positive" MF (i.e. PB and PS) denotes an increase in the MG consumption-generation balance, which is associated with an increase of the load demand or a decrease of the power generation.
  - A "Zero" MF (i.e. ZE) indicates that there has not been an energy change in the MG.

- Input SOC (n):
  - A "Negative" MF (i.e. NB and NS) specifies that the storage system is being discharged. The NB membership function indicates that the charge level of the storage system is reaching the discharging limit allowed.
  - A "Positive" MF (i.e. PB and PS) indicates that the storage system is being charged. The PB membership function indicates that the storage system is almost fully charged.
  - A "Zero" membership function (i.e. ZE) indicates that the storage system is close to the half of the battery useful capacity (i.e. close to 75% of the rated battery capacity).

From the aforementioned assumptions, the initial rule-base is built as follows:

- First, the output of the FLC should specify that besides P_{AVG} component, the use of additional power coming from the grid is not required (i.e. P_{FLC} → ZE) under the following conditions:
  - When $\dot{P}_{AVG}$ is NB and SOC is NB, given that the big energy change in the MG would be absorbed by the ESS, since the battery is discharged at this time.

RULE 1: IF $\dot{P}_{AVG}$ **IS** NB **AND** SOC **IS** NB **THEN** P_{FLC} **IS ZE**

  - When $\dot{P}_{AVG}$ is NS and SOC is NS, given that the small energy change in the MG would be absorbed by the ESS, since the amount of energy stored in the battery is lower than the half of the battery useful capacity.

RULE 7: IF $\dot{P}_{AVG}$ **IS** NS **AND** SOC **IS** NS **THEN** P_{FLC} **IS ZE**

- When $\dot{P}_{AVG}$ is ZE and *SOC* is ZE, given the amount of energy stored in close to the half of the rated battery capacity.

RULE 13: IF $\dot{P}_{AVG}$ **IS** ZE **AND** *SOC* **IS** ZE **THEN** P_{FLC} **IS ZE**

- When $\dot{P}_{AVG}$ is PS and *SOC* is PS, given that the small energy change in the MG would be handled by the ESS, since the battery lifetime is not compromised.

RULE 19: IF $\dot{P}_{AVG}$ **IS** PS **AND** *SOC* **IS** PS **THEN** P_{FLC} **IS ZE**

- When $\dot{P}_{AVG}$ is PB and *SOC* is PB, given that the big energy change in the MG would be handled by the ESS, since the battery at this time is almost fully charged.

RULE 25: IF $\dot{P}_{AVG}$ **IS** PB **AND** *SOC* **IS** PB **THEN** P_{FLC} **IS ZE**

According to the conditions mentioned above, the ZE (i.e. Zero) MF for the FLC output is initially defined as shown in Fig. 3.15. Given this initial definition, the FLC rule-base presents rules corresponding to ZE fuzzy subset in its diagonal, as shown in Fig. 3.16, which states that under those conditions, besides the component P_{AVG}, the use of extra power coming from the grid is not required.

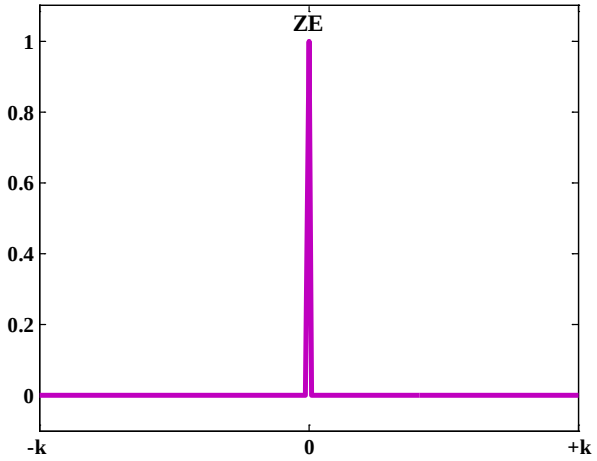

Fig. 3.15. Initial definition and distribution of the ZE fuzzy subset of the FLC output

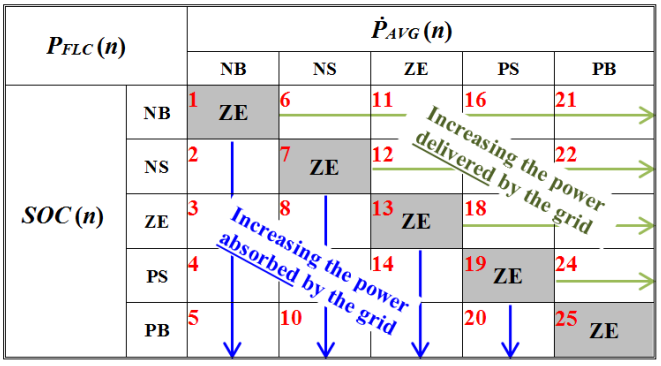

Fig. 3.16. Initial fuzzy rule-base and grid power variation with respect to the FLC inputs

- Then, the rules over the diagonal are defined to establish that the evolution of the variable $\dot{P}_{AVG}$ from a ***X*** value to a ***Y*** value involves the following statements:
  - If ***X*** < ***Y*** implies the increase of the power delivered by the grid. For instance, when *SOC* is NB, if $\dot{P}_{AVG}$ is NS the power assigned to the FLC output should be higher than the one assigned when $\dot{P}_{AVG}$ is NB (i.e. P_{FLC} will be positive). In short, when the battery is almost discharged (i.e. *SOC* is NB) and the MG energy ERoC indicates a reduction of power generation or an increase of the load demand (e.g. when $\dot{P}_{AVG}$ changes from NB to NS), besides P_{AVG} component it will be necessary the use of extra power coming from the grid in order to charge the batteries (i.e. P_{FLC} → PSS).
  - On the contrary, if ***X*** > ***Y*** implies the decrease of the power delivered by the grid.

Following these statements, the rules over the diagonal are defined as:

RULE 6: IF $\dot{P}_{AVG}$ **IS** NS **AND** *SOC* **IS** NB **THEN** P_{FLC} **IS PSS**

RULE 11: IF $\dot{P}_{AVG}$ **IS** ZE **AND** *SOC* **IS** NB **THEN** P_{FLC} **IS PS**

RULE 12: IF $\dot{P}_{AVG}$ **IS** ZE **AND** *SOC* **IS** NS **THEN** P_{FLC} **IS PSS**

RULE 16: IF $\dot{P}_{AVG}$ **IS** PS **AND** *SOC* **IS** NB **THEN** P_{FLC} **IS PM**

RULE 17: IF $\dot{P}_{AVG}$ **IS** PS **AND** *SOC* **IS** NS **THEN** P_{FLC} **IS PS**

RULE 18: IF $\dot{P}_{AVG}$ **IS** PS **AND** *SOC* **IS** ZE **THEN** P_{FLC} **IS PSS**

RULE 21: IF $\dot{P}_{AVG}$ **IS** PB **AND** *SOC* **IS** NB **THEN** P_{FLC} **IS PB**

RULE 22: IF $\dot{P}_{AVG}$ **IS** PB **AND** *SOC* **IS** NS **THEN** P_{FLC} **IS PM**

RULE 23: IF $\dot{P}_{AVG}$ **IS** PB **AND** *SOC* **IS** ZE **THEN** P_{FLC} **IS PS**

RULE 24: IF $\dot{P}_{AVG}$ **IS** PB **AND** *SOC* **IS** PS **THEN** P_{FLC} **IS PSS**

As shown in Fig. 3.16, the rules over the diagonal indicate the increase of the power delivered by the grid. In addition, this analysis leads to the definition of another four MFs for the FLC output. These MFs are uniformly distributed along the positive range of the output P_{FLC}, as shown in Fig. 3.17, and correspond to four fuzzy sets noted as PSS, PS, PM and PB where besides of P, B, and S previously defined, SS represents “Smallest” and M represents “Medium”.

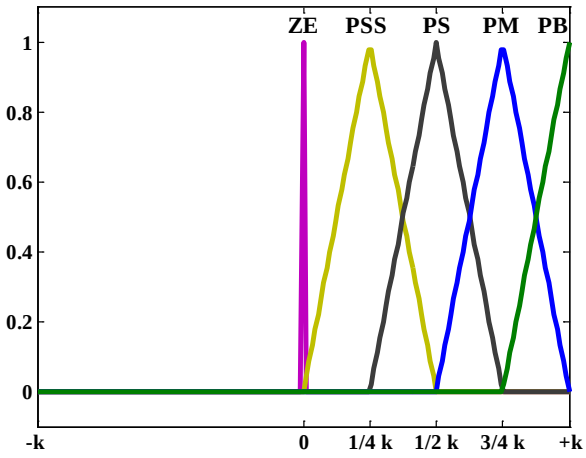

Fig. 3.17. Initial definition and distribution of the positive MFs for the FLC output

- After that, the rules below the diagonal are defined in order to preserve the battery lifetime. In this concern, these rules consider the amount of energy stored in the battery (i.e. *SOC* input) to increase the power absorbed by the grid according to the following statements:
  - An increase of the amount of energy stored in the ESS implies an increase of the power absorbed by the grid in order to not overcharge the battery. For instance, when $\dot{P}_{AVG}$ is NB, if *SOC* is NS the power assigned to the FLC output should be lower than the one assigned when *SOC* is NB (i.e. P_{FLC} will be negative, P_{FLC} → NSS).
  - Conversely, a decrease of the energy stored in the ESS implies a decrease of the power absorbed by the grid in order to avoid discharge the battery out the security limit.

Accordingly, the rules below the diagonal are defined as follows:

RULE 2: IF $\dot{P}_{AVG}$ **IS** NB **AND** *SOC* **IS** NS **THEN** P_{FLC} **IS NSS**

RULE 3: IF $\dot{P}_{AVG}$ **IS** NB **AND** *SOC* **IS** ZE **THEN** P_{FLC} **IS NS**

RULE 4: IF $\dot{P}_{AVG}$ **IS** NB **AND** *SOC* **IS** PS **THEN** P_{FLC} **IS NM**

RULE 5: IF $\dot{P}_{AVG}$ **IS** NB **AND** *SOC* **IS** PB **THEN** P_{FLC} **IS NB**

RULE 8: IF $\dot{P}_{AVG}$ **IS** NS **AND** *SOC* **IS** ZE **THEN** P_{FLC} **IS NSS**

RULE 9: IF $\dot{P}_{AVG}$ **IS** NS **AND** *SOC* **IS** PS **THEN** P_{FLC} **IS NS**

RULE 10: IF $\dot{P}_{AVG}$ **IS** NS **AND** *SOC* **IS** PB **THEN** P_{FLC} **IS NM**

RULE 14: IF $\dot{P}_{AVG}$ **IS** ZE **AND** *SOC* **IS** PS **THEN** P_{FLC} **IS NSS**

RULE 15: IF $\dot{P}_{AVG}$ **IS** ZE **AND** *SOC* **IS** PB **THEN** P_{FLC} **IS NS**

RULE 20: IF $\dot{P}_{AVG}$ **IS** PS **AND** *SOC* **IS** PB **THEN** P_{FLC} **IS NSS**

This previous analysis leads to the definition of extra four MFs for the FLC output, which correspond to four fuzzy sets noted as NSS, NS, NM and NB. These MFs are uniformly distributed along the negative range of the output P_{FLC}. Fig. 3.18 illustrates the complete initial definition of the MFs for the FLC output.

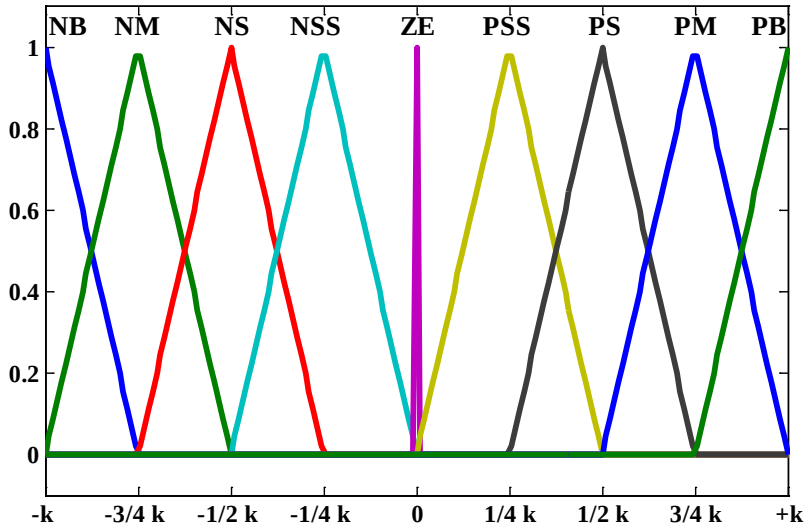

Fig. 3.18. Initial definition and distribution of the MFs for the FLC output

- Finally, the initial rule-base is presented in Table 3-8. The initial rule-base includes 25-rules which establish the evolution of the FLC output [54], [53].

Table 3-8 Initial FLC rule-base of the fuzzy ERoC strategy, © 2015, IEEE

$P_{FLC}(n)$		$\dot{P}_{AVG}(n)$				
		NB	**NS**	**ZE**	**PS**	**PB**
$SOC(n)$	**NB**	**ZE**	PSS	PS	PM	PB
	NS	NSS	**ZE**	PSS	PS	PM
	ZE	NS	NSS	**ZE**	PSS	PS
	PS	NM	NS	NSS	**ZE**	PSS
	PB	NB	NM	NS	NSS	**ZE**

STEP 2: MF adjustment of the FLC inputs and outputs

The second step consists in the adjustment of the inputs and output MFs. This process is carried out through numerical simulations using Matlab®. The procedure for the adjustment of trapezoidal MF, is described in [51]. For instance, the optimization procedure for the *SOC* input is described below:

- First, each triangular MF shown in Fig. 3.14 is parametrically defined according to:

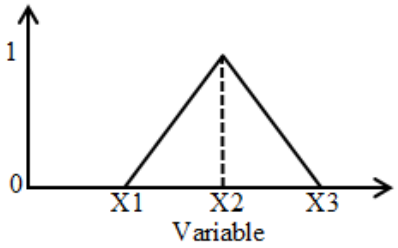

Fig. 3.19. Triangular membership function parameters

The mapping parameters X1, X2 and X3 assume that the pairs of MFs (NB, PB), (NS, PS) are mapped symmetrically with respect to the origin (i.e. 3/4 SOC_{MAX} for the *SOC* input), as shown in Fig. 3.20. Note that for input $\dot{P}_{AVG}$ and output P_{FLC}, X1 = -X3 for the particular case of the MF ZE.

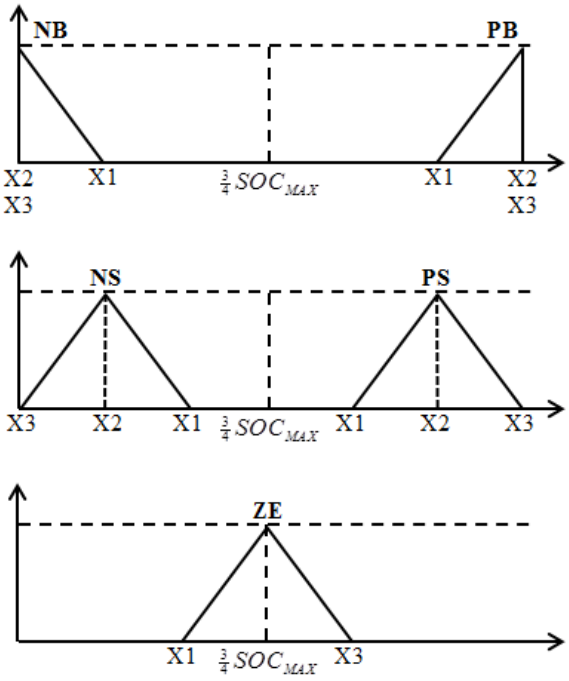

Fig. 3.20. Mapping parameters for the MFs of the *SOC* input

- Then, the mapping adjustment assumes the initial rule-base shown in Table 3-8 and is carried out for each pair of MFs and for ZE MF as follows:
  - Finding X1: the parameters X2 and X3 are fixed to the values shown in Fig. 3.14. Then, the optimum value of the parameter X1, noted as $X1_{opt}$, is obtained through numerical simulations as the value which minimizes the set of defined quality criteria.
  - Finding X2: the parameter X3 is fixed to the value shown in Fig. 3.14 and X1 is set to $X1_{opt}$. Then, the optimum value of the parameter X2, noted as $X2_{opt}$, is obtained through numerical simulations as the value which minimizes the set of defined quality criteria.
  - Finding X3: the parameters X1 and X2 are set to X1 = $X1_{opt}$ and X2 = $X2_{opt}$, respectively. Then, the optimum value of the parameter X3, noted as $X3_{opt}$, is obtained

through numerical simulations as the value which minimizes the set of defined quality criteria.

- Finally, there is a verification procedure where the parameters X3 and X2 are set to $X3 = X3_{opt}$ and $X2 = X2_{opt}$, respectively. Then, by numerical simulations the value of $X1_{opt}$ which minimizes the set of defined quality criteria is verified. If not, the adjustment procedure is repeated.

- Finally, after this process, the optimized MFs for both inputs and the output are shown in Fig. 3.21, Fig. 3.22, and Fig. 3.23, respectively [54], [53].

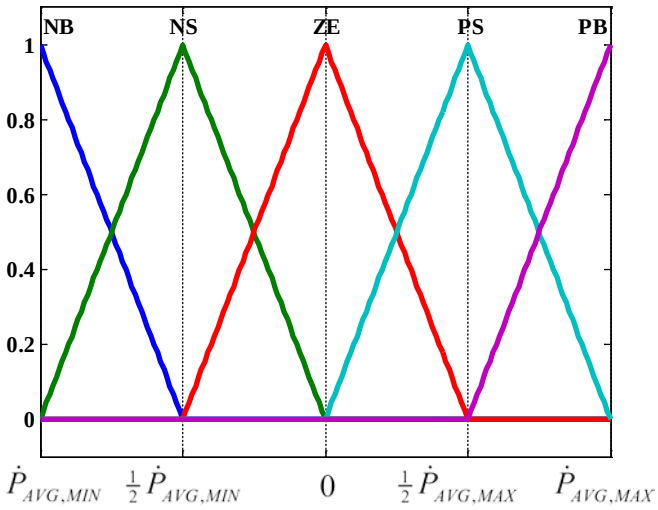

Fig. 3.21. Optimized MFs for the input variable $\dot{P}_{AVG}$, © 2016, IEEE

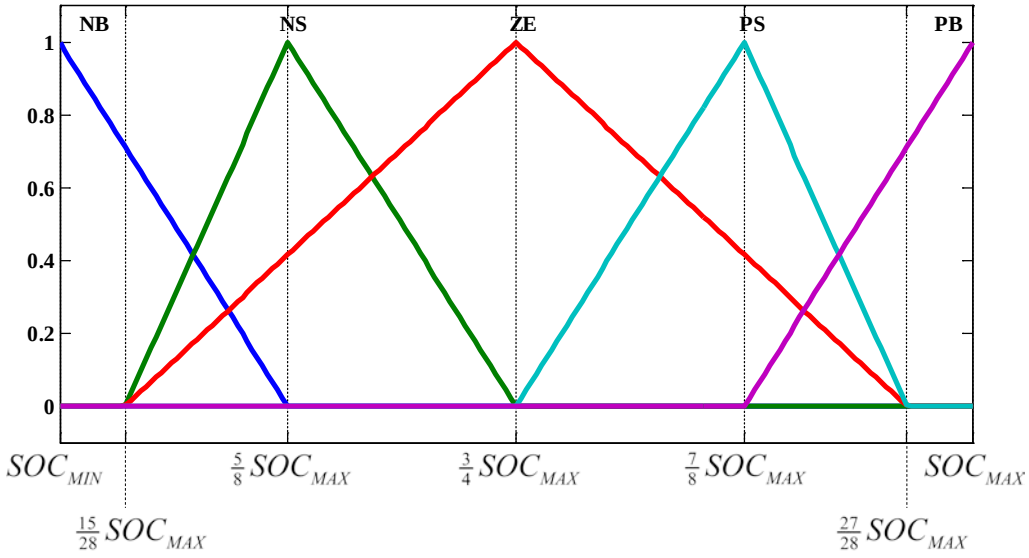

Fig. 3.22. Optimized MFs for the input variable *SOC*, © 2016, IEEE

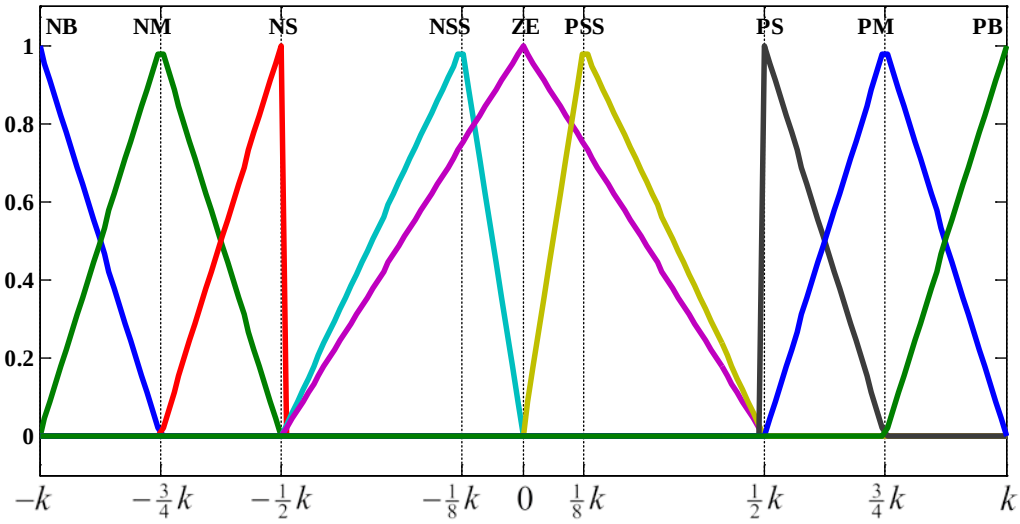

Fig. 3.23. Optimized MFs for the FLC output P_{FLC}, © 2016, IEEE

STEP 3: Optimization of the initial FLC rule-base

The final step involves the adjustment of the initial rule-base presented in table 3-8. Similarly to Step 2, the optimized rule-base is obtained by modifying the rules of the initial rule-base in order to find a set of rules which minimize the quality criteria defined in section 3.1.2. For instance, the optimization of the rules 7, 8 and 9 according to MPD criterion is shown in Fig. 3.24. As it can be seen, the lowest MPD value is obtained when rule 7 is ZE, rule 8 is NSS and rule 9 is NS.

Note that in Fig. 3.24, the number 9 represents the MF “PB”, the number 8 represents “PM”, then successively, PS=7, PSS=6, ZE=5, NSS=4, NS=3, NM=2 and NB=1.

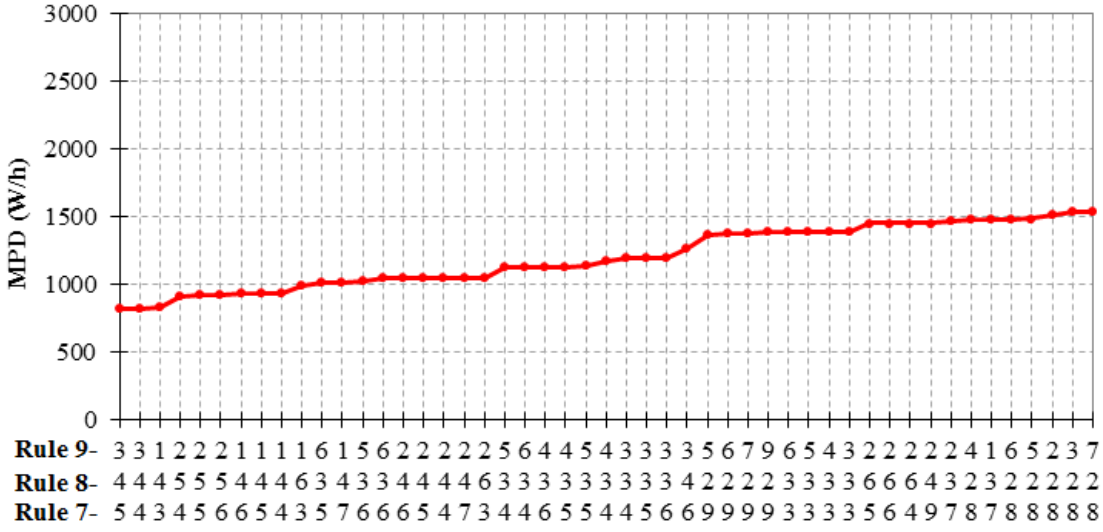

Fig. 3.24. Optimization of the rules 7, 8 and 9

Finally, this process is performed for each rule, which leads to the definition of the optimized rule-base presented in Table 3-9 [54].

Table 3-9 Optimized rule-base for the FLC of the fuzzy ERoC strategy, © 2016, IEEE

$P_{FLC}(n)$		$\dot{P}_{AVG}(n)$				
		NB	**NS**	**ZE**	**PS**	**PB**
$SOC(n)$	**NB**	PSS	PSS	PS	PM	PB
	NS	PSS	ZE	PSS	PSS	PM
	ZE	NS	NSS	ZE	PSS	PS
	PS	NSS	NS	NSS	PM	PSS
	PB	NB	NM	NSS	NSS	NSS

3.4.5. Simulation results and analysis

The simulation results of the fuzzy ERoC strategy excluding the EWH consumption are shown from Fig. 3.25 to Fig. 3.29.

Fig. 3.25(a) compares the grid power profile achieved with the SMA, the fuzzy NPT, and the fuzzy ERoC strategies. The results highlight the improved behavior of the fuzzy ERoC strategy, since the power peaks and the strong fluctuations in the grid power profile are minimized.

Moreover, Fig. 3.25(b) confirms the correct evolution of the battery SOC, which is kept within the secure bounds. As it can be seen, the battery SOC evolution achieved through the SMA strategy and the fuzzy NPT strategy reaches low values, which may cause the battery SOC falls below the secure limit, thus, compromising the battery lifetime. In contrast, the fuzzy ERoC strategy evidences a battery SOC evolution, during the year under study, close to the 75% of the rated battery capacity, which means that the ESS could further compensate net power fluctuations that may exist in the MG at any time while preserving the battery lifetime [54].

The improved behavior of the battery SOC evolution can be further appreciated in Fig. 3.26, where it can be seen that the fuzzy ERoC strategy keeps the battery SOC in a range between the 60% and 80% of the rated battery capacity during the 77% of the year under study. In contrast, the SMA strategy and the fuzzy NPT strategy keep this range in the 66% and 68% of the year under study, respectively.

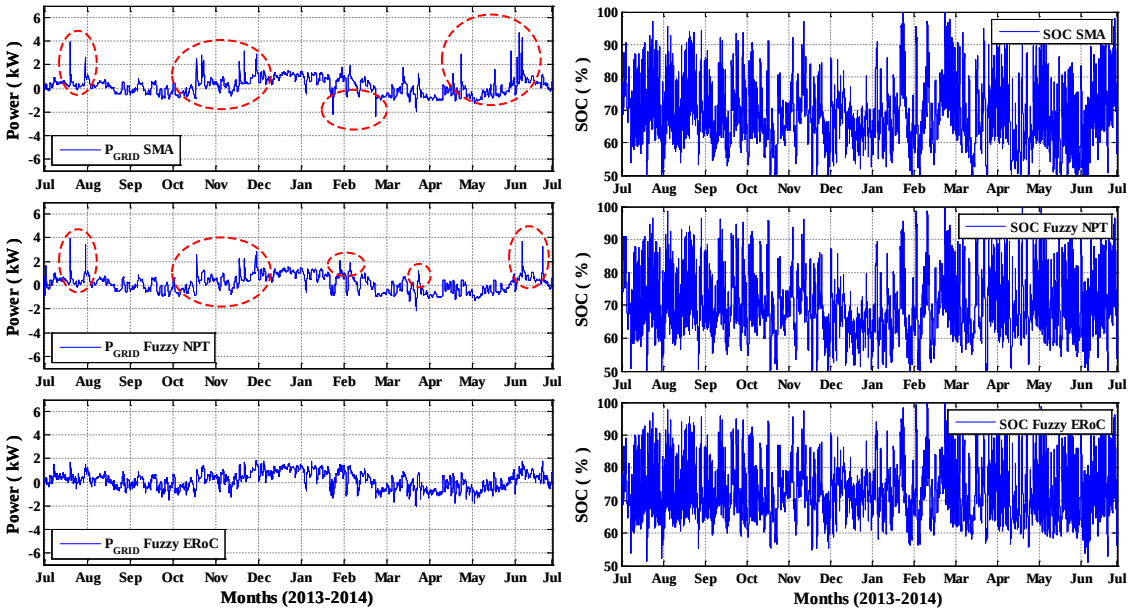

(a) (b)

Fig. 3.25. Simulation results and comparison for the SMA strategy (top), the fuzzy NPT strategy (middle), and the fuzzy ERoC strategy (bottom), (a) grid power profile, and (b) battery SOC

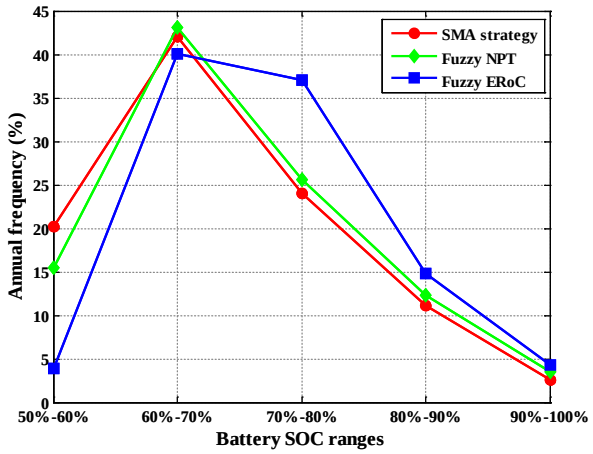

Fig. 3.26. Annual frequency of the battery SOC ranges established from the SMA, fuzzy NPT, and fuzzy ERoC strategies including the EWH consumption

Moreover, the analysis of specific days which highlights the improved grid profile of the fuzzy EMS based on the MG ERoC is presented in Fig. 3.27 and Fig. 3.28. As it can be appreciated in Fig. 3.27, the energy stored in the battery through the fuzzy EMS ERoC (green solid line) is higher than the one obtained through the SMA strategy (pink dot line) and the fuzzy NPT strategy (brown dashed line), which allows compensate the net power fluctuations. Therefore, the proper control of the battery SOC evolution is ensured at every time, and consequently, the undesirable fluctuations in the grid power profile are removed.

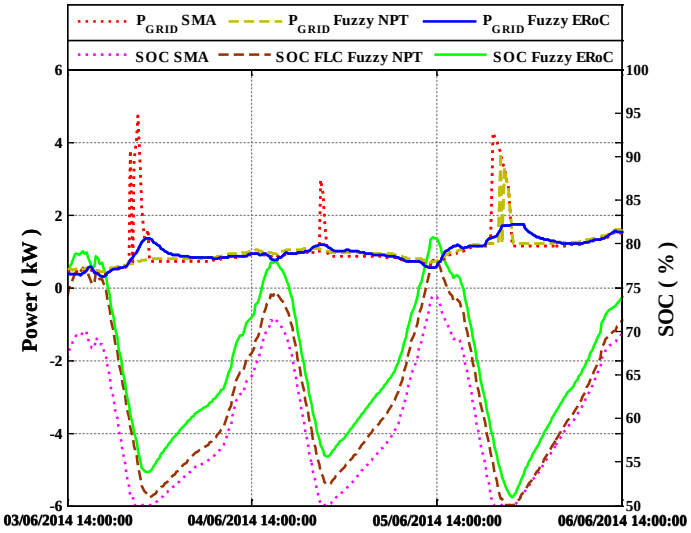

Fig. 3.27. Improved behavior of the fuzzy ERoC strategy with respect to the SMA and fuzzy NPT strategies

Furthermore, Fig. 3.28 highlights the advantage of adding the derivative input to the FLC. As it can be seen, in front of an abrupt consumption change in the MG, the fuzzy ERoC strategy rapidly increases the power delivered by the grid (blue solid line), preventing the discharge of the battery below the secure limit. On the contrary, the slow evolution of the power delivered by the grid provided through the SMA strategy (red dot line) and the fuzzy ERoC strategy (mustard-colored dashed line), leads to the battery to reach the secure limits, thus, breaking the battery SOC constraints [54].

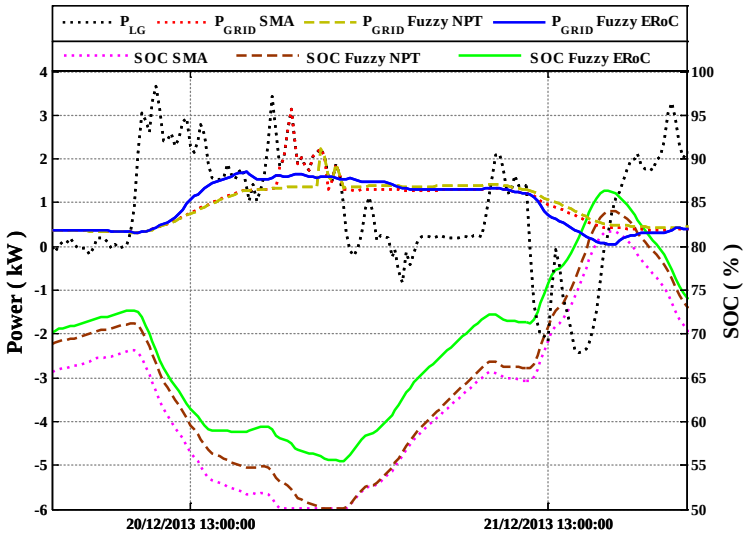

Fig. 3.28. Influence of the derivative input in the grid power profile, © 2016, IEEE

In addition, Fig. 3.29 shows the ramp-rates of the grid power profile achieved through the fuzzy ERoC strategy during the year under study. As it can be seen in Fig. 3.29(a), the grid power ramp-rates are reduced with respect to previous strategies. This result confirms the reduction of

the *MPD* criterion that reaches a maximum value of 817.9 W/h, as shown in Fig. 3.29(b), which leads to improve the quality of the grid power profile.

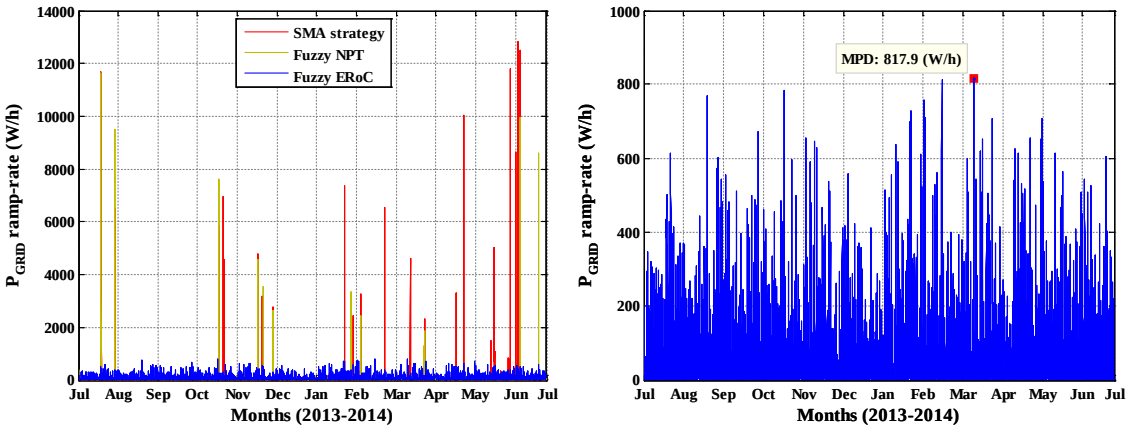

(a) (b)

Fig. 3.29. Simulation results for the fuzzy ERoC strategy excluding the EWH consumption (a) grid power profile ramp-rates comparison, and (b) maximum grid power profile ramp-rate.

The enhanced behavior of the fuzzy ERoC strategy with respect to the strategies described so far is also verified through the analysis of the resulting values of the quality criteria defined in section 3.1.2. The results are summarized in Table 3-10 [54].

Table 3-10 Quality criteria comparison for the fuzzy ERoC strategy, the fuzzy NPT strategy, the SMA strategy and the baseline values excluding the EWH consumption

EMS Strategy	$P_{G,MAX}$ **(kW)**	$P_{G,MIN}$ **(kW)**	***PVR***	***MPD*** **(W/h)**	***APD*** **(W/h)**	***PPV***
No EMS & ESS excluding the EWH consumption	5.75	-6.45	1.00	18468	1121	13.3
SMA strategy	4.71	-2.40	0.58	12839	44.42	2.51
Fuzzy NPT strategy	3.93	-2.12	0.49	11640	35.65	2.61
Fuzzy ERoC strategy	**1.83**	**-2.04**	**0.32**	**817**	**56.15**	**2.79**

As it can be seen, the fuzzy ERoC strategy achieves an important reduction in four of the defined quality criteria. With respect to the SMA strategy $P_{G,MAX}$, $P_{G,MIN}$, and *PVR* are reduced in 61% , 15%, and 45% , respectively, and 53%, 4%, and 35%, respectively, with respect to the fuzzy NPT strategy. Moreover, the main improvement of the fuzzy ERoC strategy is the high reduction of the *MPD* criterion, achieving a reduction up to 94% and 93% with respect to the SMA and the fuzzy NPT strategies, respectively. It can be noted that the improved behavior of the fuzzy ERoC strategy comes mainly from the strong reduction of the *MPD* criterion, even though the *APD* and *PPV* values are slightly higher than the other strategies [54].

Finally, for comparison purposes the analysis of the fuzzy ERoC strategy is conducted including the EWH consumption. The simulation results are shown in Fig. 3.30, where it can be appreciated a similar behavior of the grid power profile achieved through the fuzzy ERoC strategy including the EWH. In short, the grid power fluctuations are reduced as shown in Fig. 3.30(a). Moreover, the energy stored in the battery is kept between secure limits as shown in Fig. 3.30(b), with a charge of 70% to 80% during the 40.72% of the year under study as illustrated in Fig. 3.30(c). Furthermore, the grid power ramp-rates are reduced with respect to previous strategies as shown in Fig. 3.30(d) and Fig. 3.30(e). Finally, the improved behavior is reflected in the reduction of the defined quality criteria, which is summarized in Table 3-11.

Table 3-11 Quality criteria comparison for the fuzzy ERoC strategy, the fuzzy NPT strategy, the SMA strategy and the baseline values including the EWH consumption

EMS Strategy	$P_{G,MAX}$ **(kW)**	$P_{G,MIN}$ **(kW)**	***PVR***	***MPD*** **(W/h)**	***APD*** **(W/h)**	***PPV***
No EMS & ESS including the EWH consumption	6.53	-6.45	1.00	18468	1221	5.99
SMA strategy	6.25	-3.98	0.79	20006	57.41	1.23
Fuzzy EMS based on MG net power trend	5.80	-3.28	0.70	18119	50.81	1.31
Fuzzy ERoC strategy	**2.94**	**-2.52**	**0.42**	**1252**	**79.93**	**1.51**

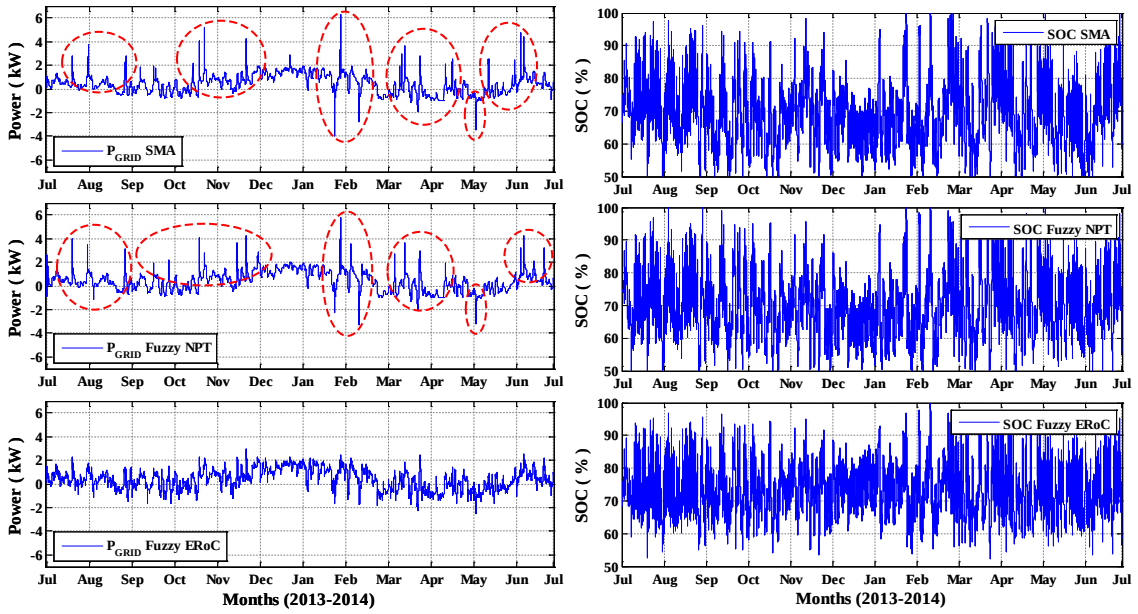

(a) (b)

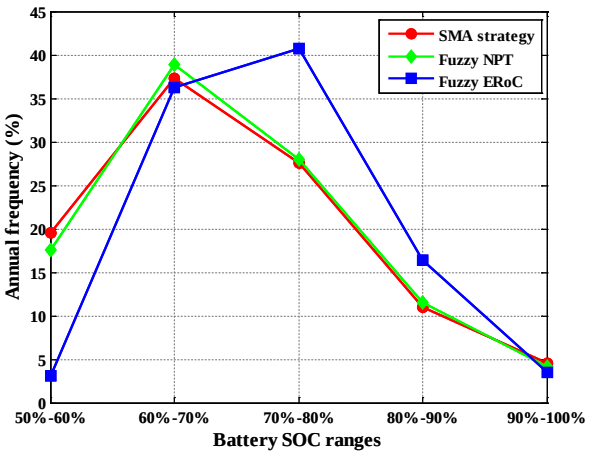

(c)

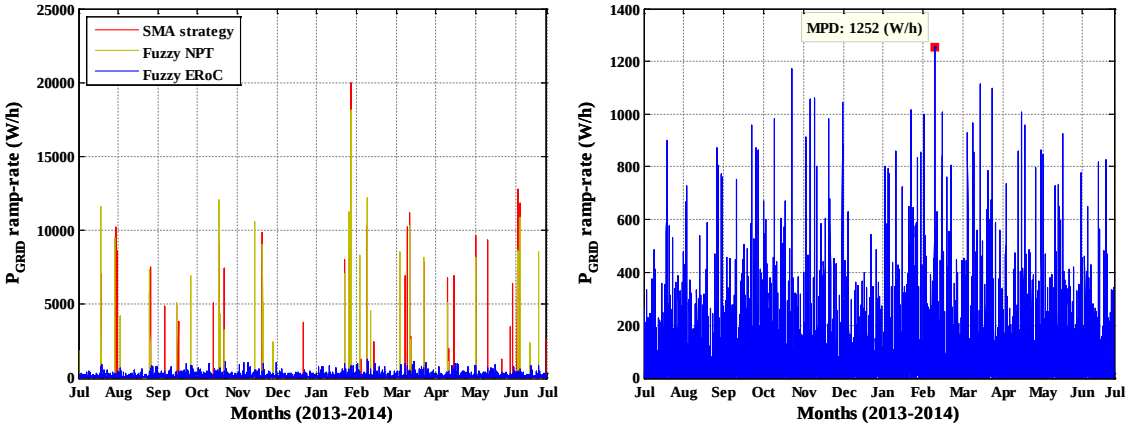

(d) (e)

Fig. 3.30. Simulation results for the fuzzy ERoC strategy including the EWH consumption (a) grid power profile, (b) battery SOC, (c) annual frequency of the battery SOC ranges established from the defined EMS strategies, (d) grid power profile ramp-rates comparison, and (e) maximum grid power profile ramp-rate.

3.5. Experimental validation of the Fuzzy ERoC strategy

The fuzzy ERoC strategy is programmed and compiled through LabVIEW® platform using the Fuzzy System Designer toolbox [97], as shown from Fig. 3.31 to Fig. 3.33. Subsequently it is sent to the NI-PXI where the EMS algorithm runs in real-time. Note that the optimization process used in the FLC design sets the maximum and minimum boundaries for each input as shown in Fig. 3.32. Therefore, an additional signal conditioning is required in order to normalize the measured physical values within those bounds; otherwise, the FLC would deliver an unknown value causing an EMS failure [54]. In addition, Fig. 3.33(a) and Fig. 3.33(b) show the FLC rule-base and the testing screenshot of the FLC created in this platform.

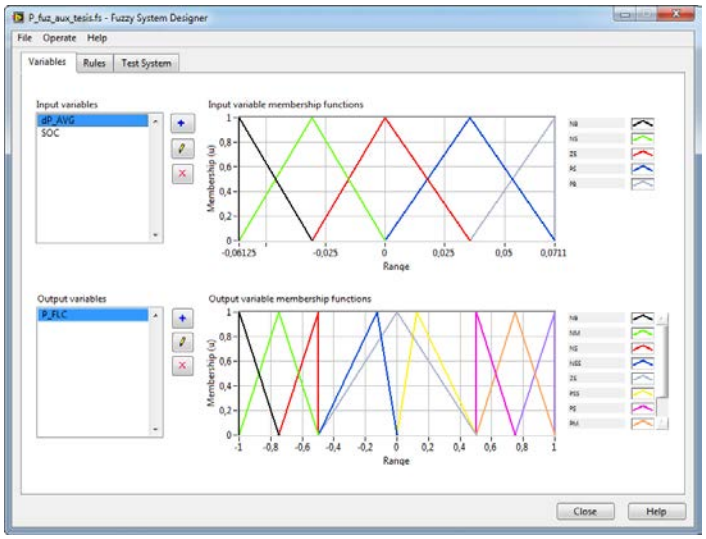

Fig. 3.31. Fuzzy logic controller design through LabVIEW® platform and the Fuzzy System Designer toolbox

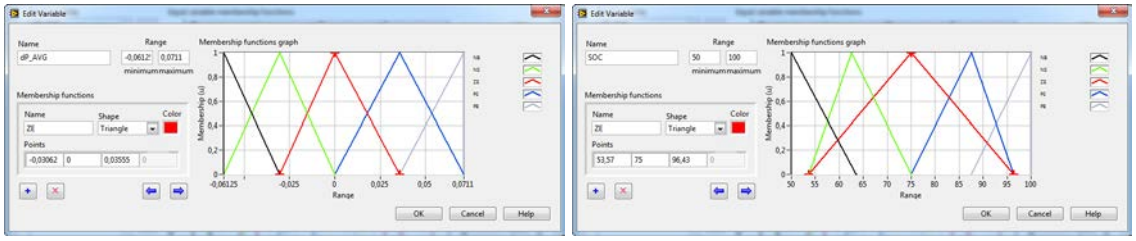

(a) (b)

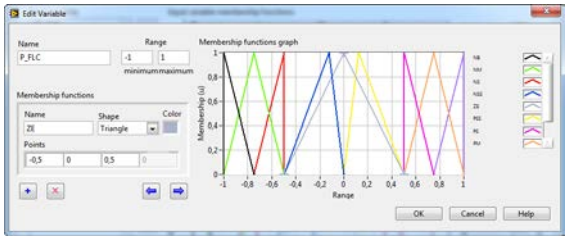

(c)

Fig. 3.32. MFs number, type, name, mapping and variation range assignment (a) MFs for the input variable $\dot{P}_{AVG}$, (b) MFs for the input variable *SOC*, and (c) MFs for the output variable P_{FLC}

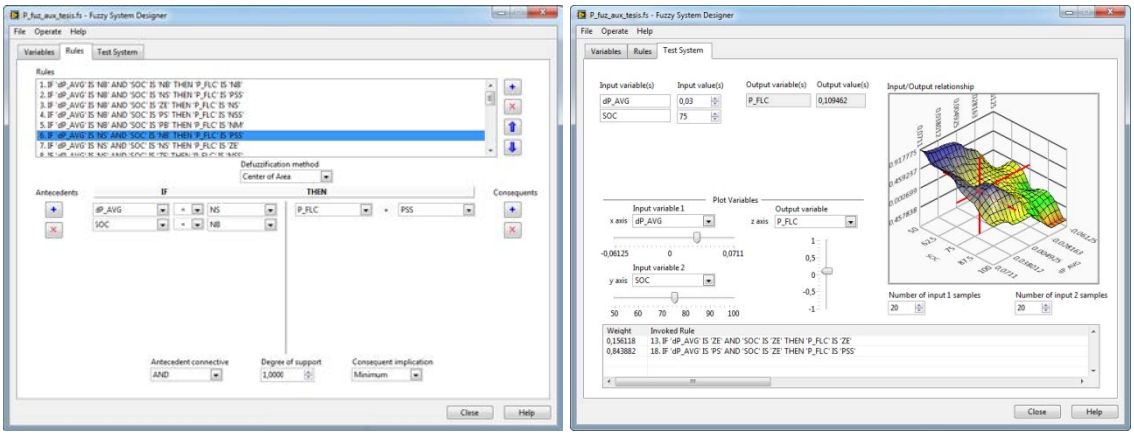

(a) (b)

Fig. 3.33. Final FLC design (a) rule-base definition and, (b) FLC testing and surface

3.5.1. Experimental results and analysis

In order to experimentally validate the fuzzy EMS strategy based on MG ERoC, the system has been tested in real conditions from Feb. 4th to Feb. 28th, 2015 [54]. Fig. 3.34 presents the real data of renewable generation and load demand, whose were recorded every second through the NI-PXI at UPNa.

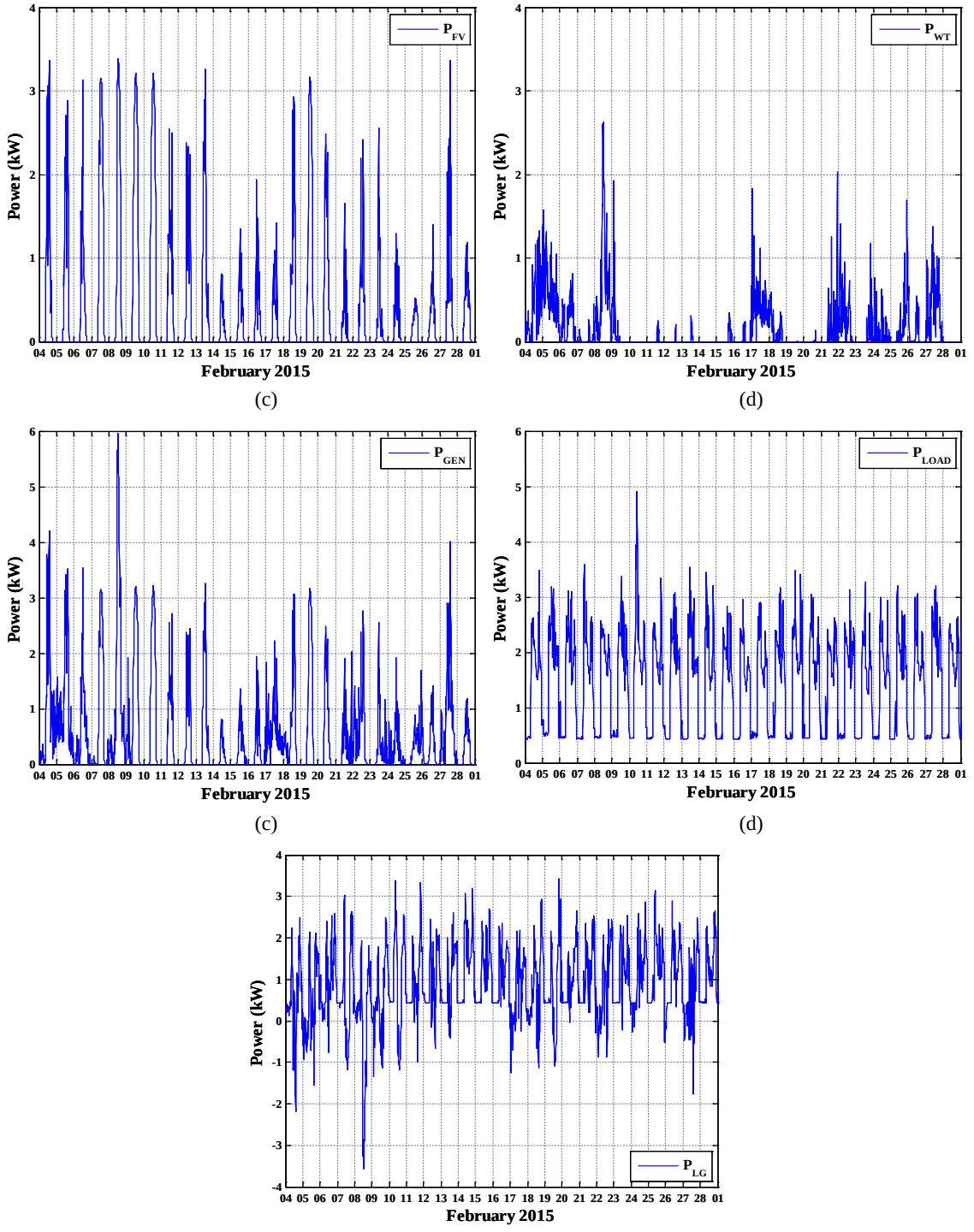

Fig. 3.34. Experimental results obtained from UPNa MG (a) photovoltaic power, (b) wind turbine power, (c) renewable power generation, (d) load power, and (d) MG net power.

In addition, Fig. 3.35 illustrates the grid power profile achieved through simulation (gray dot line) and in real conditions (red solid line). As it can be seen, the experimental grid power profile follows the evolution obtained in simulations, which confirms the correct behavior of the fuzzy ERoC strategy [54].

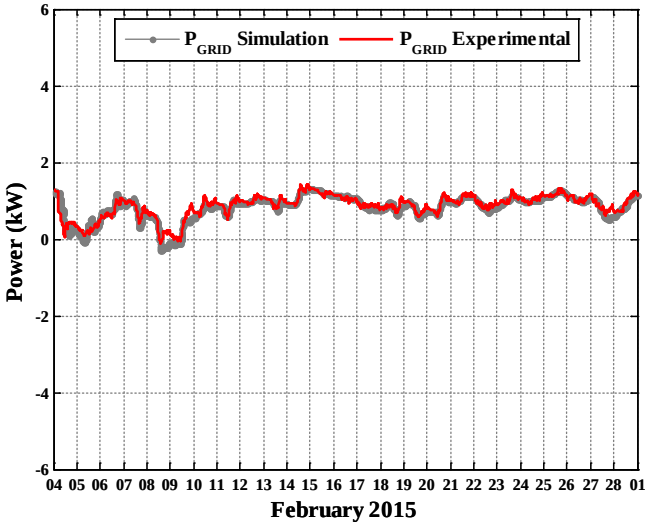

Fig. 3.35. Simulated and experimental grid power profile comparison, © 2016, IEEE

Moreover, the experimental results of the principal variables of the MG are shown in Fig. 3.36. As it can be seen, the grid power profile achieved through the fuzzy ERoC strategy (red solid line) shows minimum fluctuations despite the high fluctuations in the MG net power (black dot line). Additionally, Fig. 3.36 highlights the proper evolution of the battery SOC and also confirms the simulation results. As it can be noted the battery SOC (green solid line) oscillates around the 75% of the rated battery capacity, as expected from simulation results, thus, the improved fuzzy EMS design keeps the battery SOC evolution between secure bounds [54].

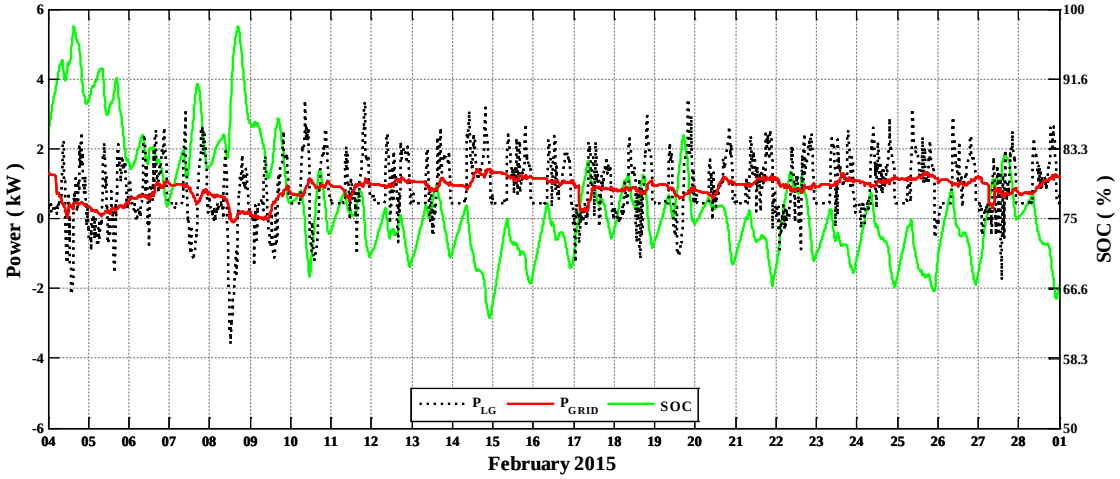

Fig. 3.36. Experimental validation of the fuzzy ERoC strategy, © 2016, IEEE

Finally, a detailed analysis of one specific day is presented in Fig. 3.37 in order to describe the behavior of the most relevant variables of the MG (i.e. MG net power, battery power, grid power and battery SOC) [54].

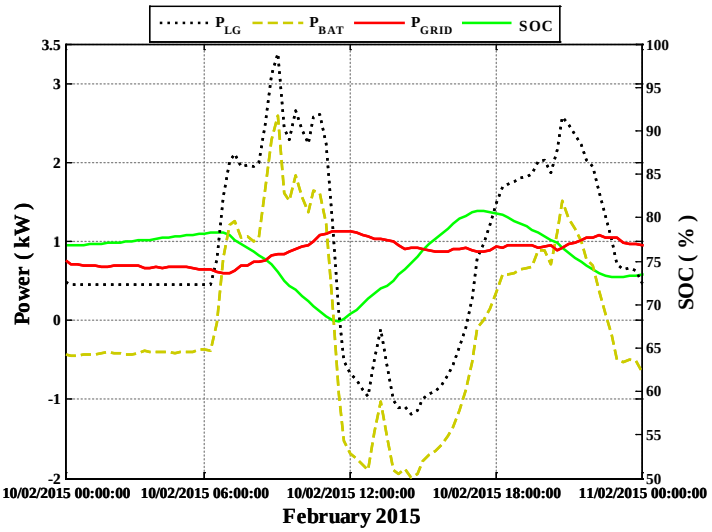

Fig. 3.37. Real power variables and battery SOC measured at UPNa MG on February 10th, 2015, © 2016, IEEE

As it can be seen, at the beginning of the day, the MG has a constant consumption (black dot line), therefore, the proposed EMS controls the grid power in order to absorb a constant power from the mains (red solid line) to supply the MG consumption and to recharge the battery (green solid line) (i.e. the battery is charging at a constant power, pink dashed line). Later, the MG presents a sudden energy change close to 6:00 AM. The proposed fuzzy EMS increases the power delivered by the grid, as expected, helping the storage system to supplying the demand required by the MG. After that, the MG presents another important energy change close to 12:00 PM. This time, the proposed fuzzy EMS increases even more the power delivered by the grid in order to recharge the battery and preserve its lifetime due to the battery SOC has dropped at the end of the previous action. Subsequently, once the battery charging process starts, the proposed fuzzy EMS design decreases the power delivered by the grid, since the MG exhibits a generation state at this time (i.e. $P_{LG} < 0$). Finally, the battery charging continues up to a range of time close to 18:00, when the EMS keeps almost constant the power delivered by the grid with the purpose of using the energy stored in the battery to supply the load demand. By this way the EMS preserves the grid power profile and avoids a battery overcharge. Note that this process is repeated for each energy change in the MG [54].

Chapter 4

FLC-based energy management strategy based on Microgrid power forecasting

This Chapter presents an enhanced FLC-based energy management strategy based on MG power forecasting (EMS-FC), for smoothing the power profile exchanged with the grid. The new design includes generation and demand forecasting to predict the future behavior of the MG so that the power forecast error will be used by the FLC to modify the grid power profile according to the battery SOC.

Moreover, this Chapter describes the forecasting of power generation and load demand, and presents the comparison between the forecasted and measured data. Moreover, in order to verify the enhanced behavior of the fuzzy energy management strategy based on MG power forecasting (EMS-FC), the Chapter presents the simulation results and the comparison with previous strategies described in Chapter 3.

Finally, this Chapter also presents the experimental results of the enhanced FLC-based strategy based on MG power forecasting carried out in a real MG at the UPNa. The results highlight the effectiveness of the proposed design, which concurrently smooths the grid power profile and keeps the battery SOC evolution between secure limits.

4.1. Microgrid power forecasting

Conversely to previous designs described in Chapter 3, the fuzzy EMS-FC strategy uses a Central Moving Average (CMA) filter to compute the average of the MG net power. Therefore, the fuzzy EMS-FC strategy removes the problem of making decisions based on the MG data of the previous 24-hours. In this regard, with the purpose of computing the central average of the MG net power, this strategy requires the forecast of both the energy production and the load demand of the MG, as addressed in the following paragraphs.

4.1.1. Power generation forecasting

The MG power generation of wind and solar RES is predicted using the weather forecast data provided by Meteogalicia THREDDS Server [98], which consists in a set of weather data acquired through the Weather Research and Forecasting (WRF) model for the Iberian Peninsula. The weather data provided by Meteogalicia THREDDS Server is updated every 12-hours with a prediction horizon of three days and includes among others the ambient temperature, the wind speed at 10 m of height above the ground, the horizontal irradiance, and the atmospheric

pressure for the following 12-hours. In addition, the server provides the weather forecast data with a resolution of 1-hour and 12x12 km grid resolution [63], [57], [46].

In this regard, the power generation forecasting is carried out by means of the Numerical Weather Prediction (NWP) [99], [100] data provided by Meteogalicia THREDDS Server and the photovoltaic and wind turbine models described in Chapter 2.2.

As mentioned in Chapter 2.3.1, the estimation of the PV power forecast, $P_{PV,FC}$, requires the transformation of the incident solar irradiance on an horizontal surface provided by Meteogalicia server, shown in Fig. 4.1(a), into the incident solar irradiance on a tilted plane. This transformation was carried out following the procedure described in [75]. The resulting incident solar irradiance on an inclined surface is shown in Fig. 4.1(b). As it can be seen, the prediction of the solar irradiance incident on a tilted plane obtained through this method follows the evolution of the real data measured in the MG at UPNa, as shown in Fig. 4.2.

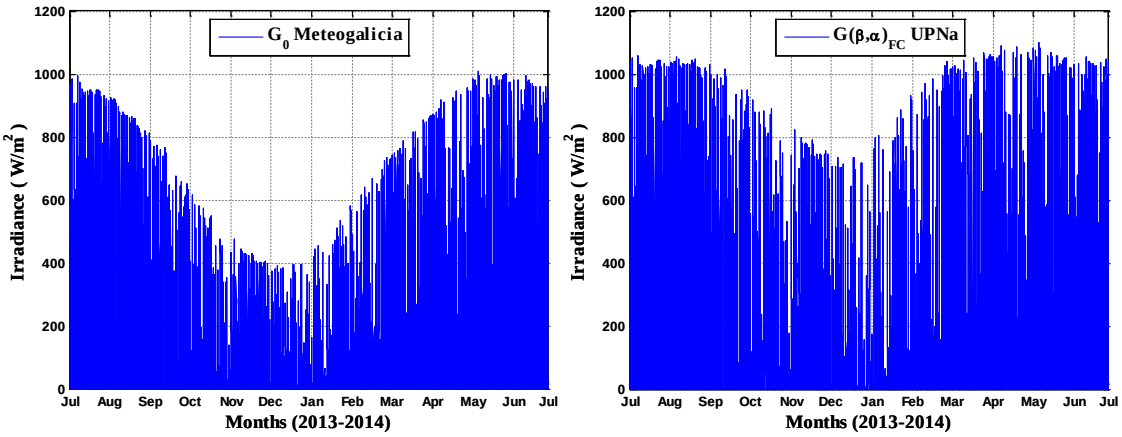

(a) (b)

Fig. 4.1. Solar irradiance of the year under study (a) forecast of the incident solar irradiance on a horizontal surface provided by Meteogalicia, and (b) forecast of the incident solar irradiance on an inclined surface at UPNa,

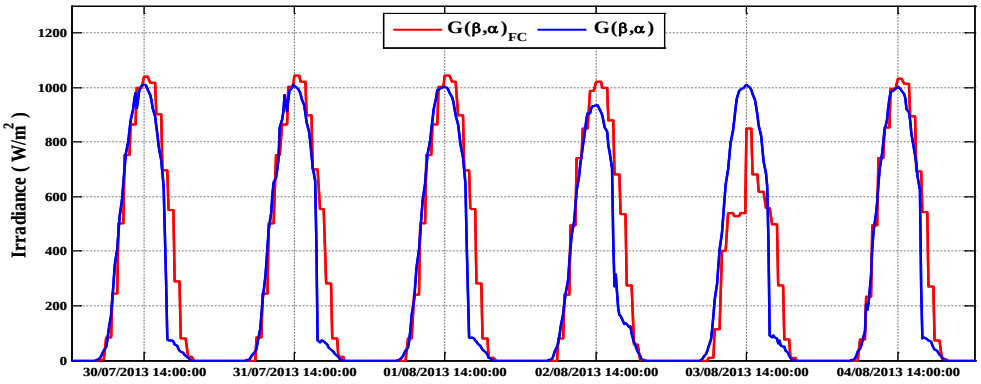

Fig. 4.2. Comparison between the forecasted and measured data of the incident solar irradiance on an inclined surface at UPNa

The forecast of the PV power is therefore obtained using the estimated solar irradiance on an inclined surface, the forecast of the ambient temperature at UPNa, and the PV model described

in Chapter 2.3.1. The forecast of the PV power generation for the year under study is presented in Fig. 4.3(a), whereas a comparison of six days between the PV generation power forecasted and measured at UPNa is presented in Fig. 4.3(b).

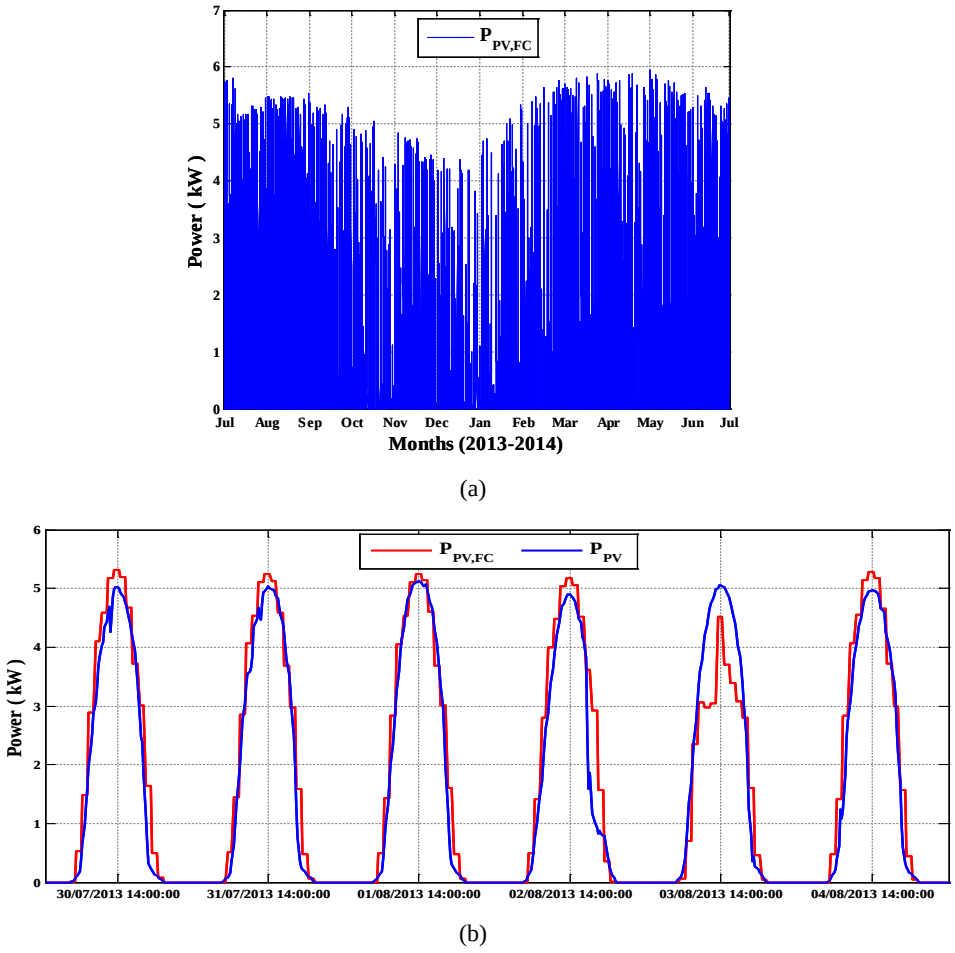

Fig. 4.3. Forecast of photovoltaic power (a) during the year under study, and (b) comparison between forecasted and measured data

Furthermore, the wind power forecasting uses the estimation of wind speed, atmospheric pressure, and temperature at UPNa. In this regard, the forecast data of wind speed provided by Meteogalicia server (i.e. measured at a height of 10 m above the ground) has to be extrapolated to the wind turbine hub-height at UPNa (i.e. 20 m above the ground). In addition, the wind speed taking into account the air density at UPNa is computed using WT model described in Chapter 2.3.2 and the forecast data provided by Meteogalicia server.

The resulting prediction of the WT power during the year under study, $P_{WT,FC}$, is displayed in Fig. 4.4(a), whereas the comparison of six days between the WT power forecasted and measured is presented in Fig. 4.4(b).

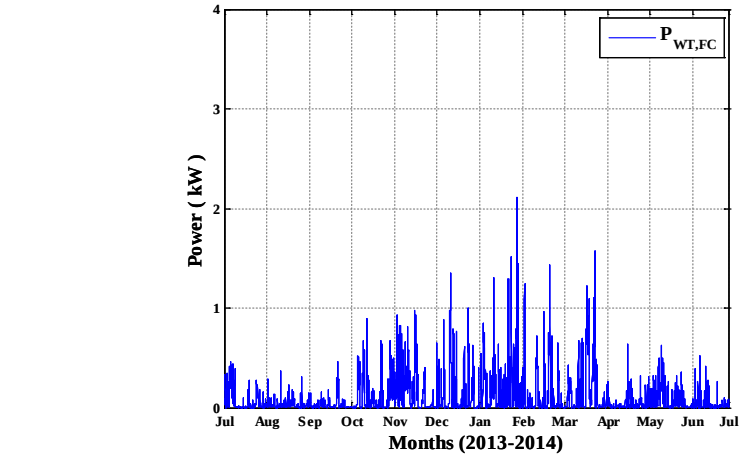

(a)

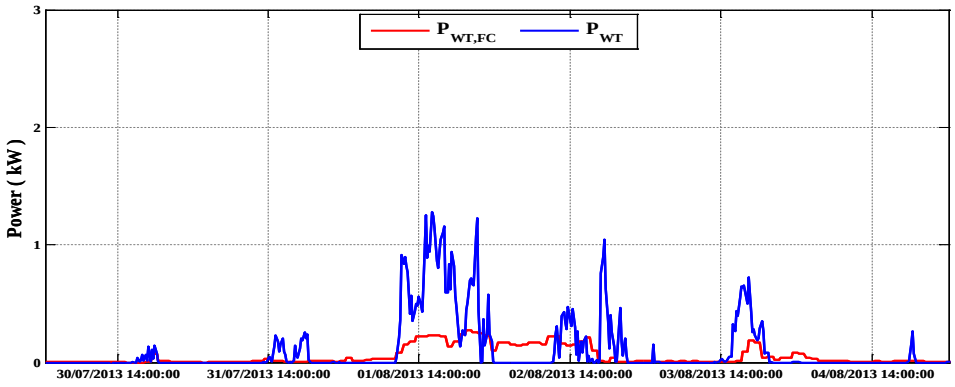

(b)

Fig. 4.4. Forecast of wind turbine power (a) during the year under study, and (b) comparison between forecasted and measured data

Finally, the forecast of power generation, $P_{GEN,FC}$, is expressed as follows:

$$P_{GEN,FC}(n) = P_{PV,FC}(n) + P_{WT,FC}(n), \tag{4.1}$$

where $P_{PV,FC}$ and $P_{WT,FC}$ are the forecast of the photovoltaic and wind turbine power, respectively. The prediction of power generation during the year under study is shown in Fig. 4.5(a). Similarly, Fig. 4.5(b) shows the comparison between the forecasted and measured data for six specific days.

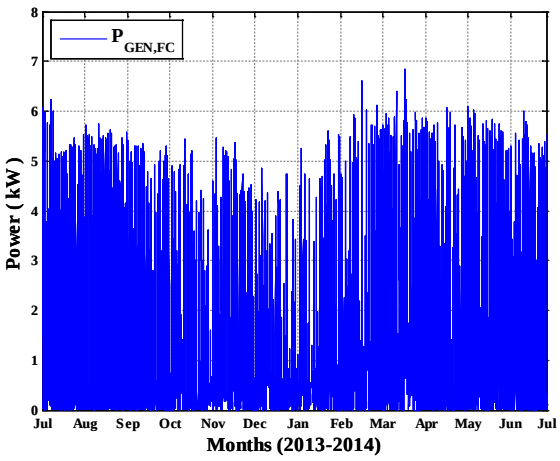

(a)

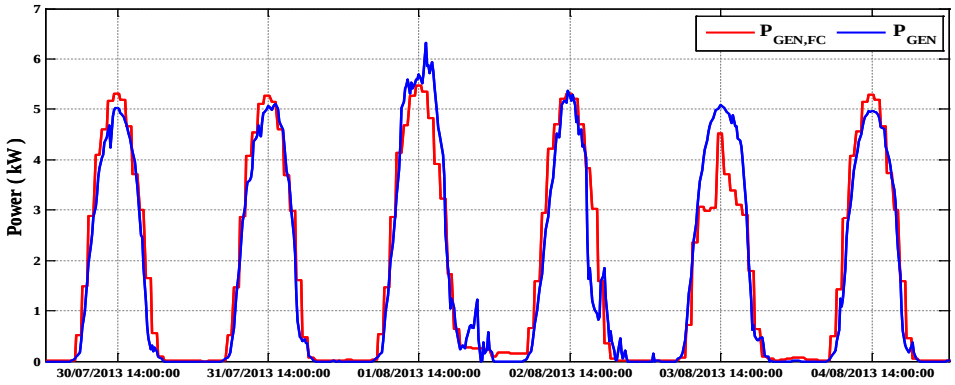

(b)

Fig. 4.5. Forecast of power generation (a) during the year under study, and (b) comparison between forecasted and measured data

4.1.2. Load demand forecasting

The load forecast is estimated through the persistence forecast model assuming that the daily consumption pattern is not very distinct and steady from one day to another. In this regard, persistence model uses past data as the forecast for the next time period [62], [63], [48], [101], [102]. Thus, the load demand profile for the next day will be similar as the previous day, namely:

$$P_{LOAD,FC}(n+M) = P_{LOAD}(n), \tag{4.2}$$

being $P_{LOAD,FC}$ the load forecast. Note that in this study the differences of load demand between weekdays and weekends or holydays are not considered.

The load forecast and the load power demand measured in six days on winter and summer seasons at UPNa are shown in Fig. 4.6(a) and Fig. 4.6(b), respectively. As it can be seen, the behavior of the persistence model could be considered acceptable.

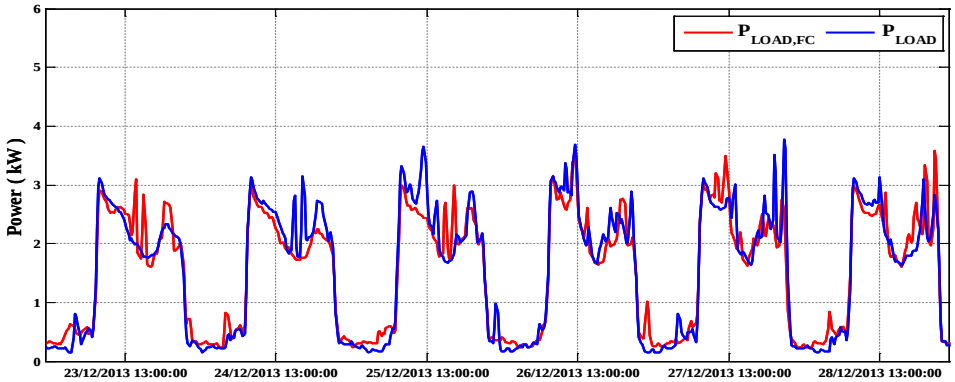

(a)

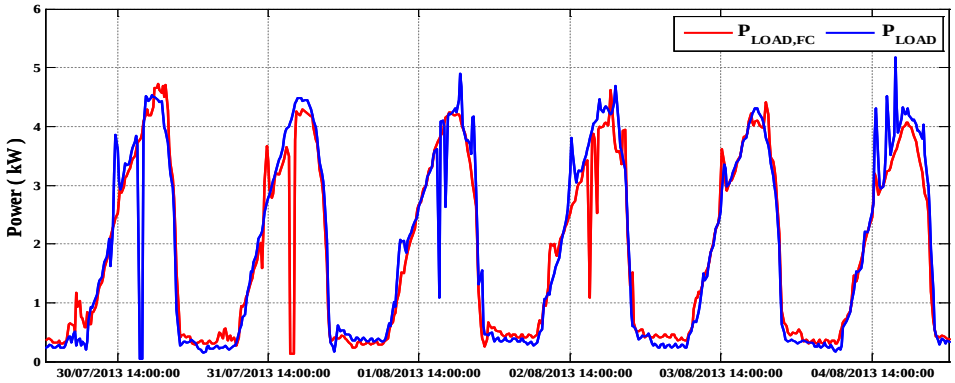

(b)

Fig. 4.6. Comparison between the predicted load power demand and the load power demand measured at UPNa microgrid (a) winter season data, and (b) summer season data

4.1.3. Net power forecasting

According to (2.3) the forecast of the MG net power, $P_{LG,FC}$, is expressed as follows [62], [63]:

$$P_{LG,FC}(n) = P_{LOAD,FC}(n) - P_{GEN,FC}(n). \tag{4.3}$$

Fig. 4.7 shows the comparison between the forecast of the MG net power and the MG net power measured at UNPa microgrid. As it can be seen, there is an error between the measured and the expected values (i.e. forecast error P_E), therefore, the EMS design should consider this error to take the appropriate control decision in order to concurrently improve the grid power profile and to protect the battery bank from a deep discharge [62]. The MG forecast error is defined as follows [62], [63]:

$$P_E(n) = P_{LG}(n) - P_{LG,FC}(n), \tag{4.4}$$

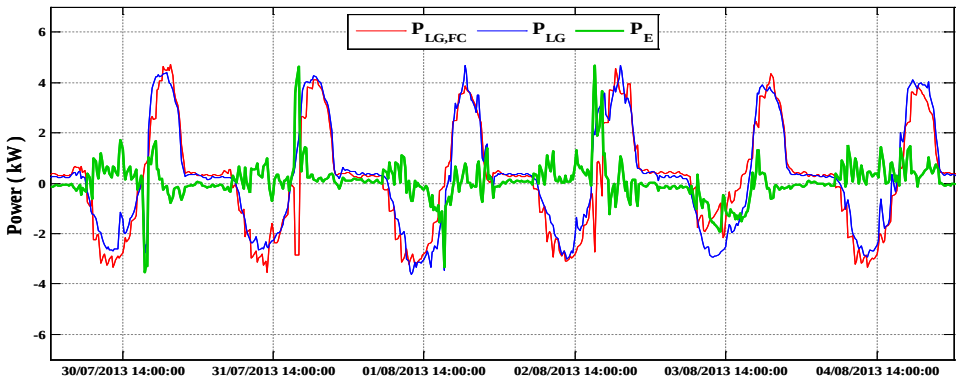

Fig. 4.7. Comparison between the prediction of the MG net power and the MG net power measured at UPNa microgrid

4.2. Fuzzy EMS design based on MG power forecasting

The block diagram of the fuzzy EMS strategy based on MG power forecasting is shown in Fig. 4.8 and includes the following blocks [62], [63]:

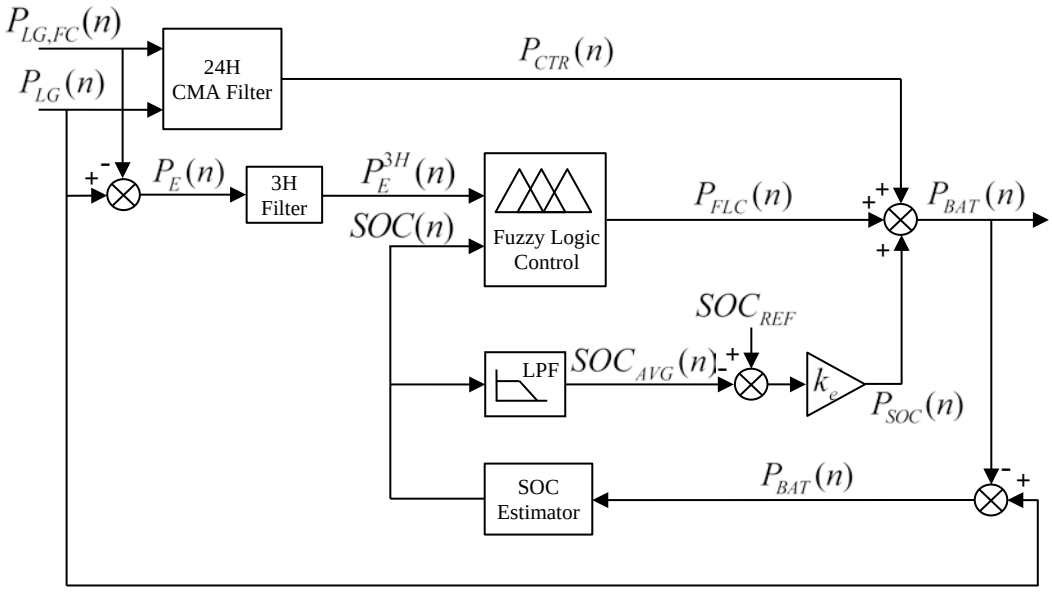

Fig. 4.8. Fuzzy EMS based on MG power forecasting block diagram

1. A Central Moving Average (CMA) filter block, used for computing the MG average net power $P_{CTR}(n)$,
2. A 3H filter block, used for both computing the average forecast error of the previous 3-hours, $P_E^{3H}(n)$, and reducing the high variability associated with the forecast error P_E,
3. A LPF block, used for computing the average battery SOC of the previous 24-hours, $SOC_{AVG}(n)$,
4. A battery SOC Estimator block, used to estimate the SOC of the battery according to the battery model described in Chapter 2.3.3, and

5. A Fuzzy Logic Control block, used for improving the grid power profile according to the battery SOC and the MG forecast error of the previous 3-hours.

As shown in Fig. 4.8 the grid power profile of the fuzzy EMS-FC strategy is defined as the sum of three variables P_{CTR}, P_{SOC} and P_{FLC}, where each variable plays a particular role in the energy management strategy. The grid power profile is expressed as follows [62], [63]:

$$P_{GRID}(n) = P_{CTR}(n) + P_{SOC}(n) + P_{FLC}(n), \tag{4.5}$$

The first variable, P_{CTR} (n), is computed by means of a Central Moving Average (CMA) filter [103], which uses the past and the future data of the MG net power to estimate the central average of the MG net power. The CMA filter uses a window size of 24-hours, which contains the MG net power of the previous 12-hours and the forecast of the MG net power for the following 12-hours. The central average of the MG net power, P_{CTR}, is expressed as follows [62], [63]:

$$P_{CTR}(n) = \frac{1}{2} \cdot \left[P_{LG}^{-12H}(n) + P_{LG,FC}^{+12H}(n) \right], \tag{4.6}$$

$$P_{LG}^{-12H}(n) = \frac{1}{M_{12}} \sum_{k=1}^{M_{12}} P_{LG}(n-k), \tag{4.7}$$

$$P_{LG,FC}^{+12H}(n) = \frac{1}{M_{12}} \sum_{k=1}^{M_{12}} P_{LG,FC}(n+k), \tag{4.8}$$

where P_{LG}^{-12H} is the average value of MG net power of the previous 12-hours, $P_{LG,FC}^{+12H}$ is the average value of the MG net power forecast for the next 12-hours, and M_{12} is the number of samples in 12-hours.

The second variable of the grid power profile, P_{SOC} (n), is used to keep the battery SOC centered close to the 75% of the rated battery capacity [57]. In this regard, P_{SOC} (n) is proportional to the error between the reference value of the battery SOC and the average value of the battery SOC of the previous 24-hours. This component is expressed as follows [62], [63]:

$$P_{SOC}(n) = k_e \cdot \left[SOC_{REF} - SOC_{AVG}(n) \right], \tag{4.9}$$

$$SOC_{AVG}(n) = \frac{1}{M} \sum_{k=1}^{M} SOC(n-k), \tag{4.10}$$

where SOC_{REF} is the reference value of the battery SOC which is set to 75% for the case under study, SOC_{AVG} is the average value of the battery SOC of the previous 24-hours, and k_e is the proportional gain constant which is set to 0.05 kW/% in order to obtain a high enough phase margin in the battery SOC control loop [57].

The third variable, P_{FLC}, is used to improve the grid power profile according to both the battery SOC and the forecast error of the MG of the previous 3-hours. This component is computed by a FLC that assumes a Mamdani-based inference and defuzzyfication of Center of Gravity of two-input, one-output and 25 rules. The inputs of the FLC are the current battery state-of-charge SOC (n) and the power forecast error of the previous 3-hours, P_E^{3H} (n), which is defined as follows [62], [63]:

$$P_E^{3H}(n) = \frac{1}{M_3}\sum_{k=1}^{M_3} P_E(n-k), \tag{4.11}$$

being M_3 the number of samples in the previous 3-hours.

Finally, according to (2.4) the battery power is defined as follows:

$$P_{BAT}(n) = P_{LG}(n) - P_{GRID}(n). \tag{4.12}$$

Regarding the FLC design, similarly to the previous fuzzy EMS strategies, the adjustment of all parameters involved in the fuzzy controller design was performed by an off-line optimization process [51] considering the real recorded data and the forecasted data of the renewable electricity production and load demand with the purpose of minimizing the energy management quality criteria defined in Chapter 3.1.2. The optimization procedure was described in Chapter 3.4.4. Therefore, only the results from this procedure are presented in this Chapter.

As a result, five triangular MFs are defined for the input variables P_E^{3H} (n) and SOC (n). As illustrated in Fig. 4.9, these MFs are associated with five fuzzy sets noted as NB, NS, ZE, PS and PB, and are distributed along the variation range defined for each input. In this regard, the variation range for the input SOC (n) has to satisfy the battery constraints defined in Chapter 2.3.3, whereas the variation range for the input P_E^{3H} is defined as follows [62], [63]:

$$-P_e \le P_E^{3H}(n) \le +P_e, \tag{4.13}$$

being P_e the maximum forecast error. Note that the case under study assumes a maximum forecast error of 6 kW.

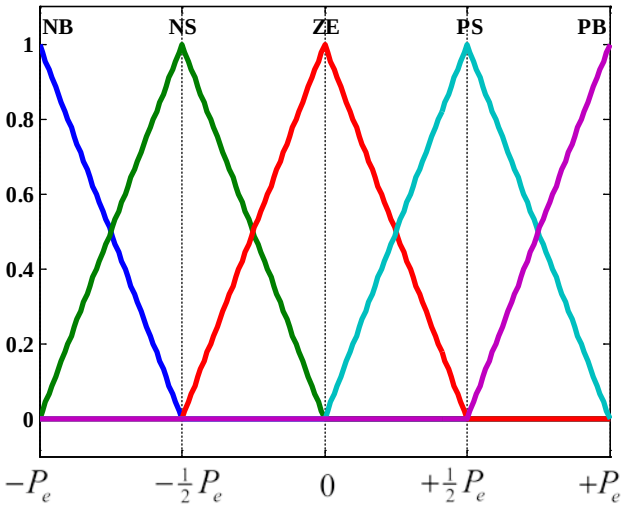

(a)

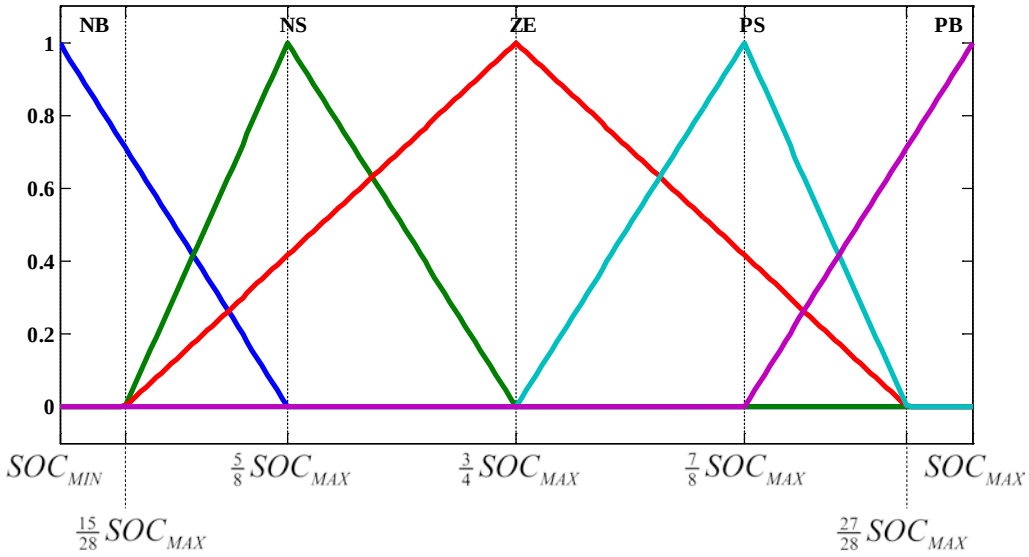

(b)

Fig. 4.9. Optimized MFs for the FLC inputs of the fuzzy EMS-FC strategy (a) MG forecast error, and (b) battery SOC

Moreover, nine triangular MFs are defined for the controller output P_{FLC}, which are associated with nine fuzzy sets noted as NB, NM, NS, NSS, ZE, PSS, PS, PM and PB, as illustrated in Fig. 4.10 [62], [63]. The MFs of the FLC output are distributed along the variation range defined as follows:

$$P_N \le P_{FLC}(n) \le P_P, \tag{4.14}$$

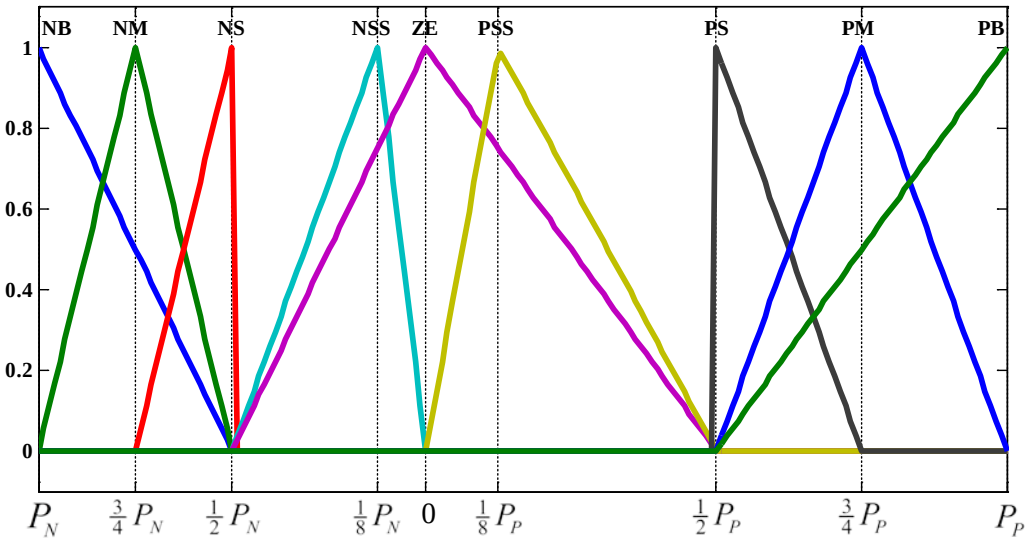

Fig. 4.10. MFs for the FLC output of the fuzzy EMS-FC strategy

where P_N and P_P are the minimum and maximum power assigned through the controller output, respectively. From the optimization process, the variation range of the FLC output is established between P_N = -0.3 kW and P_P = 0.45 kW [62], [63].

Finally, the optimized fuzzy rule-base consists in 25-rules which are presented in Table 4-1 [63]. Note that the optimized rule-base is built in order to concurrently smooth the grid power profile and to minimize the energy management quality criteria defined in Chapter 3.1.2.

Table 4-1 Optimized rule-base for the fuzzy EMS based on MG power forecasting

$P_{FLC}(n)$		$P_E^{3H}(n)$				
		NB	**NS**	**ZE**	**PS**	**PB**
***SOC* (*n*)**	**NB**	PB	PB	PSS	PS	PB
	NS	PM	NS	PSS	PS	PS
	ZE	PSS	ZE	ZE	PSS	PM
	PS	NS	PM	NSS	NS	NSS
	PB	NS	NSS	NSS	NM	NB

Note that $P_E^{3H}(n)$ is negative when the measured load demand is lower than the forecasted one or when the measured power generation is higher than the forecasted one. Conversely, $P_E^{3H}(n)$ is positive when the measured load demand is higher than forecasted or when the measured power generation is lower than forecasted.

4.3. Simulation results and analysis

The simulation results of the fuzzy EMS-FC strategy excluding the EWH consumption are presented from Fig. 4.11 to Fig. 4.16.

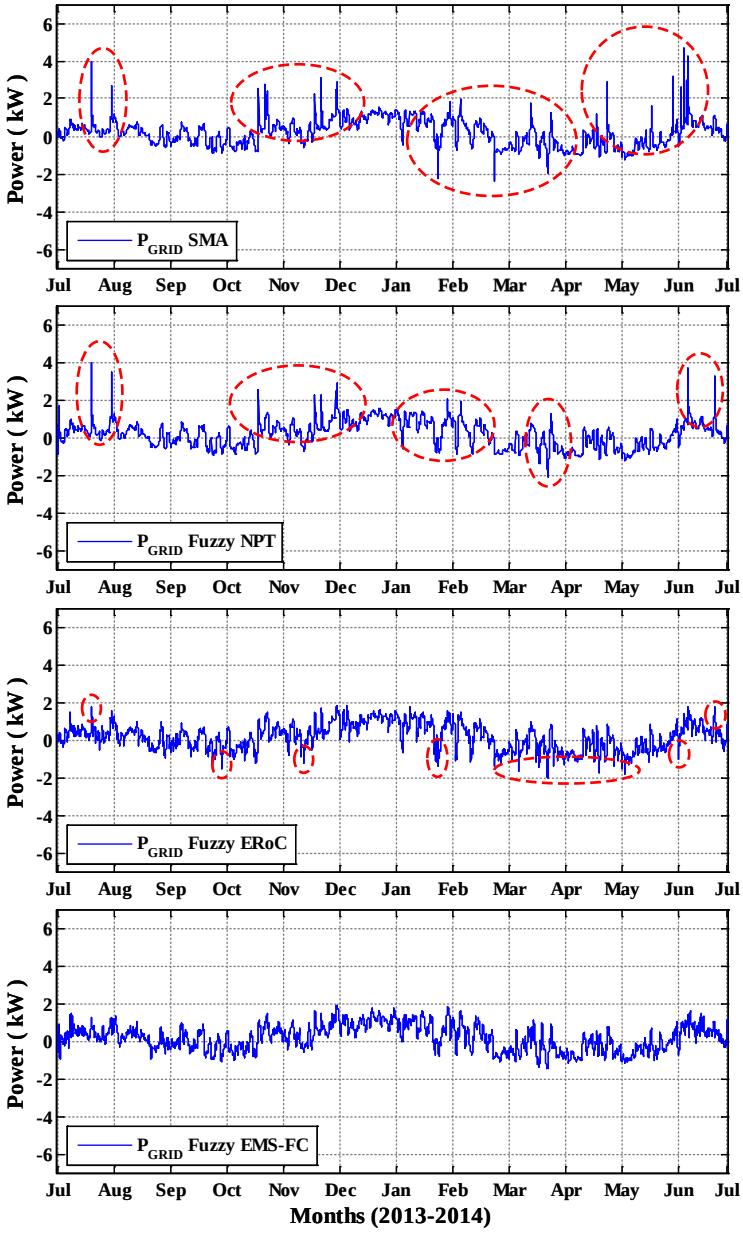

Fig. 4.11. Grid power profile comparison for the SMA, the fuzzy NPT, the fuzzy ERoC and the fuzzy EMS-FC strategies

Fig. 4.11 shows the grid power profile achieved with the energy management strategies described so far. As it can be seen, the fuzzy EMS-FC strategy minimizes the grid power fluctuations with respect to previous strategies described in Chapter 3. In addition, although the results achieved through the fuzzy ERoC strategy are positive, the fuzzy EMS-FC strategy minimizes the negative power peaks in the grid power profile, since the control decisions are

made according to the forecast power of the MG. This improved behavior can be appreciated in Fig. 4.12.

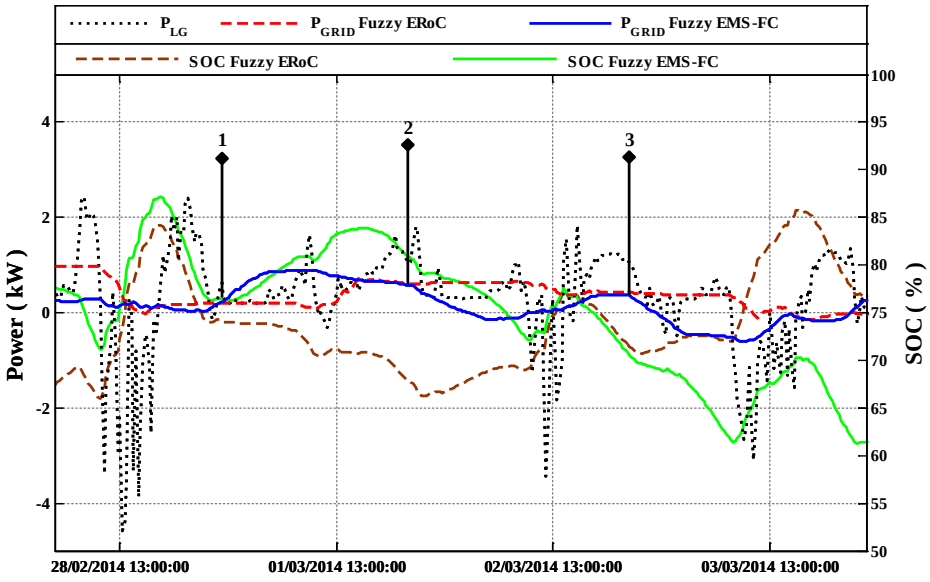

(a)

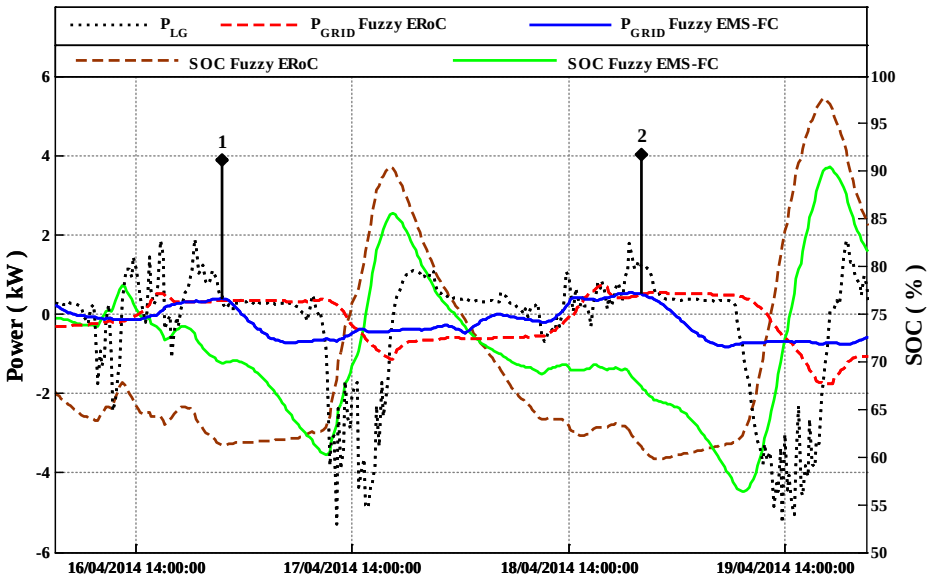

(b)

Fig. 4.12. Improved grid power profile evolution of the fuzzy EMS-FC strategy with respect to the fuzzy ERoC strategy

As shown in Fig. 4.12, the use of the forecast power allows the controller to anticipate to the events occurring in the MG. As it can be appreciated in Fig. 4.12(a) [62], [63], the lack of RES for the next day is predicted hence increasing the amount of power delivered by the grid during the night in order to prepare the batteries for the next day. Conversely, for a previous design, where power forecasting is not included, the grid power is kept constant, which produces the battery discharge. Similarly, at point #2, an increase in generation is predicted for the next day in the MG. Hence, the proposed fuzzy strategy decreases the grid power, which permits the

battery discharge in order to prepare the ESS for absorbing the future power generation. Finally, a similar behavior than that at point #2 occurs at point #3, as even more generation is predicted for the following day. In addition, this improved behavior leads to minimize the grid power fluctuations, which is evidenced in Fig. 4.12(b) where the negative peaks in the grid power profile are reduced [62], [63].

Moreover, Fig. 4.13 confirms the improved evolution of the battery SOC accomplished through the fuzzy EMS-FC strategy, resulting in a battery SOC further centered close to the 75% of the rated battery capacity.

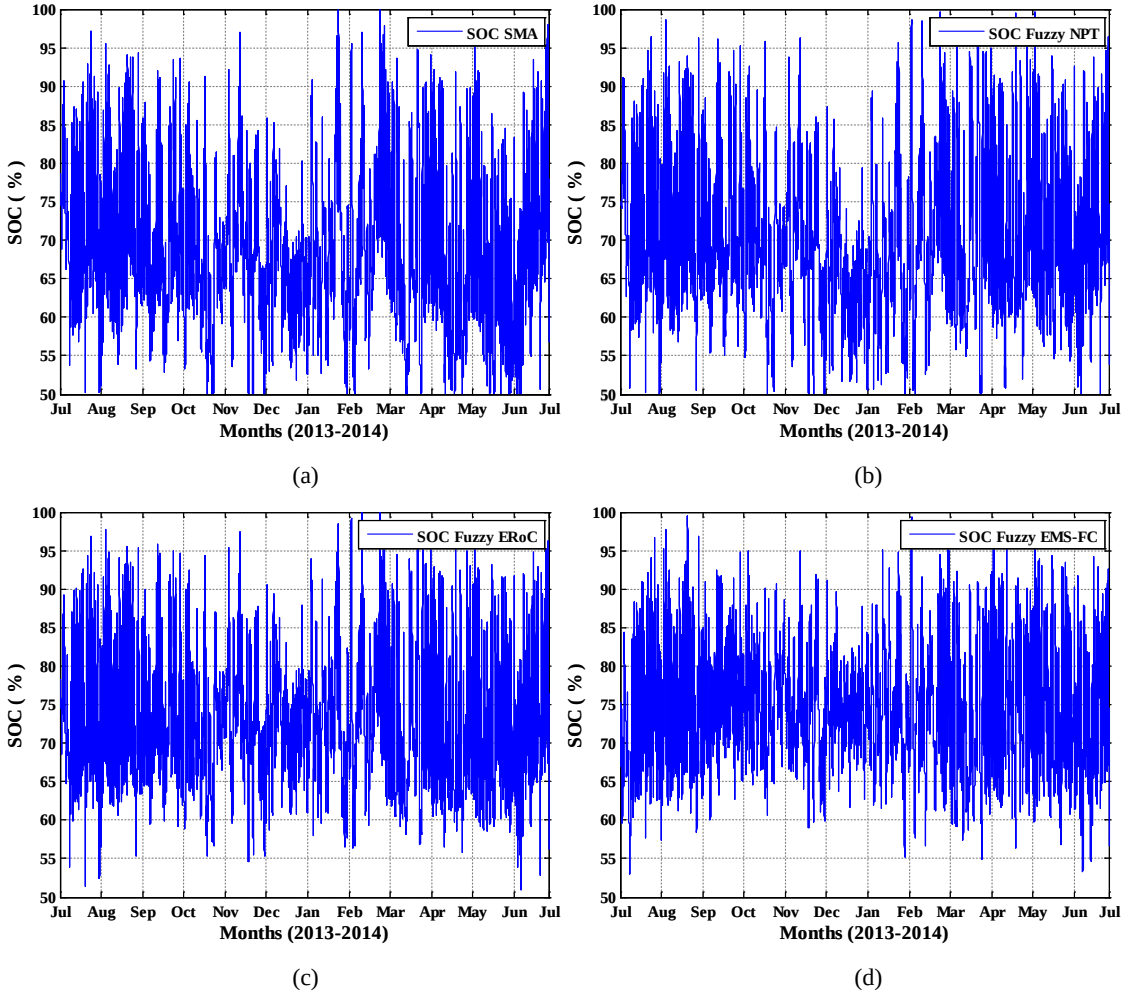

Fig. 4.13. Battery SOC evolution during the year under study (a) SMA strategy, (b) fuzzy NPT strategy, (c) fuzzy ERoC strategy, and (d) fuzzy EMS-FC strategy

In addition, Fig. 4.14 displays the daily average profile of the battery SOC during the year under study obtained with the EMS strategies described so far.

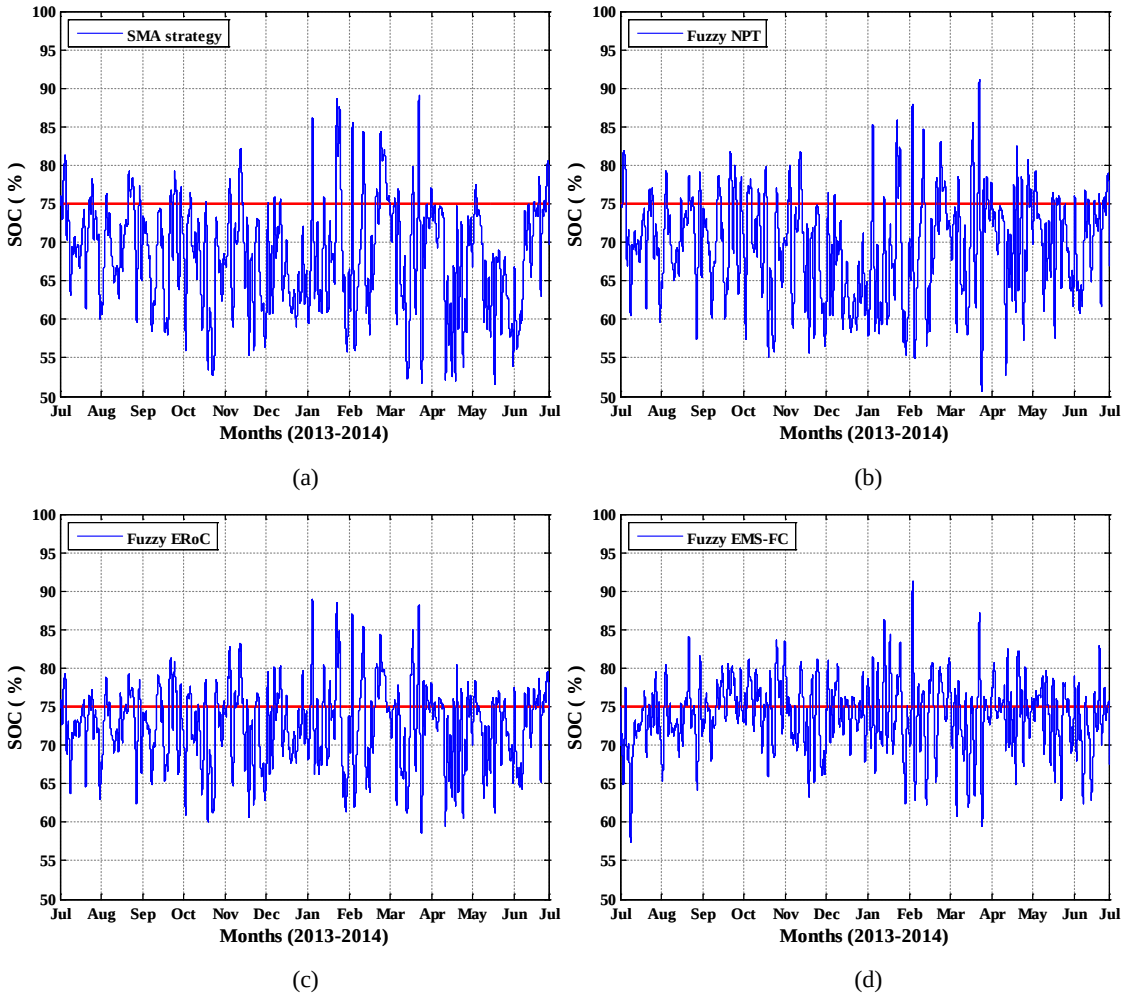

Fig. 4.14. Daily average profile of the battery SOC during the year under study (a) SMA strategy, (b) fuzzy NPT strategy, (c) fuzzy ERoC strategy, and (d) fuzzy EMS-FC strategy

As it can be seen, the daily average profile of the battery SOC achieved with the SMA strategy, shown in Fig. 4.14(a), and the fuzzy NPT strategy, shown in Fig. 4.14(b), reaches low values, which may cause the battery SOC falls below the secure limit, thus compromising the battery lifetime. In contrast, the fuzzy ERoC strategy, shown in Fig. 4.14(c), and the fuzzy EMS-FC strategy, shown in Fig. 4.14(d), evidences a daily average profile close to the 75% of the rated battery capacity during the year under study. However, the daily average SOC achieved through the fuzzy EMS-FC strategy is further centered close to the 75% of the rated battery capacity, which means that the fuzzy EMS-FC strategy allows the storage system to further compensate the MG net power fluctuations while preserving the battery lifetime.

Furthermore, the improved evolution of the battery SOC achieved through the fuzzy EMS-FC strategy is verified through the analysis of the SOC interval where the battery is located the most of the year under study. The intervals for the EMSs described so far is shown in Fig. 4.15 [63].

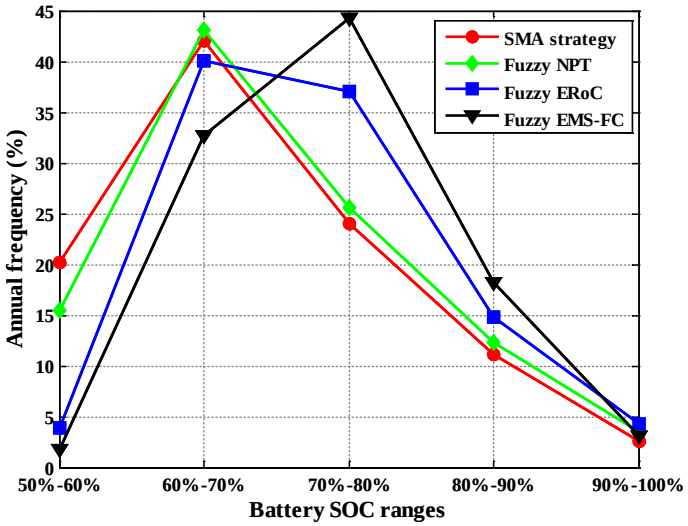

Fig. 4.15. Annual frequency of the battery SOC ranges established from the SMA, fuzzy NPT, fuzzy ERoC, and fuzzy EMS-FC strategies including the EWH consumption

As it can be seen, the fuzzy EMS-FC strategy leads to keep the battery SOC in a range between the 70% and 80% of the rated battery capacity during the 45% of the year under study. In contrast, the SMA, the fuzzy NPT, and the fuzzy ERoC strategies keep the battery SOC in this range the 24%, 26% and 33% of the year under study, respectively.

In addition, the improved behavior of the fuzzy EMS-FC strategy with respect to the strategies described so far is verified by computing the energy management quality criteria defined in Chapter 3.1.2. The results are reported in Table 4-2.

Table 4-2 Quality criteria comparison for the fuzzy EMS-FC strategy, the fuzzy ERoC strategy, the fuzzy NPT strategy, the SMA strategy and the baseline values excluding the EWH consumption

EMS Strategy	$P_{G,MAX}$ **(kW)**	$P_{G,MIN}$ **(kW)**	***PVR***	***MPD*** **(W/h)**	***APD*** **(W/h)**	***PPV***
No EMS & ESS excluding the EWH consumption	5.75	-6.45	1.00	18468	1121	13.3
SMA strategy	4.71	-2.40	0.58	12839	44.42	2.51
Fuzzy NPT strategy	3.93	-2.12	0.49	11640	35.65	2.61
Fuzzy ERoC strategy	1.83	-2.04	0.32	817	56.15	2.79
Fuzzy EMS-FC strategy	**1.89**	**-1.48**	**0.28**	**480**	**51.79**	**2.76**

As it can be seen in Table 4-2, the fuzzy EMS-FC strategy achieves an important reduction in the performance indicators with respect to previous strategies. In short, the maximum power fed into the grid $P_{G,MIN}$, *PVR*, *MPD*, *APD* and *PPV* quality criteria have been reduced in 27.4%, 12.5%, 41.2%, 7.8%, and 1.1%, respectively, with respect to the fuzzy ERoC strategy. Therefore, the slightly increase of the $P_{G,MAX}$ criterion can be considered irrelevant.

Finally, Fig. 4.16 compares the grid power ramp-rates achieved through the EMS strategies described so far. As it can be seen in Fig. 4.16(a) and Fig. 4.16(b), the grid power ramp-rates are reduced through the fuzzy EMS-FC strategy, which confirms the reduction of the *MPD* criterion reaching a maximum value of 480.5 W/h, as shown in Fig. 4.16(c).

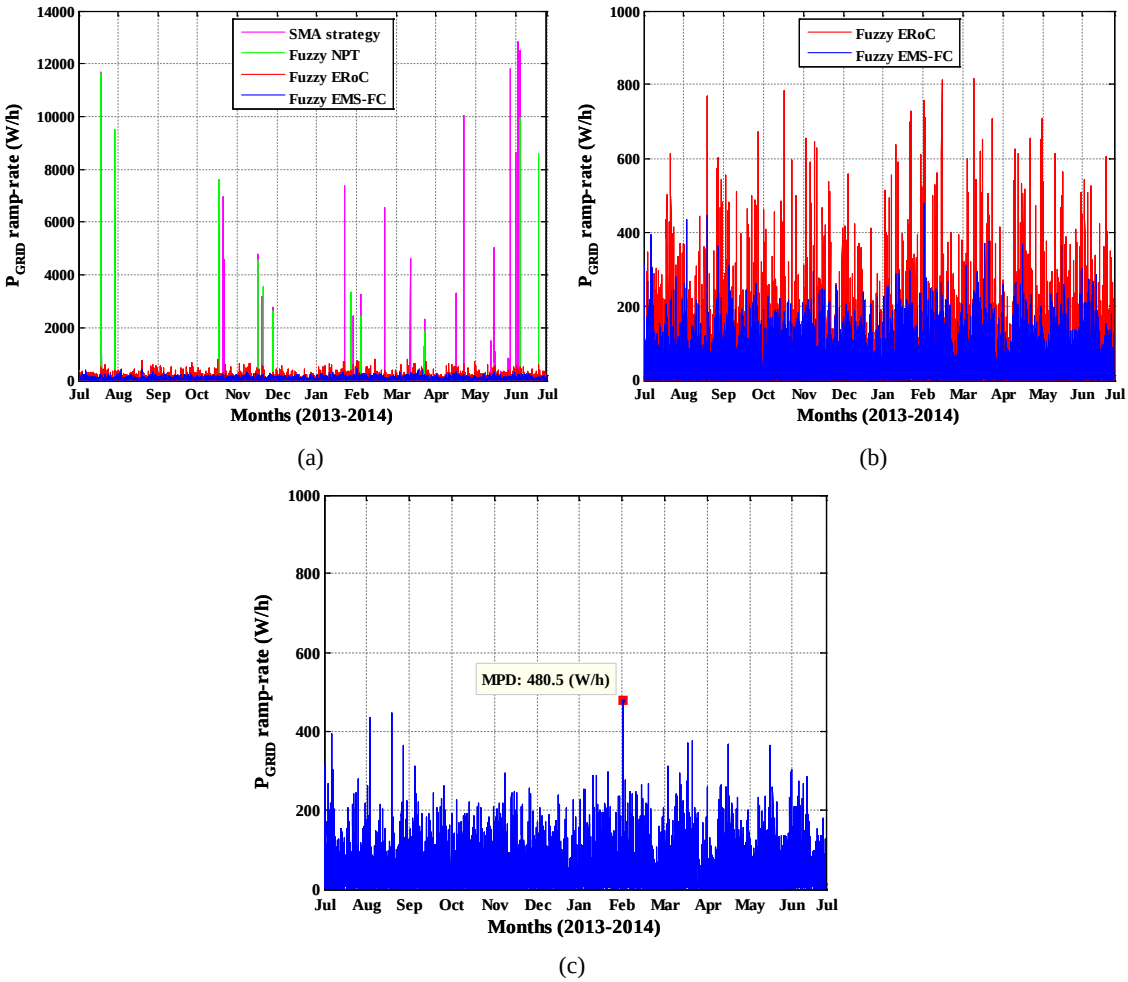

Fig. 4.16. Simulation results for the fuzzy EMS-FC strategy excluding the EWH consumption (a) grid power ramp-rates comparison, (b) grid power ramp-rates comparison with respect to the fuzzy ERoC strategy, and (c) maximum grid power profile ramp-rate

In the same manner of previous strategies, for comparison purposes the analysis of the fuzzy EMS-FC strategy is conducted including the EWH consumption. The simulation results are illustrated in Fig. 4.17 and Fig. 4.18, where it can be appreciated the enhanced behavior of the fuzzy EMS-FC strategy. In short, with respect to previous strategies, the grid power fluctuations are reduced, as shown in Fig. 4.17(a), while the energy stored in the battery is kept between secure limits, as illustrated in Fig. 4.17(b). In addition, the energy stored in the battery is kept in a range between the 70% and 80% of the rated battery capacity during the 47% of the year under study, as it can be seen in Fig. 4.17(c). Furthermore, the grid power ramp-rates are reduced with respect to previous strategies, as shown in Fig. 4.18(a) and Fig. 4.18(b), reaching a maximum grid power ramp-rate of 983.1 W/h, as is depicted in Fig. 4.18(c). Finally, this

improved behavior is reflected in the reduction of the defined quality criteria summarized in Table 4-3.

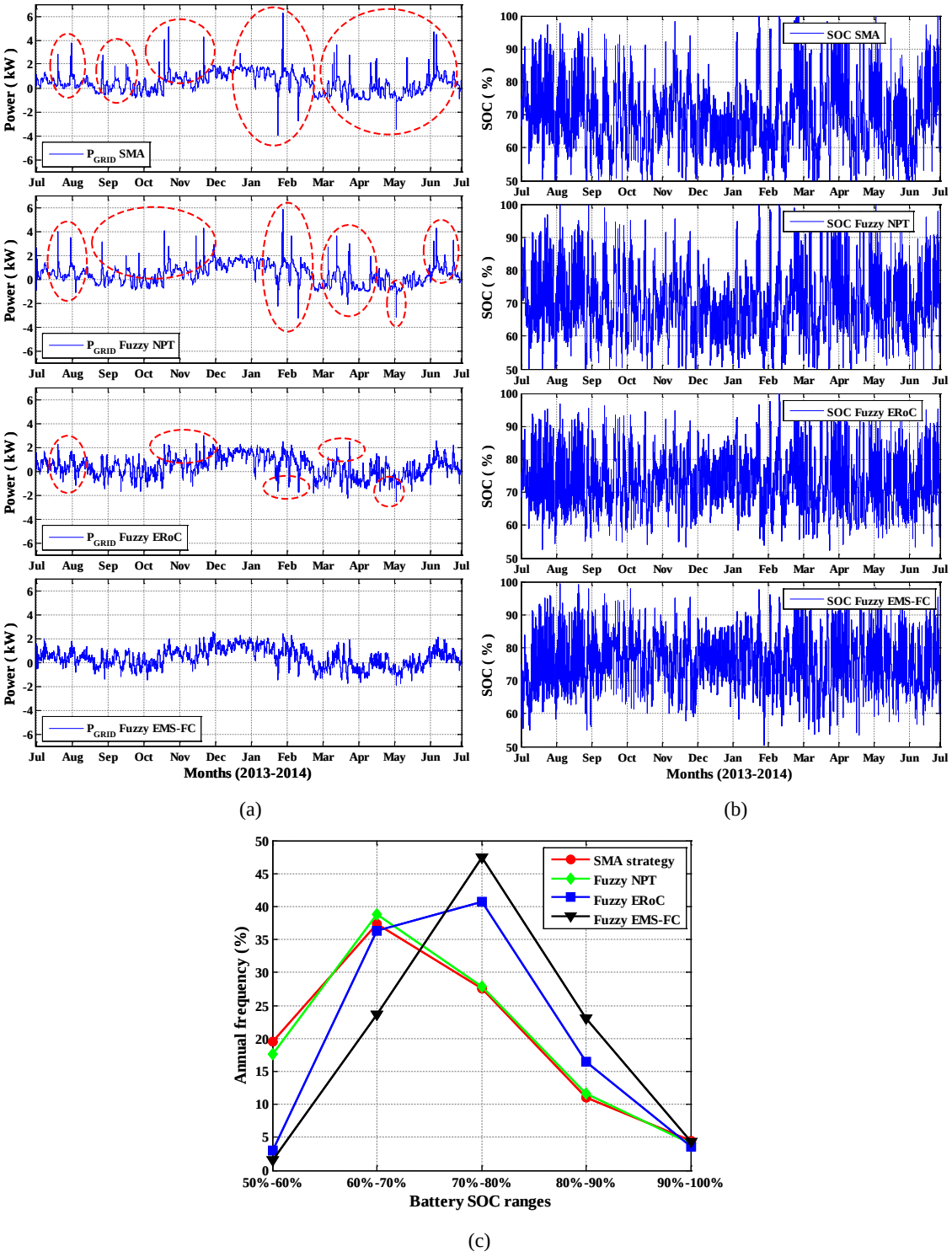

Fig. 4.17. Simulation results accomplished through the defined EMS strategies including the EWH (a) grid power comparison, (b) battery SOC comparison, and (c) annual frequency of the battery SOC ranges

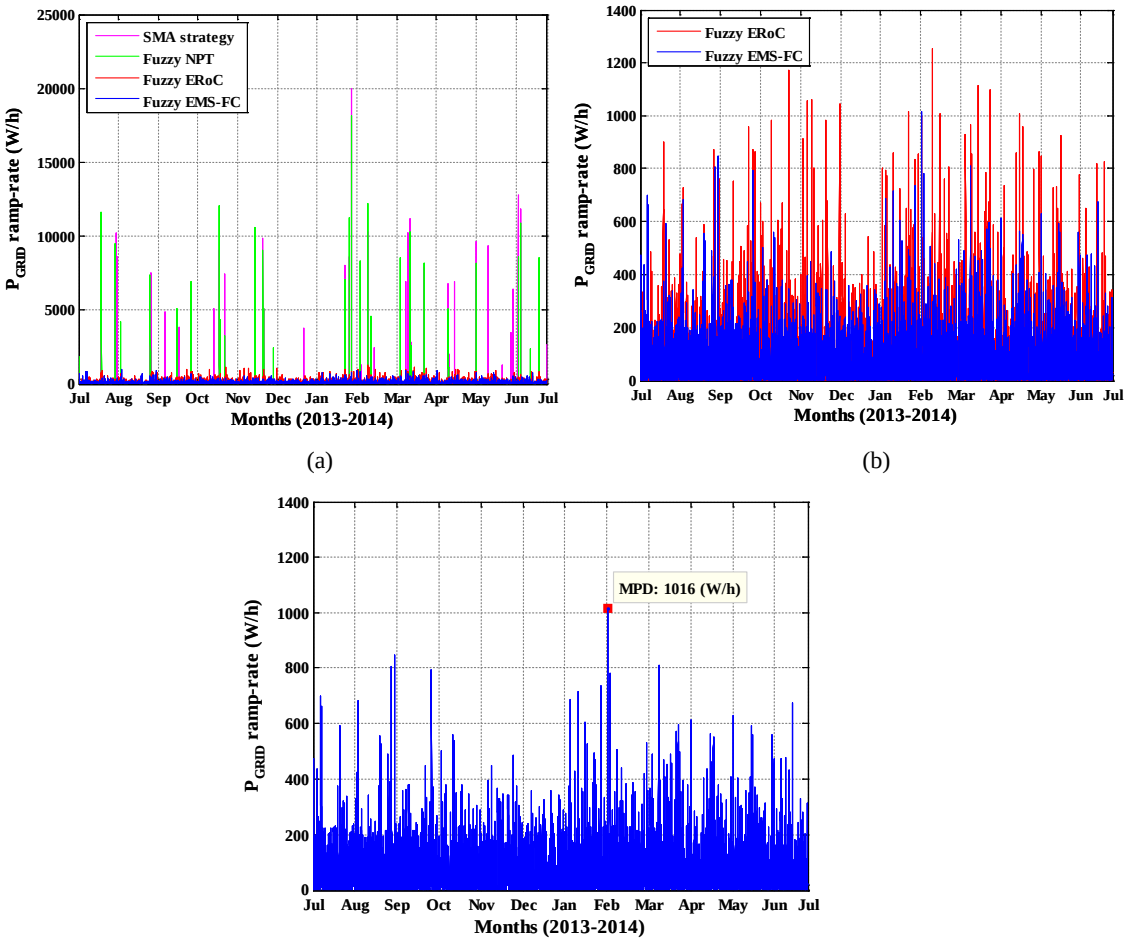

Fig. 4.18. Simulation results for the fuzzy EMS-FC strategy including the EWH consumption (a) grid power ramp-rates comparison with respect to the designed EMSs, (b) grid power ramp-rates comparison with respect to the fuzzy ERoC strategy, and (c) maximum grid power profile ramp-rate

Table 4-3 Quality criteria comparison for the fuzzy EMS-FC strategy, the fuzzy ERoC strategy, the fuzzy NPT strategy, the SMA strategy and the baseline values including the EWH consumption

EMS Strategy	$P_{G,MAX}$ (kW)	$P_{G,MIN}$ (kW)	*PVR*	*MPD* (W/h)	*APD* (W/h)	*PPV*
No EMS & ESS including the EWH consumption	6.53	-6.45	1.00	18468	1221	5.99
SMA strategy	6.25	-3.98	0.79	20006	57.41	1.23
Fuzzy NPT strategy	5.80	-3.28	0.70	18119	50.81	1.31
Fuzzy ERoC strategy	2.94	-2.52	0.42	1252	79.93	1.51
Fuzzy EMS-FC strategy	**2.46**	**-1.92**	**0.33**	**1016**	**75.93**	**1.42**

4.4. Experimental validation and analysis

In the same manner that the fuzzy ERoC strategy, the fuzzy EMS strategy based on MG power forecasting is accomplished and compiled through LabVIEW® platform. The fuzzy EMS-FC strategy is experimentally tested from Sep. 1st to Oct. 25th, 2015. The experimental results for different months are presented from Fig. 4.19 to Fig. 4.22 [63].

Fig. 4.19 presents the forecasted and measured data from Sep. 8th to Sep. 14th, 2015 obtained by the MG at UPNa. As it can be seen, excluding the WT power generation shown in Fig. 4.19(b), the magnitude and evolution of the forecast data is similar than measured [63]. Although, these differences (i.e. forecast error) are compensated by the fuzzy EMS-FC strategy as shown in Fig. 4.20.

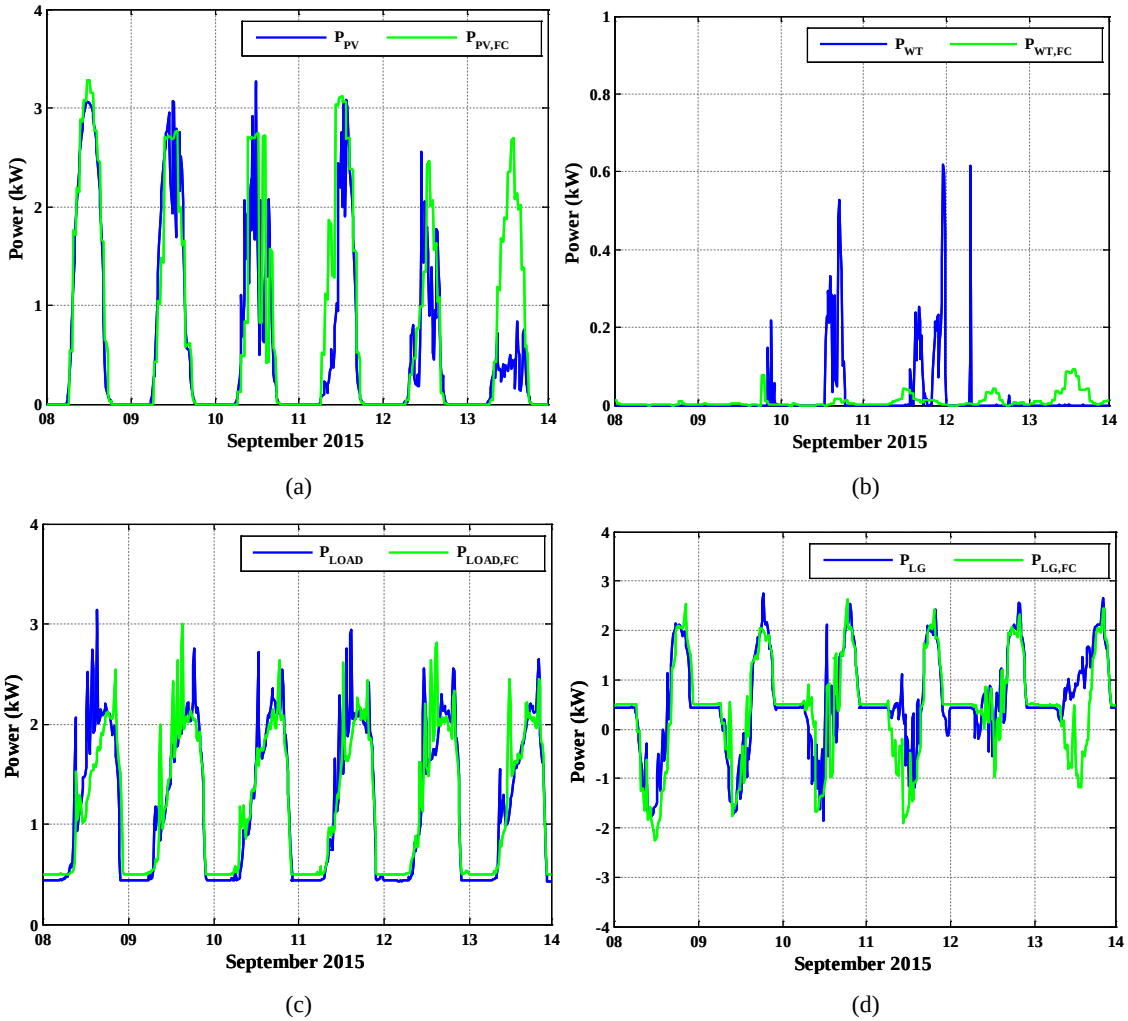

Fig. 4.19. Forecasted and measured data obtained at UPNa MG from Sep. 08th to Sep.14th, 2015. (a) Photovoltaic power, (b) wind turbine power, (c) load power, and (d) MG net power

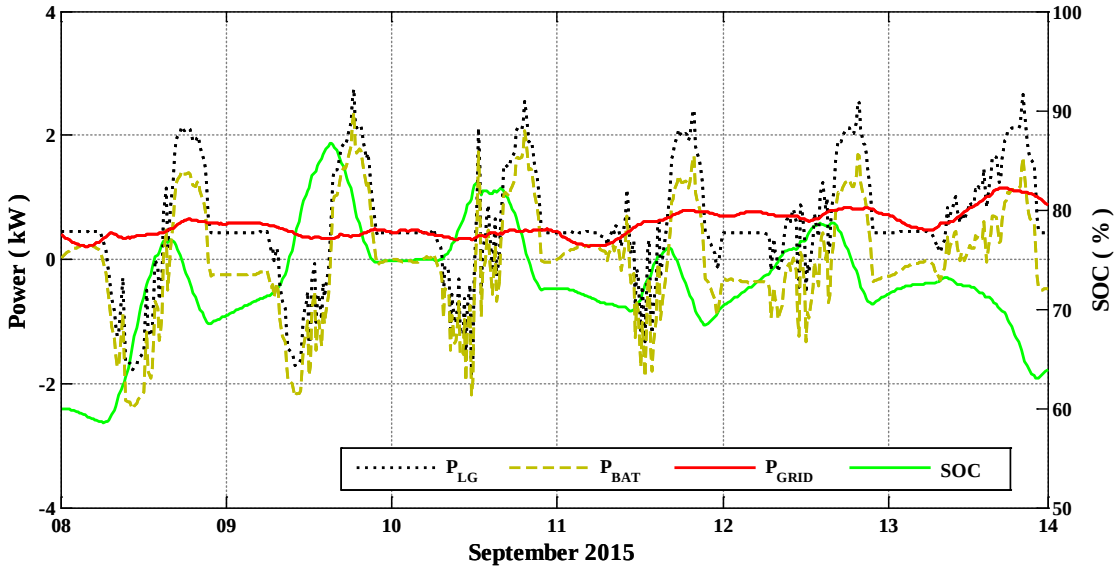

Fig. 4.20. Experimental results through the fuzzy EMS-FC strategy from Sep. 8th to Sep. 14, 2015 at UPNa MG

As it can be seen in Fig. 4.20, the fuzzy EMS-FC strategy manages the battery power in order to absorb the MG net power fluctuations, consequently smoothing the grid power profile.

Similarly, Fig. 4.21 illustrates the forecasted and measured data from Oct. 10th to Oct. 25th, 2015 obtained by the MG at UPNa [63].

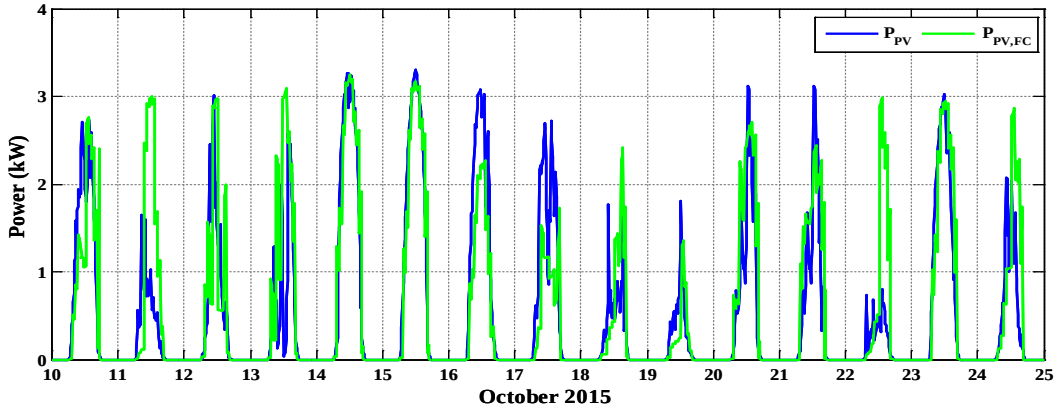

(a)

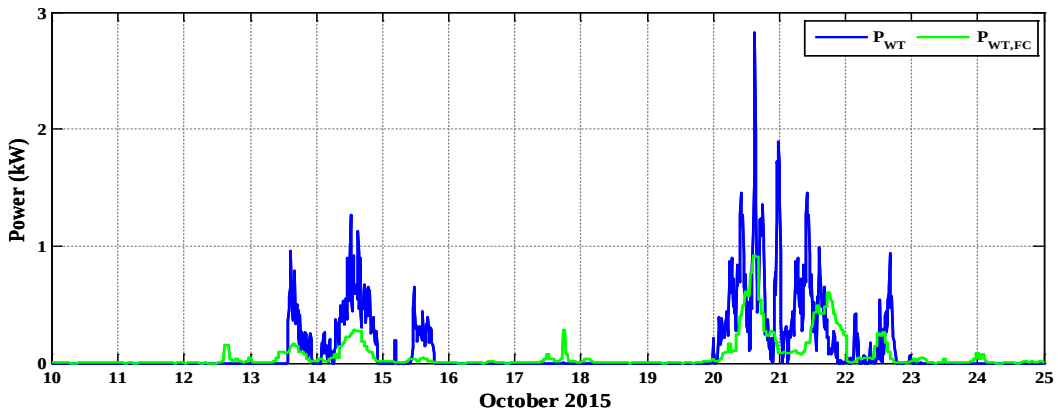

(b)

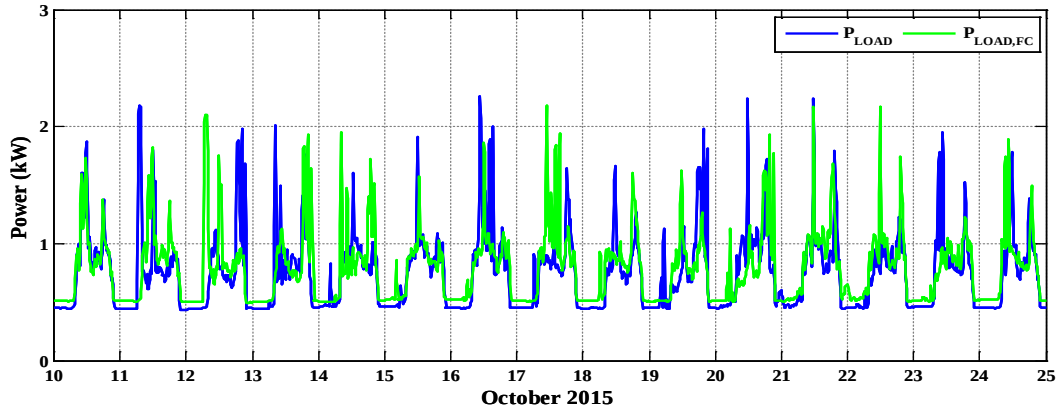

(c)

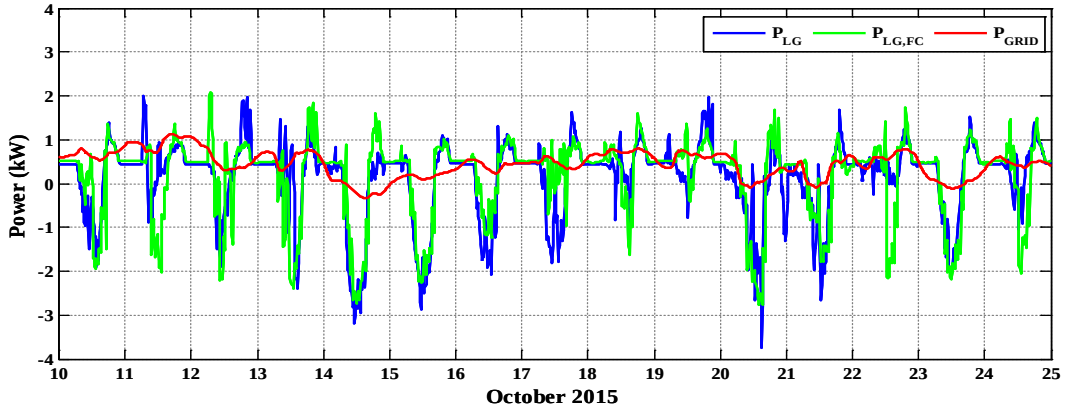

(d)

Fig. 4.21. Forecasted and measured data obtained at UPNa MG from Oct. 10th to Oct. 25th, 2015 (a) PV power generation, (b) WT power generation, (c) load demand, and (d) MG net power and resulting grid power profile

Finally, Fig. 4.22 shows the resulting behavior featured by the fuzzy EMS-FC strategy, which validates the fuzzy EMS-FC strategy that concurrently minimizes the power profile exchanged with the grid and keeps the battery SOC between secure limits [63].

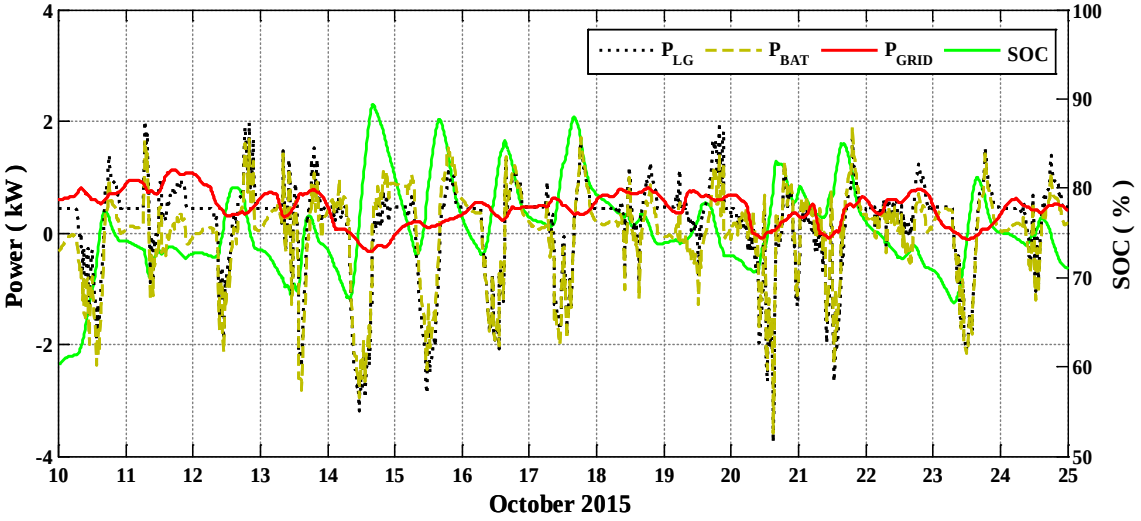

Fig. 4.22. Experimental results achieved through the fuzzy EMS based on MG power forecasting from Oct. 10th to Oct. 25th, 2015 at UPNa MG

Chapter 5

FLC-based Energy management strategies for a residential grid-connected electro-thermal microgrid

This Chapter presents the design and comparison of a fuzzy EMS strategies applied to an electro-thermal MG scenario. The electro-thermal MG scenario under study, shown in Fig. 5.1, includes renewable generation system (i.e. photovoltaic and wind generation), electric storage system (i.e. lead-acid battery bank), thermal generation system (i.e. electric water heater and solar thermal collectors), thermal storage system (i.e. water storage tank), and electric and thermal load demand (i.e. electrical appliances and domestic hot water consumption). In this new scenario, the main goal of the EMS strategy is to use the surplus power of the MG to supply the power required by the EWH in order to keep the water temperature in the storage tank between specific ranges.

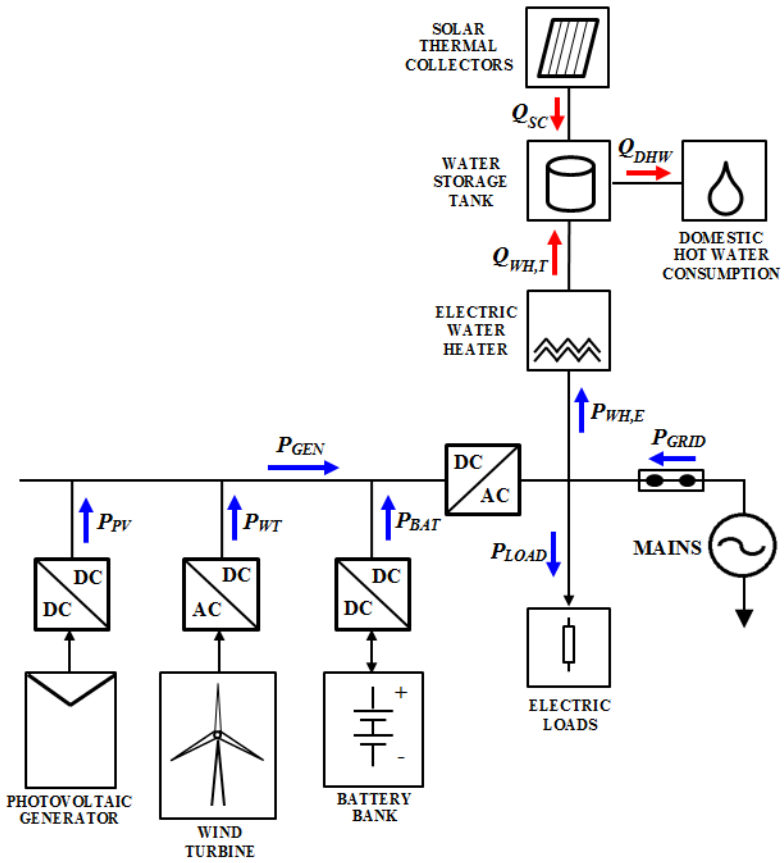

Fig. 5.1. Residential grid-connected electro-thermal microgrid

In this regard, given the positive results achieved through the fuzzy EMS strategies described in Chapter 3.4 and Chapter 4 (i.e. fuzzy ERoC and fuzzy EMS-FC strategies), this Chapter

proposes the use of the fuzzy-based EMS strategies in an electro-thermal MG scenario. Therefore, some variations in the control algorithms of the previous strategies are introduced with the purpose of using the energy stored in the ESS to supply part of the energy required by the EWH. In this manner, the EMS strategies minimize both the grid power profile and the amount of energy supplied by the mains to satisfy the EWH demand.

5.1. Fuzzy EMS strategy based on MG energy rate-of-change applied to an electro-thermal microgrid

5.1.1. Introduction

The EMS strategy developed in Chapter 3.4 (i.e. fuzzy ERoC strategy) is now applied for an electro-thermal MG scenario, now referred as fuzzy ERoC ETH-MG strategy. In this scenario, the appropriate control of the EWH leads to concurrently minimize both the grid power consumption and the fluctuations in the power exchanged to the grid [55], [56]. The goal of the EMS strategy is the suitable use of the energy stored in the ESS to meet the load demand required by the EWH in order to keep the water temperature in the storage tank between the established limits. According to the configuration shown in Fig. 5.1 the grid power profile and the MG net power are defined as follows:

$$P_{GRID} = P_{LG} - P_{BAT}, \tag{5.1}$$

$$P_{LG} = P_{LOAD} - P_{GEN} + P_{WH,E}. \tag{5.2}$$

5.1.2. Controller design

The design follows the control policies described in Chapter 3.4 and includes some additional policies for the EWH control. The design includes an electric water heater (EWH) control block, which is used to calculate the amount of energy that the ESS supplies to the EHW, $P_{WH}^{B}(n)$. By this way, the power required by the EWH is handled by the ESS and the mains, thus, reducing the MG net power (5.2) since now part of the energy is provided by the ESS instead by the mains. In this regard, the MG net power is modified as follows:

$$P_{LG}^{*}(n) = P_{LG}(n) - P_{WH}^{B}(n), \tag{5.3}$$

where $P_{WH}^{B}(n)$ is the amount of power delivered by the battery for the EWH consumption, which is assigned as follows:

$$P_{WH}^{B}(n)=\begin{cases}P_{WH,E}(n), & \text{if } SOC(n)>SOC_{R1}\wedge P_{WH,E}(n)>0\\ 0, & \text{otherwise}\end{cases}, \tag{5.4}$$

where SOC_{R1} is the threshold which allows the power injection from the ESS.

Equation (5.4) highlights that the ESS will provide the EWH power as long as the battery has enough energy at the time that the EWH requires it. Therefore, according to (5.3) the amount of energy supplied by the mains is reduced. On the contrary, $P_{WH}^{B}(n)$ is null for other cases, which implies that the energy supplied by the mains is maintained.

As presented in Chapter 3.4, the grid power profile of the fuzzy ERoC strategy is defined as follows:

$$P_{GRID}(n)=P_{AVG}^{*}(n)+P_{FLC}(n), \tag{5.5}$$

being $P_{AVG}^{*}(n)$ the average net power of $P_{LG}^{*}(n)$, which is computed as follows:

$$P_{AVG}^{*}(n)=\frac{1}{M}\sum_{k=1}^{M}P_{LG}^{*}(n-k), \tag{5.6}$$

In addition, the $P_{FLC}(n)$ component is computed by means of a FLC, which uses as input variables the battery SOC and the modified MG ERoC over time, $\dot{P}_{AVG}^{*}(n)$. In this concern, the modified energy rate-of-change of the MG is defined as follows:

$$\dot{P}_{AVG}^{*}(n)=\left[P_{AVG}^{*}(n)-P_{AVG}^{*}(n-1)\right]/T_s. \tag{5.7}$$

In contrast to the EMS strategy described in Chapter 3.4, the battery power $P_{BAT}(n)$, is now defined as the sum of two components as follows:

$$P_{BAT}(n)=P_{BAT}^{MG}(n)+P_{WH}^{B}(n), \tag{5.8}$$

$$P_{BAT}^{MG}(n)=P_{GRID}(n)+P_{LG}(n), \tag{5.9}$$

where $P_{BAT}^{MG}(n)$ is computed through (5.1) and $P_{WH}^{B}(n)$ is the power supplied by the ESS for the EWH consumption according to the conditions defined in (5.4).

In this regard, the use of the energy stored in the ESS to supply part of the energy required by the EWH leads to the reduction of the energy supplied by the mains, which reduces the

operation cost of the MG. The amount of energy saved in a year, E_{saved}, through the fuzzy ERoC strategy for an electro-thermal can be quantified as follows:

$$E_{saved} = E_{WH,E} - E_{WH}^{G}, \tag{5.10}$$

$$E_{WH}^{G} = E_{WH,E} - E_{WH}^{B}, \tag{5.11}$$

$$E_{WH,E} = \frac{1}{T_s} \cdot \sum_{n=1}^{N} P_{WH,E}(n), \tag{5.12}$$

$$E_{WH}^{B} = \frac{1}{T_s} \cdot \sum_{n=1}^{N} P_{WH}^{B}(n), \tag{5.13}$$

where $E_{WH,E}$ is the annual energy required by the EWH, E_{WH}^{B} is the annual energy supplied by the mains for the EWH consumption, and E_{WH}^{B} is the annual energy supplied by the ESS for the EWH consumption.

The new block diagram of the fuzzy ERoC strategy applied to an electro-thermal MG is depicted in Fig. 5.2 and includes the following blocks:

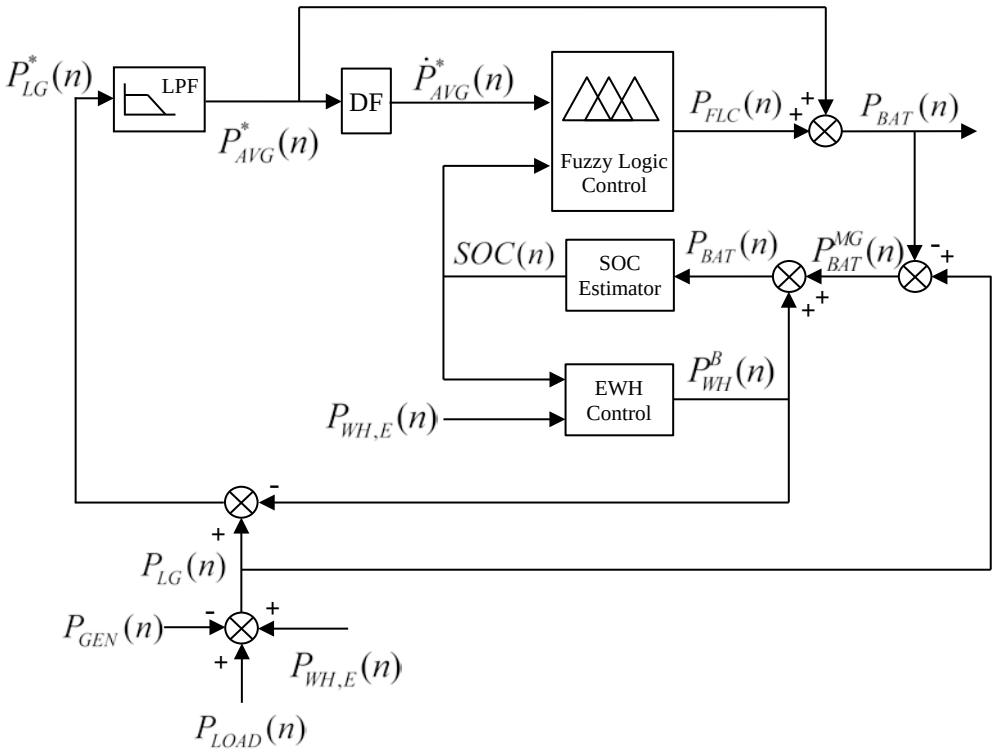

Fig. 5.2. Block diagram of the Fuzzy ERoC strategy applied to an electro-thermal microgrid

1. A Low-Pass filter block (LPF), used for computing the MG average net power according to (5.6),
2. A digital Derivative and Filter block (DF), used for concurrently obtaining $\dot{P}^{*}_{AVG}(n)$, according to (5.7), and limiting the high-frequency gain and noise associated with the derivative term [95],
3. A battery SOC Estimator block, used to estimate the SOC of the battery according to the battery model described in Chapter 2.3.3,
4. A Fuzzy Logic Controller block (FLC), used for computing the second component, $P_{FLC}(n)$, of the grid power profile defined in (5.5), and
5. A EWH Control block, used for computing the amount of energy supplied by the ESS for the EWH consumption, $P^{B}_{WH}(n)$.

5.1.3. Fuzzy logic controller design

The FLC block used for this strategy is similar as the one presented in Chapter 3.4.3. In short, the FLC assumes a Mamdani-based inference and defuzzyfication of Center of Gravity with two inputs, $SOC(n)$ and $\dot{P}^{*}_{AVG}(n)$, and one output $P_{FLC}(n)$, where the variation range of each variable is defined as follows:

$$SOC_{MIN} \leq SOC(n) \leq SOC_{MAX}, \tag{5.14}$$

$$-\dot{P}_{AVG} \leq \dot{P}^{*}_{AVG}(n) \leq \dot{P}_{AVG}, \tag{5.15}$$

$$-P_{N} \leq P_{FLC}(n) \leq P_{P}, \tag{5.16}$$

where SOC_{MIN} and SOC_{MAX} are the boundaries of the battery SOC defined in Chapter 2.3.3, $\dot{P}_{AVG}$ is maximum variation of the derivative term defined through (3.30), and P_N and P_P are the minimum and maximum power assigned through the controller output, respectively. Note that this approach considers only the maximum variation of the derivative term. In addition, from the optimization process, the variation range of the FLC output is established between P_N = -1.4 kW and P_P = 1.5 kW.

As in Chapter 3.4.3, the adjustment of all parameters involved in the FLC design is performed by an off-line optimization procedure described in [51] with the purpose of minimizing the energy management quality criteria defined in Chapter 3.1.2. As a result, five triangular MFs are defined for each input variable and nine triangular MFS are defined for the output variable. The MFs are illustrated in Fig. 5.3.

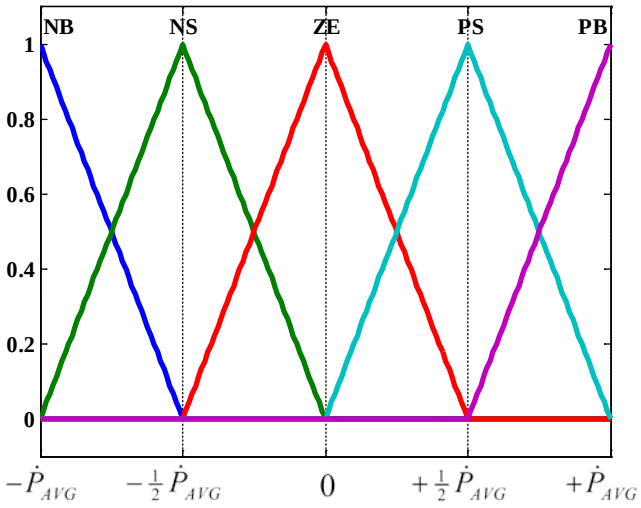

(a)

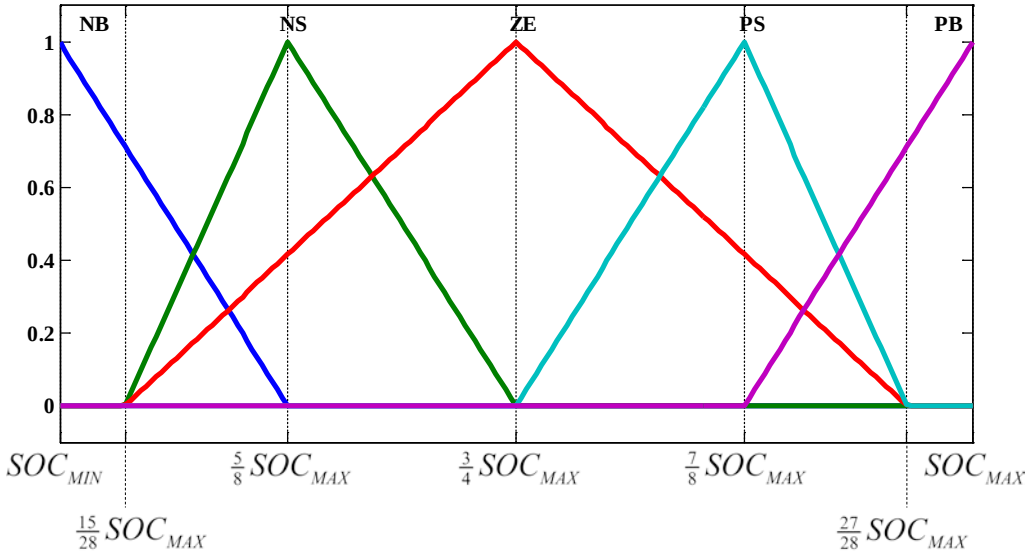

(b)

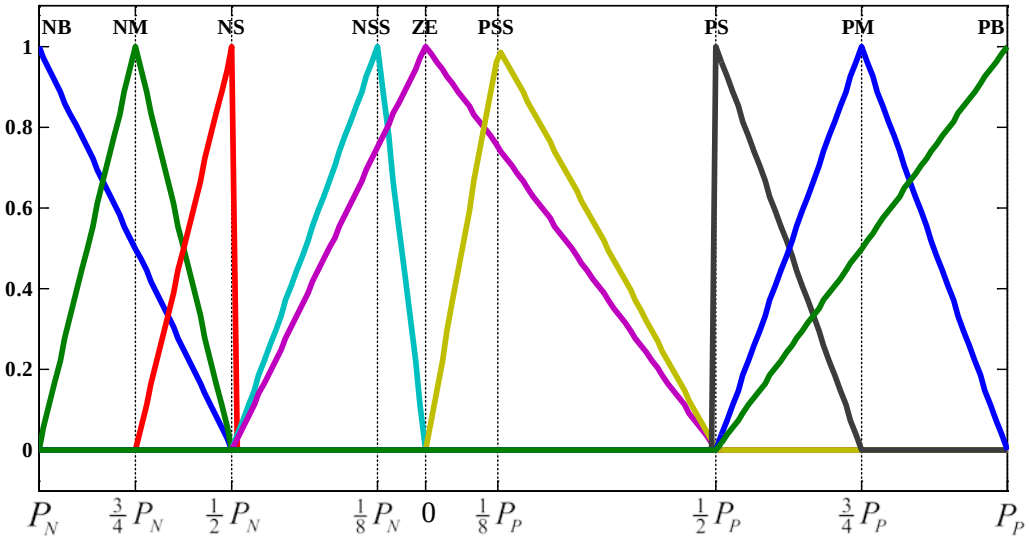

(c)

Fig. 5.3. MFs of the FLC for the fuzzy ERoC strategy applied to an electro-thermal MG (a) MFs for the input variable $\dot{P}^{*}_{AVG}$, (b) MFs for the input variable *SOC*, and (c) MFs for the output variable P_{FLC}

Finally, the optimized rule-base of the fuzzy ERoC strategy applied to an electro-thermal microgrid is presented in Table 5-1.

Table 5-1 Optimized fuzzy rule-base of the FLC for the fuzzy ERoC strategy applied to an electro-thermal microgrid

$P_{FLC}(n)$		$\dot{P}^*_{AVG}(n)$				
		NB	**NS**	**ZE**	**PS**	**PB**
***SOC* (*n*)**	**NB**	PB	PM	PSS	PM	PB
	NS	PM	PS	PSS	PS	PM
	ZE	ZE	NSS	ZE	NSS	NSS
	PS	NM	NSS	NS	NM	NM
	PB	NB	NB	NSS	NM	NB

5.1.4. Simulation results and analysis

The simulation results of the fuzzy ERoC strategy applied to an electro-thermal microgrid are shown in Fig. 5.4 to Fig. 5.10.

As mentioned in the controller design, the energy management strategy for an electro-thermal MG uses the energy stored in the ESS to supply part of the power required by the EWH. Therefore, as it can be seen in Fig. 5.4, the amount of power supplied by the mains required for the EWH consumption is reduced so is the MG net power.

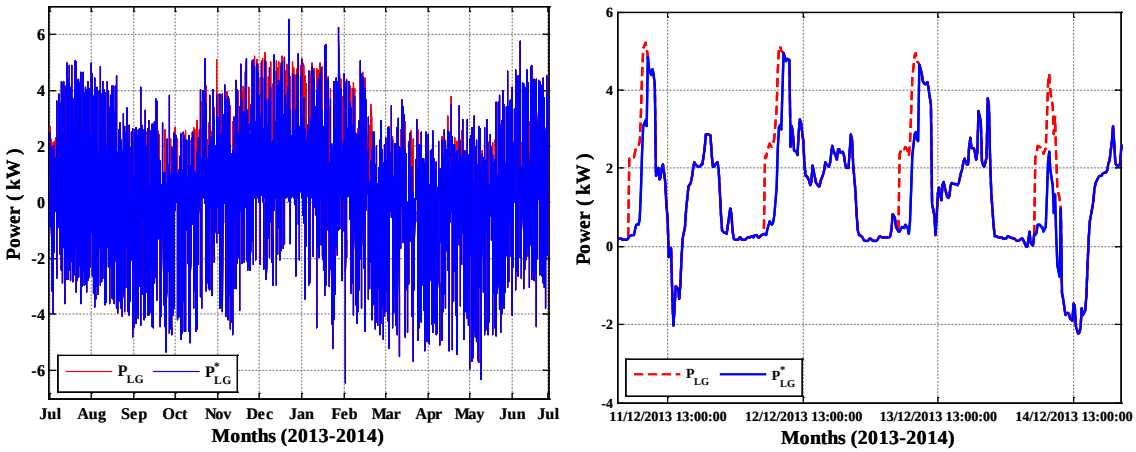

(a) (b)

Fig. 5.4. MG net power profile (a) comparison between the MG net power including the EWH consumption and the modified MG net power achieved through the fuzzy ERoC strategy applied to an electro-thermal MG, (b) reduction of the MG net power profile

As a consequence of this behavior and according to (5.8) the energy management strategy increases the battery power in order to supply the remaining power required by the EWH. The increase of the battery power with respect to the fuzzy ERoC strategy is illustrated in Fig. 5.5.

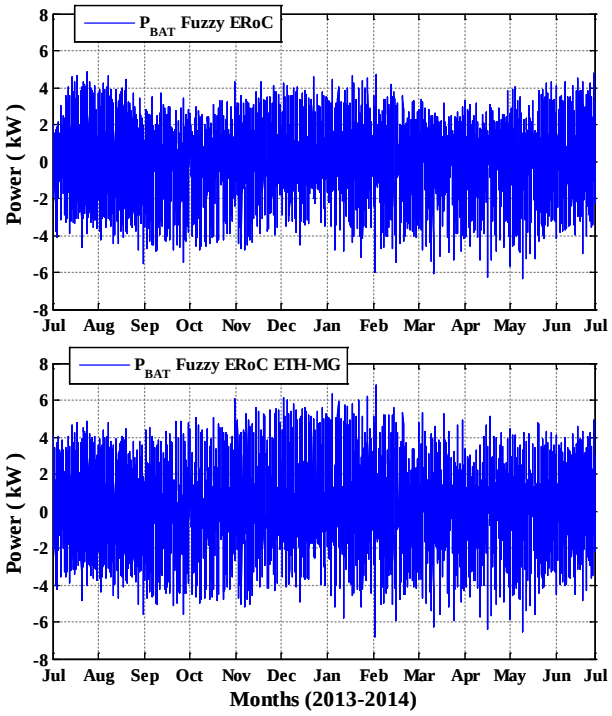

Fig. 5.5. Battery power comparison between the fuzzy ERoC strategy including the EWH consumption and the fuzzy ERoC strategy applied to an electro-thermal MG

In addition, Fig. 5.6 presents the distribution of the energy supplied by the mains and the ESS for the EWH consumption. As it can be seen, the ESS contributes significantly to the consumption needed by the EWH to keep the water temperature in the deposit tank between 45 °C and 65 °C. The ESS supplies an energy of E_{WH}^{B} = 936 kWh during the year under study, which is equivalent to 54.40 % of the total energy required by the EWH. It is worth noting that the energy provided by the ESS represents the energy saved E_{saved} by the MG.

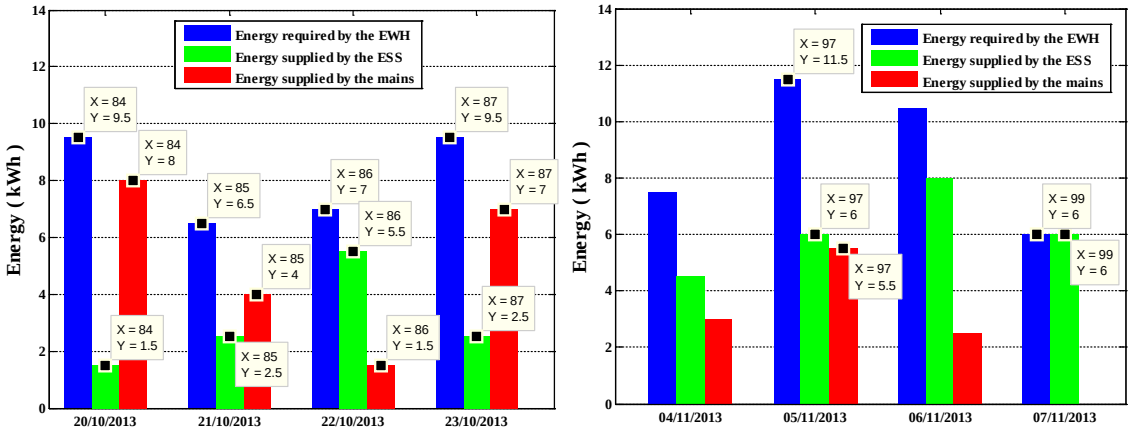

Fig. 5.6. Distribution of the energy required for the EWH in two different periods of the year under study

Moreover, Fig. 5.9(a) compares the grid power profile achieved through the energy management strategies including the EWH consumption described in Chapter 3 and the fuzzy ERoC strategy applied to an electro-thermal MG. As it can be appreciated, the grid power fluctuations are minimized through the use of the electro-thermal MG (i.e. P_{GRID} fuzzy ERoC ETH-MG).

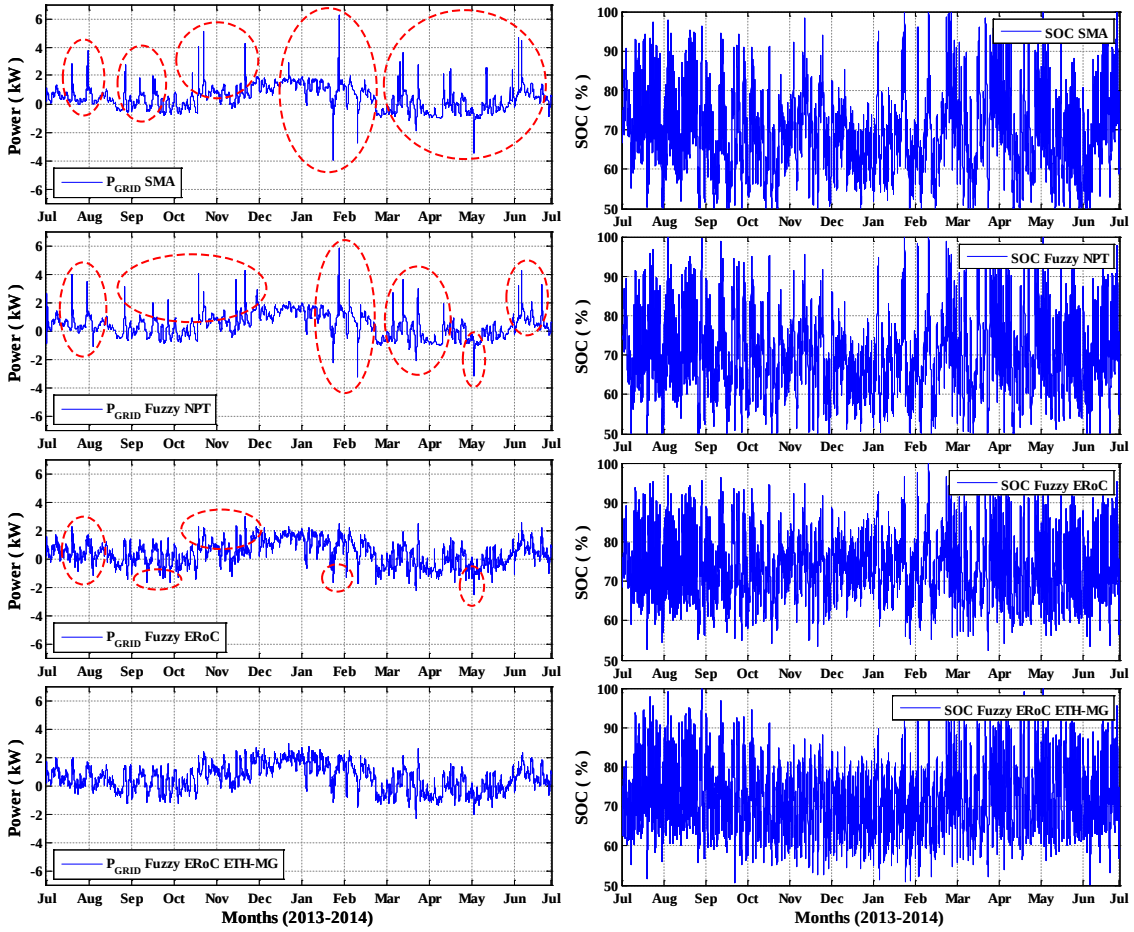

(a) (b)

Fig. 5.7. Grid power profile (a) and battery SOC comparison (b) for the SMA, fuzzy NPT, and fuzzy ERoC strategies including the EWH consumption and the fuzzy ERoC strategy applied to an electro-thermal MG

Conversely, as displayed in Fig. 5.9(b), the use of the energy stored in the battery to supply part of the power required by the EWH leads to a reduction of the battery SOC evolution during the year under study. In this regard, the energy stored in the battery is kept in a range between the 70% and 80% of the rated battery capacity during the 36.96% of the year under study. This result is higher than the 27% obtained through both the SMA and fuzzy NPT strategies including the EWH consumption, but is lower than the 40.72% reached through the fuzzy ERoC strategy including the EWH consumption as can be appreciated in Fig. 5.8. However, analyzing the range interval between the 60% and 80% of the rated battery capacity, both strategies (i.e. fuzzy ERoC including EWH consumption and fuzzy ERoC ETH-MG) have similar results keeping the battery SOC in this range the 77% of the year under study.

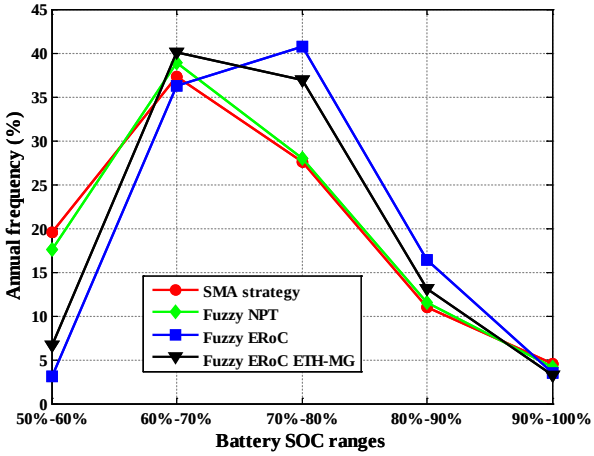

Fig. 5.8. Annual frequency of the battery SOC ranges established through the SMA, fuzzy NPT, fuzzy ERoC strategies including the EWH consumption and the fuzzy ERoC strategy applied to an electro-thermal MG

Furthermore, in order to highlight the effectiveness of the fuzzy ERoC strategy applied to an electro-thermal MG, Fig. 5.9 presents the comparison of the principal variables of the MG during three consecutive days between the fuzzy ERoC strategy including the EWH consumption and the fuzzy ERoC ETH-MG strategy.

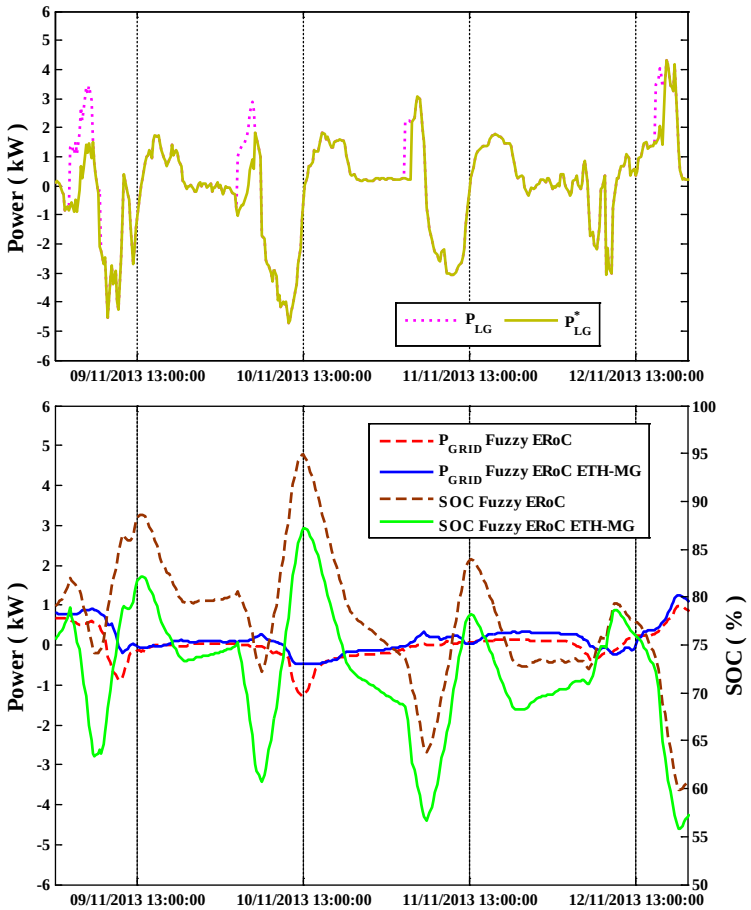

Fig. 5.9. Grid power profile and battery SOC comparison between the fuzzy ERoC strategy including the EWH consumption and the fuzzy ERoC strategy applied to an electro-thermal MG

As it can be seen in Fig. 5.9(top), part of the power required by the EWH is supplied by the ESS; therefore, the MG net power (pink dot line) is reduced (mustard-colored solid line). Accordingly, the battery discharges reducing the energy stored in the ESS (green solid line) as shown in Fig. 5.9 (bottom). In addition, as shown in Fig. 5.9 (bottom), this behavior minimizes the grid power fluctuations (blue solid line) with respect to the fuzzy ERoC strategy including the EWH consumption (red dashed-line), since the ESS can absorb the future power generation produced by both RES, as it can be appreciated on Nov. 9th and 10th close to 13:00 PM.

The proper behavior of the fuzzy ERoC strategy applied to an electro-thermal MG is verified through the analysis of the energy management quality criteria defined in Chapter 3.1.2, which are summarized in Table 5-2.

Table 5-2 Quality criteria comparison for the fuzzy ERoC strategy applied to an electro-thermal microgrid, the fuzzy ERoC, the fuzzy NPT strategy, the SMA strategy and the baseline values including the EWH consumption

EMS Strategy	$P_{G,MAX}$ **(kW)**	$P_{G,MIN}$ **(kW)**	***PVR***	***MPD*** **(W/h)**	***APD*** **(W/h)**	***PPV***
No EMS & ESS including the EWH consumption	6.53	-6.45	1.00	18468	1221	5.99
SMA strategy	6.25	-3.98	0.79	20006	57.41	1.23
Fuzzy EMS based on MG net power trend	5.80	-3.28	0.70	18119	50.81	1.31
Fuzzy ERoC strategy including the EWH consumption	2.94	-2.52	0.42	1252	79.93	1.51
Fuzzy ERoC strategy applied to an electro-thermal MG	**2.95**	**-2.31**	**0.41**	**1052**	**75.67**	**1.26**

As it can be noticed, the fuzzy ERoC strategy applied to an electro-thermal MG achieves a reduction in five of the energy management quality criteria. In short, $P_{G,MIN}$, *PVR*, *MPD*, *APD*, and *PPV* criteria are reduced in 8.3%, 2.4%, 16%, 5.3%, and16.6% with respect to the fuzzy ERoC strategy including the EWH consumption. Conversely, $P_{G,MAX}$ criterion exhibits a negligible increase that has not a negative impact on the global strategy features.

Finally, the comparison of the grid power profile ramp-rates through the EMS strategies including the EWH consumption described in Chapter 3 and the fuzzy ERoC strategy applied to an electro-thermal MG is presented in Fig. 5.10.

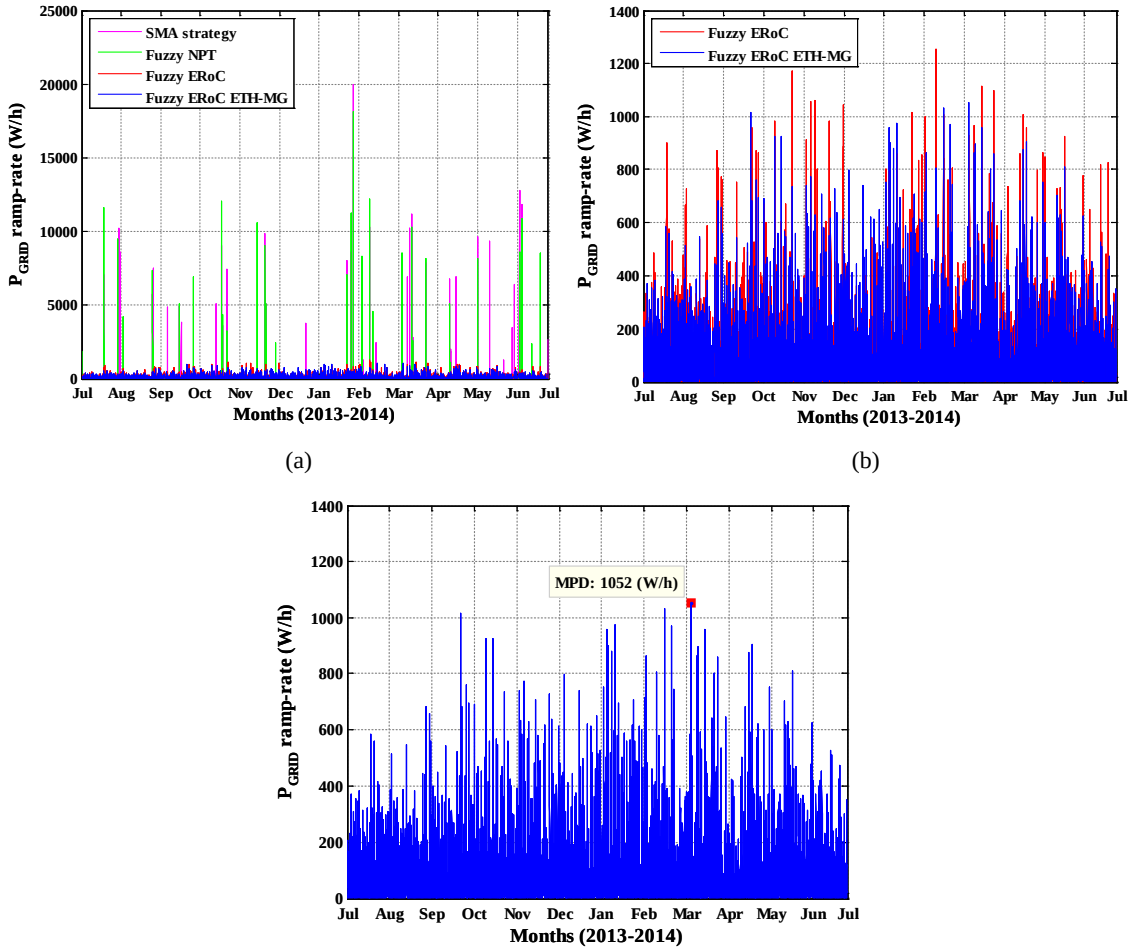

Fig. 5.10. Grid power profile ramp-rates analysis (a) grid power ramp-rates comparison for the described EMS strategies, (b) grid power ramp-rates comparison with respect to the fuzzy ERoC strategy including the EWH consumption, and (c) maximum grid power profile ramp-rate achieved through the fuzzy ERoC ETH-MG strategy

As it can be seen in Fig. 5.10(a) and Fig. 5.10(b), the grid power ramp-rates are reduced through the use of the electro-thermal MG, which confirms the reduction of the *MPD* criterion reaching a maximum value of 1052 W/h, as shown in Fig. 5.10(c).

5.2. Fuzzy EMS strategy based on MG power forecasting applied to an electro-thermal microgrid

5.2.1. Introduction

Similarly to the previous design, the energy management strategy based on MG power forecasting is applied to an electro-thermal MG scenario. Similarly, the goal of the strategy is to control the ESS power to supply part of the power required by the EWH to keep the water temperature in the storage tank between the established limits.

5.2.2. Controller design

The block diagram of the fuzzy EMS-FC strategy presented in Chapter 4.2 is modified to include the EWH control block. In this regard, the new block diagram is illustrated in Fig. 5.11 and includes the blocks described in Chapter 4.2 as well as the EWH Control block presented in section 5.1.2.

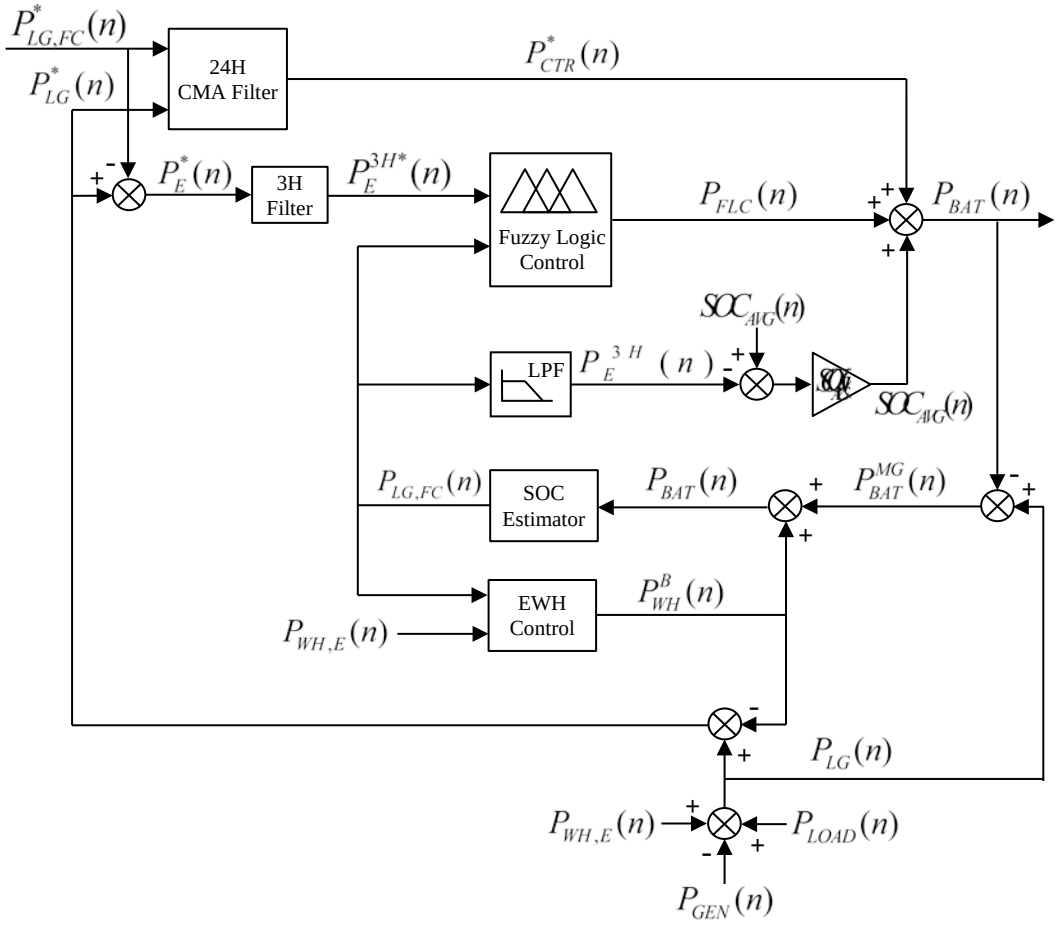

Fig. 5.11. Block diagram of the Fuzzy EMS-FC strategy applied to an electro-thermal microgrid

In this regard, the control strategy developed in Chapter 4 is adapted in order to use the energy stored in the ESS to supply, as much as possible, the power required by the EWH. Similarly to the previous design, the use of the battery power, $P^B_{WH}(n)$, to supply part of the power required by the EWH implies the reduction of the MG load demand. Thus, the load demand is modified as follows:

$$P^*_{LOAD}(n) = P_{LOAD}(n) - P^B_{WH}(n). \tag{5.17}$$

Consequently, the load forecast is affected, thus, is necessary to recalculate the load forecast considering the modified load demand, $P^{*}_{LOAD}(n)$. Hence, $P_{LOAD,FC}$ is changed into $P^{*}_{LOAD,FC}(n)$. In addition, according to (4.3) the forecast of the MG net power is modified as follows:

$$P^{*}_{LG,FC}(n) = P^{*}_{LOAD,FC}(n) - P_{GEN,FC}(n). \tag{5.18}$$

The block diagram to calculate the forecast of the modified MG net power, $P^{*}_{LG,FC}(n)$ is displayed in Fig. 5.12. Note that the renewable generation power is not affected by the use of the EWH, thus, the forecast of power generation is maintained.

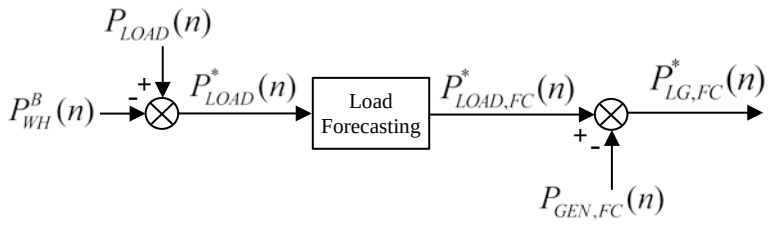

Fig. 5.12. Net power forecasting block diagram

Since a part of the power required by the EWH is supplied by the ESS the MG net power is modified as follows:

$$P^{*}_{LG}(n) = P_{LG}(n) - P^{B}_{WH}(n). \tag{5.19}$$

According to (4.5) the grid power for the fuzzy EMS-FC applied to an electro-thermal MG scenario (fuzzy EMS-FC ETH-MG) is defined as follows:

$$P_{GRID}(n) = P^{*}_{CTR}(n) + P_{SOC}(n) + P_{FLC}(n), \tag{5.20}$$

where $P^{*}_{CTR}(n)$ is the modified average net power of the MG, which is calculated at each sample by means of both the modified MG net power $P^{*}_{LG}(n)$ and the modified forecast of the MG net power $P^{*}_{LG,FC}(n)$. Note that for computing the modified average of the MG net power it is necessary to use the expressions from (4.6) to (4.8), which are defined in Chapter 4.2 by means of replacing P_{LG} and $P_{LG,FC}$ for $P^{*}_{LG}(n)$ and $P^{*}_{LG,FC}(n)$, respectively. Additionally, in order to compute the $P_{FLC}(n)$ component it is necessary to determine the modified forecast error of the MG for the previous 3-hours $P^{3H*}_{E}(n)$, which now is calculated as follows:

$$P^{*}_{E}(n) = P^{*}_{LG}(n) - P^{*}_{LG,FC}(n), \tag{5.21}$$

$$P_E^{3H^*}(n) = \frac{1}{M_3}\sum_{k=1}^{M_3} P_E^*(n-k), \tag{5.22}$$

Finally, the battery power and the energy saved during the year under study through the fuzzy EMS-FC strategy applied to an electro-thermal MG scenario are computed using from (5.8) to (5.13)

5.2.3. Fuzzy logic controller design

The FLC design follows the procedure described in Chapter 4.2, but considering the modified power forecast error of the MG. In short, the FLC uses the same configuration (i.e. Mamdani-based inference and defuzzyfication of Center of Gravity), inputs [i.e. $P_E^{3H^*}(n)$ and $SOC(n)$], output [i.e. $P_{FLC}(n)$], and MFs number (i.e. 5 MFs for each input and 9 MFs for the output), type (i.e. triangular), and mapping (see Fig. 4.9) of the fuzzy EMS-FC strategy described in Chapter 4.2. However, due to the reduction of the MG net power, the reassignment of the limits of the FLC output is needed. Consequently, the optimization process will deliver a new set of rules to minimize the energy management quality criteria defined in Chapter 3.1.2 according to the new MG conditions.

In this regard, the variation range for the output variable is established between P_N = -0.8 kW and P_P = 1.35 kW by the optimization procedure. The resulting rule-base is presented in Table 5-3.

Table 5-3 Optimized fuzzy rule-base for the FLC of the fuzzy EMS-FC strategy applied to an electro-thermal microgrid

$P_{FLC}(n)$		$P_E^{3H^*}(n)$				
		NB	**NS**	**ZE**	**PS**	**PB**
***SOC* (*n*)**	**NB**	PB	PM	PS	PM	PB
	NS	PM	PS	PSS	PS	PM
	ZE	NS	ZE	ZE	PSS	NSS
	PS	NM	NS	NSS	NS	NM
	PB	NB	NSS	NM	NM	NB

Finally, the block diagram of the FLC is shown in Fig. 5.13. Similarly to previous designs, the FLC assumes a Mamdani-based inference and defuzzyfication of Center of Gravity with two inputs, $P_E^{3H^*}(n)$ and $SOC(n)$, one output $P_{FLC}(n)$ and 25-rules.

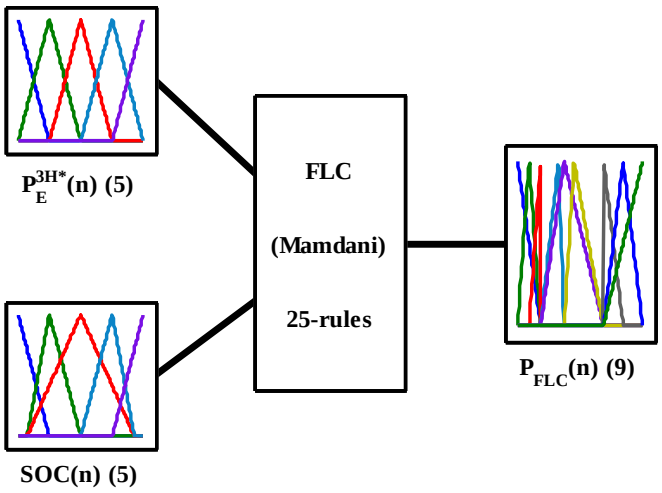

Fig. 5.13. Fuzzy logic system: 2 inputs, 1 output, and 25-rules

5.2.4. Simulation results and analysis

The simulations results of the fuzzy EMS-FC strategy applied to an electro-thermal MG scenario are presented from Fig. 5.14 to Fig. 5.18. As aforementioned in section 5.2.2, the main objective of the strategy is to use the energy stored in the ESS to supply part of the energy required by the EWH, which results in minimizing the total load required by the MG, as can be seen in Fig. 5.14(a). Consequently, the EMS strategy should recalculate the load demand forecast considering its reduced value, this leading to decrease the load forecast, as can be appreciated in Fig. 5.14(b). Hence, the MG net power and its forecasts are modified, as displayed in Fig. 5.14(c) and Fig. 5.14(d).

In the same manner, this behavior modifies the average net power profile of the MG, which now is lower than the initial value due to the reduction of the load demand, as can be illustrated in Fig. 5.15(a). Consequently, the new strategy reduces the grid power profile with respect to the fuzzy EMS-FC strategy, as can be seen in Fig. 5.15(b).

In addition, Fig. 5.16 shows the grid power profile and the battery SOC comparison for the EMS strategies including the EWH consumption described in Chapter 3 and Chapter 4, and the fuzzy EMS-FC strategy applied to an electro-thermal MG scenario. As it can be seen, the use of the energy stored in battery to supply part of the energy required by the EWH leads to the reduction of the grid power profile, as shown in Fig. 5.16(a), since the discharge of the battery allows the ESS to absorb greater amount of energy produced by the RES. Additionally, Fig. 5.15(b) shows the battery SOC evolution during the year under study. As it can be seen, the fuzzy EMS-FC ETH-MG strategy satisfies the ESS constraints defined in Chapter 2.3.3.

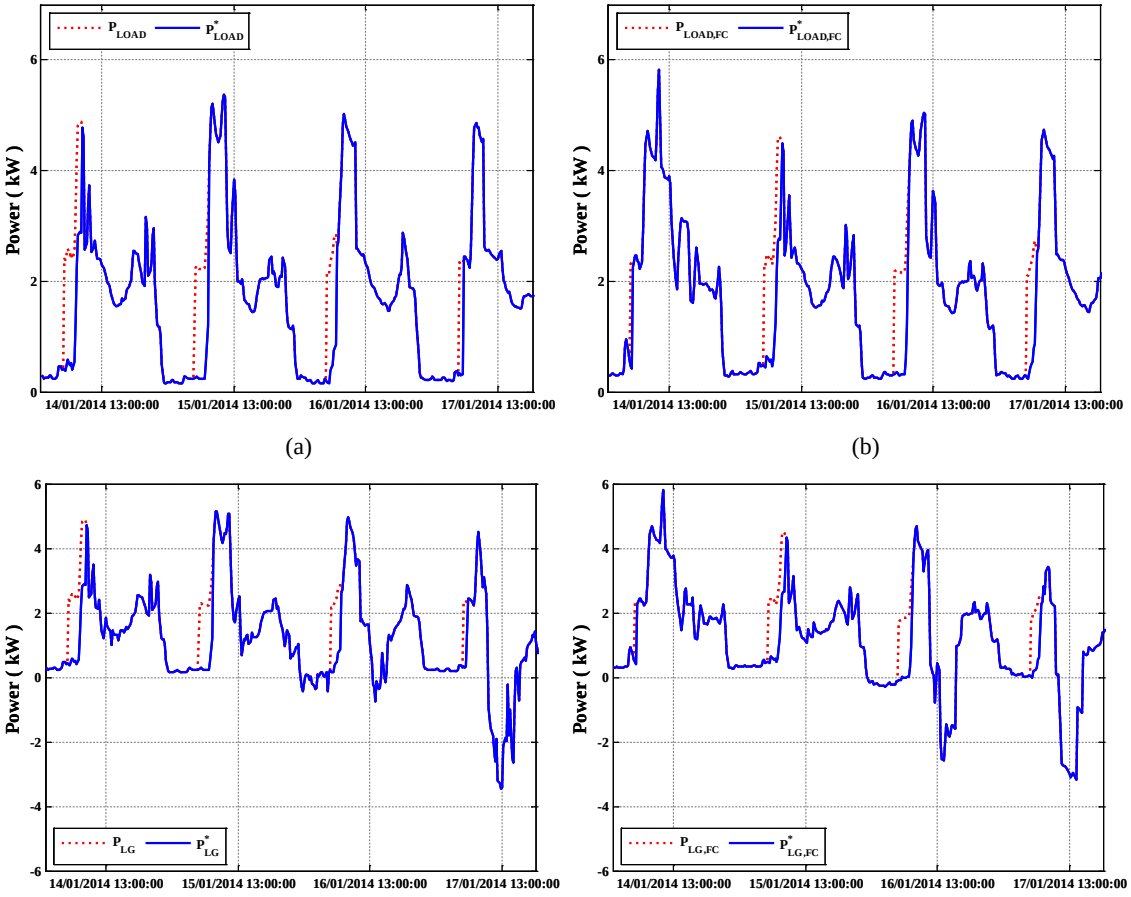

Fig. 5.14. Comparison between the initial and the modified variables of the MG (a) load demand comparison, (b) load demand forecast comparison, (c) MG net power comparison, and (d) forecast of the MG net power comparison

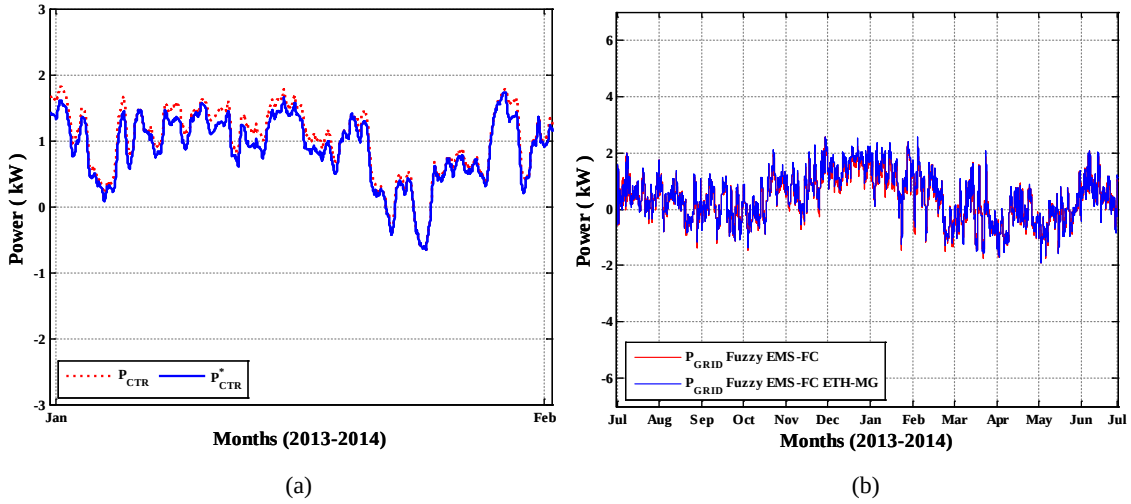

Fig. 5.15. (a) Initial and modified average net power of the MG, (b) Grid power profile comparison between the fuzzy EMS-FC strategy including the EWH consumption and the fuzzy EMS-FC strategy applied to an electro-thermal MG

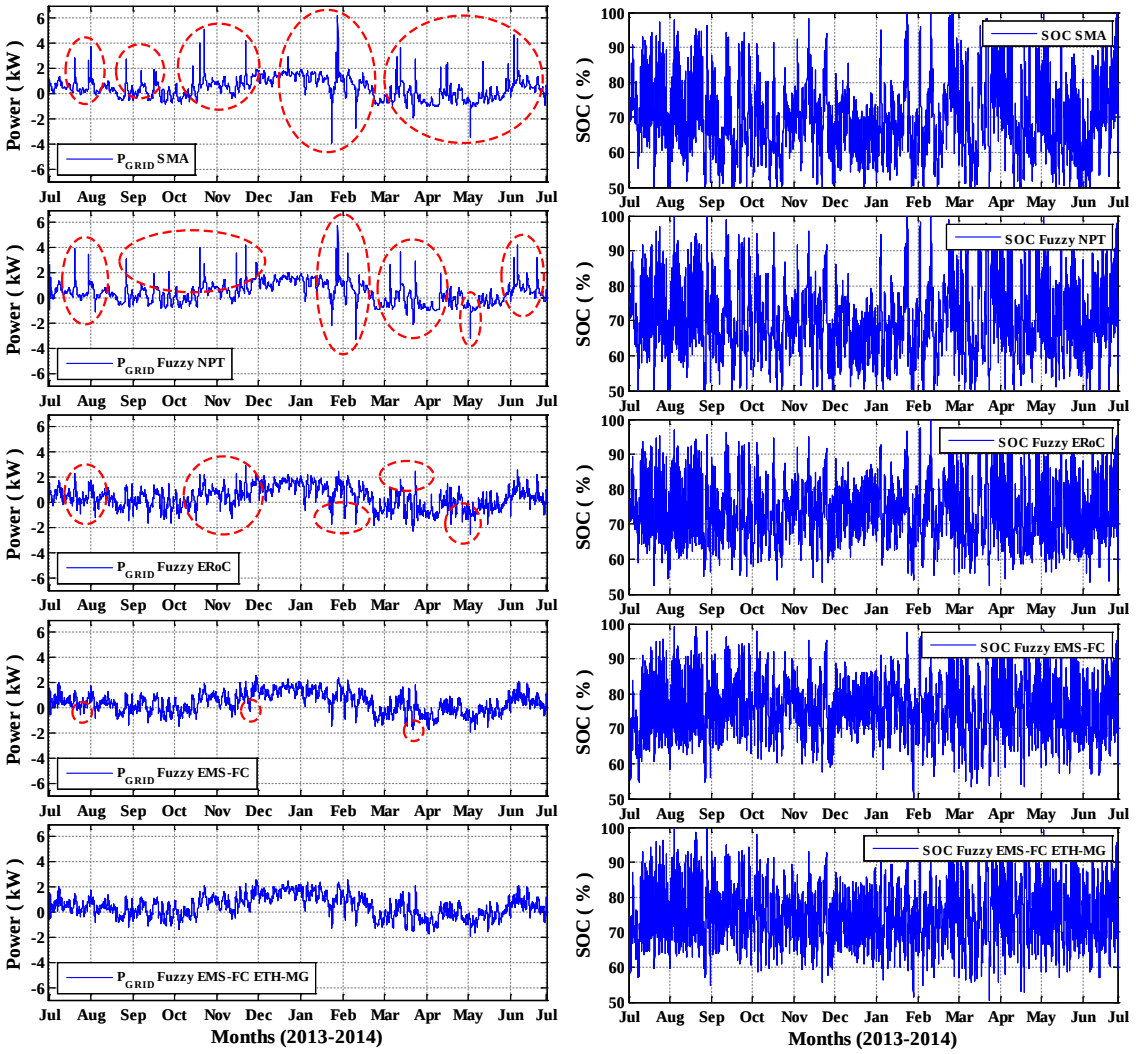

(a) (b)

Fig. 5.16. Grid power profile and battery SOC comparison for the SMA, the fuzzy NPT, the fuzzy ERoC, and the fuzzy EMS-FC strategies including the EWH consumption and the fuzzy EMS-FC strategy applied to an electro-thermal MG

Moreover, Fig. 5.17(a) depicts the distribution of the energy required by the EWH between the ESS and the mains. As it can be seen, the grid has a major contribution for the EWH consumption. Conversely, the ESS supplies an energy of only E_{WH}^{B} = 318.5 kWh during the year under study, which represents an 18.5% savings in the EWH consumption.

Furthermore, Fig. 5.17(b) illustrates the SOC intervals where the battery is located the most of the year under study. As it can be seen, the results obtained through the fuzzy EMS-FC ETH-MG are similar than those obtained through the fuzzy EMS-FC including the EWH consumption. In short, the battery SOC is kept in the 70%-80% range of the rated battery capacity over the 45% of the year under study, which means that the ESS could further compensate the MG net power fluctuations while preserving the battery lifetime.

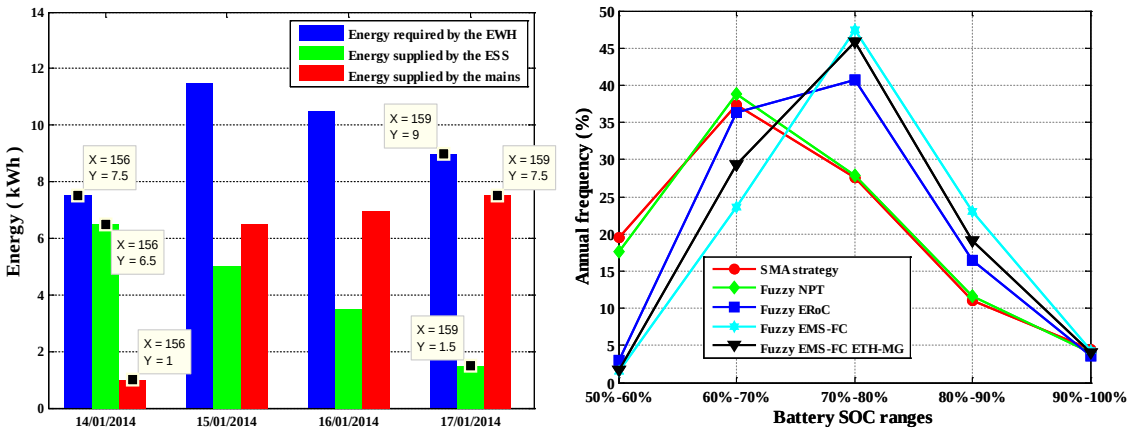

(a) (b)

Fig. 5.17. (a) Contribution of the energy required by the EWH achieved through the fuzzy EMS-FC ETH-MG strategy, (b) Annual frequency of the battery SOC ranges achieved through the SMA, fuzzy NPT, fuzzy ERoC, the fuzzy EMS-FC strategies including the EWH consumption and the fuzzy EMS-FC strategy applied to an electro-thermal MG

Moreover, the resulting values for the energy management quality criteria defined in Chapter 3.1.2 are summarized in Table 5-4 and confirm the proper behavior of the fuzzy EMS-FC strategy applied to an electro-thermal MG.

Table 5-4 Quality criteria comparison for the fuzzy EMS-FC strategy applied to an electro-thermal microgrid, the fuzzy EMS-FC strategy, the fuzzy ERoC strategy, the fuzzy NPT strategy, the SMA strategy and the baseline values including the EWH consumption

EMS Strategy	$P_{G,MAX}$ (kW)	$P_{G,MIN}$ (kW)	*PVR*	*MPD* (W/h)	*APD* (W/h)	*PPV*
No EMS & ESS including the EWH consumption	6.53	-6.45	1.00	18468	1221	5.99
SMA strategy	6.25	-3.98	0.79	20006	57.41	1.23
Fuzzy EMS based on MG net power trend	5.80	-3.28	0.70	18119	50.81	1.31
Fuzzy ERoC strategy including the EWH consumption	2.94	-2.52	0.42	1252	79.93	1.51
Fuzzy EMS-FC strategy including the EWH consumption	2.46	-1.92	0.33	1016	75.93	1.42
Fuzzy EMS-FC strategy applied to an electro-thermal MG	**2.56**	**-1.89**	**0.34**	**846**	**75.13**	**1.26**

It can be noticed that the fuzzy EMS-FC strategy applied to an electro-thermal MG minimizes four of the defined quality criteria. *MPD* and *PPV* criteria are reduced in 16.7% and 11.2% with respect to the fuzzy EMS-FC strategy including the EWH consumption. Conversely, $P_{G,MIN}$ and *APD* criteria reach a minimum reduction, whereas $P_{G,MAX}$ and *PVR* criteria present an slightly increase, which do not represent a significant influence in the overall strategy performance.

Finally, the comparison of the grid power profile ramp-rates is presented in Fig. 5.18. As it can be seen, the grid power ramp-rates are reduced through the fuzzy EMS-FC strategy applied to an electro-thermal MG reaching a maximum value of 846 W/h.

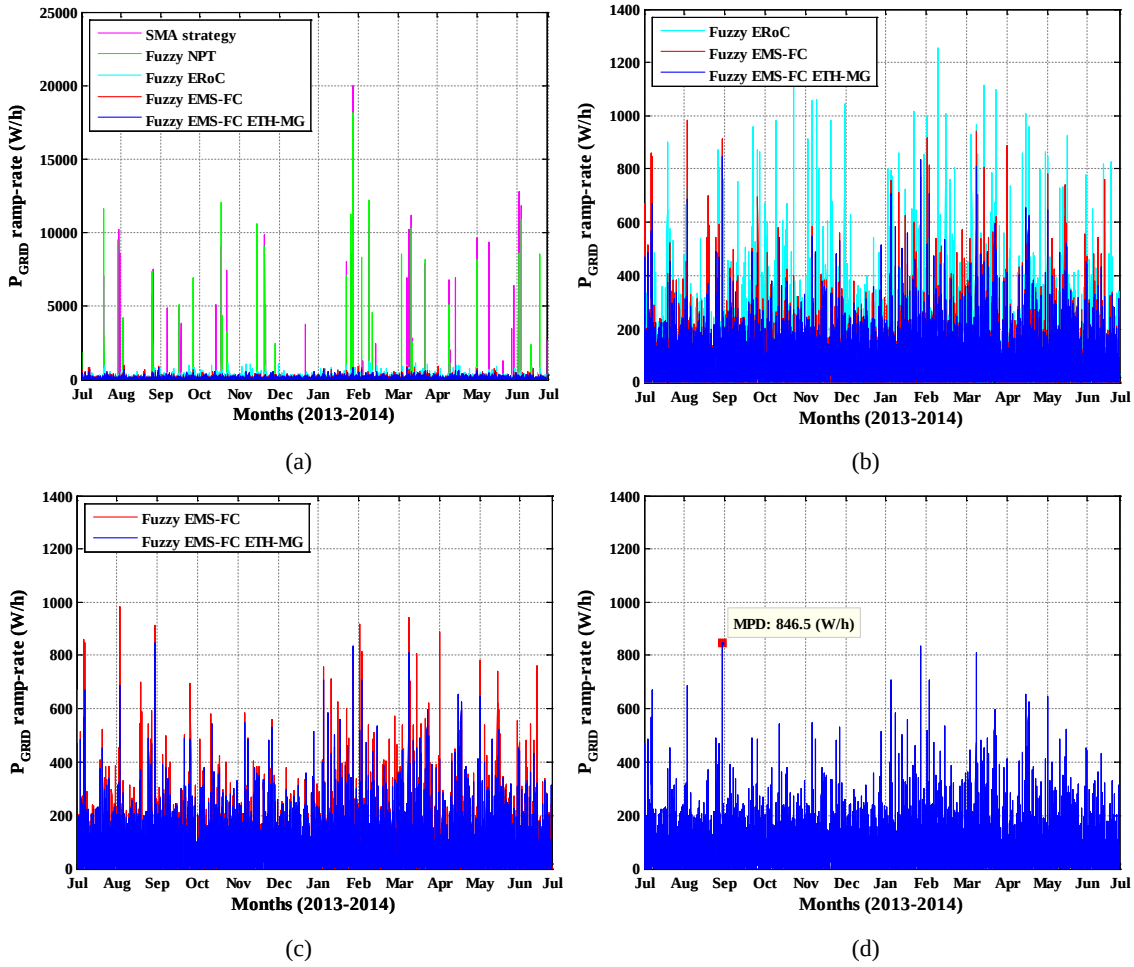

Fig. 5.18. Grid power profile ramp-rates analysis (a) grid power ramp-rates comparison for the described EMS strategies, (b) grid power ramp-rates comparison for the fuzzy ERoC, the fuzzy EMS-FC strategies including the EWH consumption and the fuzzy EMS-FC ETH-MG strategy, (c) comparison of the grid power profile ramp-rates between the fuzzy EMS-FC including the EWH consumption and the fuzzy EMS-FC ETH-MG strategy, and (d) maximum grid power profile ramp-rate achieved through the fuzzy EMS-FC strategy applied to an electro-thermal MG

Chapter 6
Conclusions and future works

6.1. Conclusions

This study has addressed the design of different energy management strategies based on Fuzzy Logic Control for a grid-connected residential microgrid with solar and wind renewable sources. The analysis of two different power architectures namely, only electrical and electro-thermal residential microgrids has been addressed. The first architecture only includes the renewable generation and domestic load demand of the residence. Conversely, the electro-thermal microgrid has considered, beside all the elements of the electrical microgrid, the thermal requirements, i.e., electric water heater, solar thermal collectors, water storage tank, and domestic hot water consumption of the residence. The designs presented in this work have been using real recorded data of electrical power generation and consumption from July 2013 to July 2014 of the residential microgrid under study.

The main objective selected for the design of the energy management strategy of these architectures has been the reduction of the power fluctuations in the power exchanged with the grid, while keeping the energy storage system within secure limits to preserve its life. Reaching this objective will facilitate the integration of the RES into the mains and contribute to the reduction of both the electricity bill and the mains overload.

First of all, a set of quality criteria was defined in order to quantify the behavior of the grid power profile resulting from an EMS design. The enhanced behavior of an EMS strategy is reflected by the minimization of the resulting value of each quality criterion. These quality criteria were additionally used to adjust the parameters of the FLC presented in this work by an off-line learning process using the real recorded data referred above.

For further comparison purposes, the analysis started with the study of the classical strategy to smooth the grid power profile namely, the Simple Moving Average (SMA) approach. The simulation results evidenced that this strategy works properly as long as no significant energy changes occur in the MG from one day to the next one but leads the Energy Storage System (EES) to exceed the secure limits during several time intervals when these changes are noticeable. This preliminary study also concluded that this undesirable ESS behavior comes from the fact that the net power fluctuations in the MG have not been taken into account in the strategy design. Based on this conclusion, a first fuzzy-based strategy referred as Net Power Trend (NPT) was suggested. This strategy uses the MG net power, the battery capacity status

respect to its half-rated capacity and the MG Net Power Trend as a controller inputs to quantify the MG net power fluctuations. As a result, a 3 inputs one output FLC of 50 rules was designed and tested. Even if the simulation results evidenced an improved behavior of the fuzzy NPT strategy with respect to the SMA one, the battery SOC evolution still exceeded secure limits.

In a second step, an improved fuzzy EMS design is carried out by means of a two-input, one-output, and 25-rules FLC, which uses the MG energy Rate-of-Change (ERoC) as a controller input to quantify the magnitude of the energy changes in the MG, and the battery SOC to increase, decrease or maintain the power delivered/absorbed by the mains. A set of numerical simulations has shown that this design allows the EMS to react quickly against the MG energy changes to set the battery SOC close to the 75% of the rated battery capacity, so that the available dynamic range of the battery can compensate the MG net power fluctuations, thus smoothing the grid power profile while keeping the SOC between secure limits. This new design has evidenced the importance of a correct selection of the fuzzy logic controller inputs since they have a major influence on the effectiveness of the energy management strategy.

This study has also faced the FLC design when power forecast data are available. A new FLC design referred as fuzzy-based energy management strategy based on MG power forecasting (EMS-FC) includes the MG power forecasting to predict the future behavior of the MG so that the power forecast error is used by the FLC to modify the grid power profile according to the battery SOC. The fuzzy EMS-FC strategy computes the grid power as the sum of three components: the first component is used to obtain the average of the MG net power through a CMA filter; the second component is used to maintain the battery SOC close to the 75% of the rated battery capacity, and the third component, which is computed by means of a two-input, one-output and 25-rules FLC, is used for smoothing the grid power profile according to the forecast error and the battery SOC. The simulation results and further comparison proved the feasibility of this strategy which concurrently holds the SOC of the battery close to the 75% of the rated battery capacity and minimizes the grid power fluctuations with respect to previous strategies.

The experimental validation of the enhanced fuzzy-based EMS strategies, i.e., fuzzy ERoC and fuzzy EMS-FC strategies, were executed in a real residential microgrid implemented at Public University of Navarre. The experimental validation results confirmed the robustness and the effectiveness of the fuzzy-based EMSs designs.

The enhanced fuzzy-based EMS strategies were also applied to electro-thermal MG architecture. The results demonstrated that an additional degree of freedom in the MG (i.e., the thermal elements of the MG) facilitates the control of the grid power profile. In this regard, the use of the Electric Water Heater (EWH) and the water storage tank allowed the improvement of

the power exchanged with the grid. In addition, the thermal elements also allowed the reduction of the amount of power supplied by the mains required to meet the domestic hot water consumption, which implies a cost reduction for the user.

Finally, this work has evidenced the feasibility of using a FLC for the EMS strategy in electric and electro-thermal MG scenarios, since it simplifies the strategy design. FLC allows transforming the linguistic knowledge about the MG behavior in the form of linguistic rules, making easier their understanding and implementation in a real environment. The results of this work have demonstrated the effectiveness of the fuzzy logic control approach in a MG scenario which improves the grid power profile quality with respect to previous control techniques described in the literature.

6.2. Future works

Despite the progress made in this study, the energy management o for a grid-connected microgrid is still a topic of ongoing research. Therefore, several aspects for improving both the reliability of the microgrid and the energy management strategy design can be recommended for future consideration:

- The analysis of the EMS strategy under a microgrid scenario including more freedom degrees, such as, controllable loads, would allow the integration of a Demand Side Management (DSM) or Demand Respond (DR) techniques, which improve the system performance.

- The addition of multiple storage elements in the microgrid scheme would allow the integration of a multi-agent based management to perform a cooperative control of the microgrid.

- The expansion of the EMS strategy design for the case of multiple interconnected microgrids would allow sharing the energy requirements of each microgrid so that they can be supplied for another microgrid, with the aim of improving the performance of the microgrids at the local and global level.

- Additional technical aspects could be considered for the estimation of the state-of-charge of the energy storage system, for instance, number of charge-discharge cycles, and charging/discharging power rates and limits, which would help to preserve the storage system lifetime.

- The parameter optimization of the fuzzy logic controller developed in this study could be compared with the optimization accomplished through sophisticated algorithms, for instance, Particle Swarm Optimization (PSO) and Cuckoo optimization algorithms.

- The feasibility of this study could be further improved by means of including a cost function, which involves all the benefits of the defined quality criteria and additionally considers the electricity market price with the purpose of minimizing the operational cost of the microgrid.

- The formulation of the cost function allows the use of complex control techniques for the EMS strategy design. For instance a Model Predictive Control (MPC) approach can be envisaged for the EMS design for a residential grid-connected microgrid scenario.

6.3. Contributions

The list of contributions delivered from this study is presented next.

Accepted Journal papers

- **D. Arcos-Aviles**, J. Pascual, L. Marroyo, P. Sanchis, and F. Guinjoan, "Fuzzy Logic-Based Energy Management System Design for Residential Grid-Connected Microgrids," *IEEE Trans. Smart Grid*, vol., no., pp. 1–14, Apr. 2016.

- **D. Arcos-Aviles**, F. Guinjoan, L. Marroyo, "Estrategia de gestión energética mediante controladores fuzzy logic para sistemas de almacenamiento de una microrred electro-térmica con conexión a red," *Revista Ciencia*, vol. 16, no. 2, pp. 193-207, Sep. 2014.

Journal papers under review:

- **D. Arcos-Aviles**, J. Pascual, L. Marroyo, P. Sanchis, and F. Guinjoan, "Fuzzy logic controller design for energy management in a grid-connected residential microgrid with generation and demand forecasting," *Energy Conversion and Management*.

Accepted Conference papers:

- **D. Arcos-Aviles**, J. Pascual, L. Marroyo, P. Sanchis, F. Guinjoan, and M. P. Marietta, "Optimal Fuzzy Logic EMS design for residential grid-connected microgrid with hybrid renewable generation and storage," in *Proc. IEEE 24th Int. Symp. Ind. Electron. (ISIE)*, Armação dos Búzios, Brazil, Jun. 2015, pp. 742–747.

- **D. Arcos-Aviles**, N. Espinosa, F. Guinjoan, L. Marroyo, and P. Sanchis, “Improved Fuzzy Controller Design for Battery Energy Management in a Grid Connected Microgrid,” in *Proc. IECON 40th Annu. Conf. IEEE Ind. Electron. Soc.*, Dallas, TX, USA, Oct. 2014, pp. 2128–2133.

- **D. Arcos-Aviles**, C. Vega, F. Guinjoan, L. Marroyo, and P. Sanchis, “Fuzzy logic controller design for battery energy management in a grid connected electro-thermal microgrid,” in *Proc. IEEE 23th Int. Symp. Ind. Electron. (ISIE)*, Istambul, Turkey, Jun. 2014, pp. 2014–2019

- **D. A. Avilés**, F. Guinjoan, J. Barricarte, L. Marroyo, P. Sanchis, and H. Valderrama, “Battery management fuzzy control for a grid-tied microgrid with renewable generation,” in *Proc. IECON 38th Annu. Conf. IEEE Ind. Electron. Soc.*, Montreal, QC, Canada, Oct. 2012, pp. 5607–5612.

Conference papers under review:

- **D. Arcos-Aviles**, J. Pascual, L. Marroyo, P. Sanchis, and F. Guinjoan, “Energy management strategy for a grid-tied residential microgrid based on fuzzy logic and power forecasting,” *IECON 2016 – 42th Annual Conference on IEEE Industrial Electronics Society*, submitted Apr. 2016.

References

[1] International Energy Agency, "Key World Energy Statistics 2015," pp. 1–81, 2015.

[2] International Energy Agency, "CO2 Emissions from Fuel Combustion Highlights," *IEA Stat.*, no. IEA - STATISTICS, pp. 1–15, 2015.

[3] M. Soshinskaya, W. H. J. Crijns-Graus, J. M. Guerrero, and J. C. Vasquez, "Microgrids: Experiences, barriers and success factors," *Renew. Sustain. Energy Rev.*, vol. 40, pp. 659–672, Dec. 2014.

[4] International Energy Agency, "Excerpt from Renewables Information (2015 Edition)," pp. 1–8, 2015.

[5] H. Kanchev, D. Lu, F. Colas, V. Lazarov, and B. Francois, "Energy Management and Operational Planning of a Microgrid With a PV-Based Active Generator for Smart Grid Applications," *IEEE Trans. Ind. Electron.*, vol. 58, no. 10, pp. 4583–4592, Oct. 2011.

[6] K. Rahbar, J. Xu, and R. Zhang, "Real-Time Energy Storage Management for Renewable Integration in Microgrid: An Off-Line Optimization Approach," *IEEE Trans. Smart Grid*, vol. 6, no. 1, pp. 124–134, Jan. 2015.

[7] P. Basak, S. Chowdhury, S. Halder nee Dey, and S. P. Chowdhury, "A literature review on integration of distributed energy resources in the perspective of control, protection and stability of microgrid," *Renew. Sustain. Energy Rev.*, vol. 16, no. 8, pp. 5545–5556, Oct. 2012.

[8] W. Huang, M. Lu, and L. Zhang, "Survey on Microgrid Control Strategies," *Energy Procedia*, vol. 12, pp. 206–212, 2011.

[9] E. Unamuno and J. A. Barrena, "Hybrid ac/dc microgrids—Part I: Review and classification of topologies," *Renew. Sustain. Energy Rev.*, vol. 52, pp. 1251–1259, Dec. 2015.

[10] D. E. Olivares, A. Mehrizi-Sani, A. H. Etemadi, C. a. Cañizares, R. Iravani, M. Kazerani, A. H. Hajimiragha, O. Gomis-Bellmunt, M. Saeedifard, R. Palma-Behnke, G. a. Jiménez-Estévez, and N. D. Hatziargyriou, "Trends in microgrid control," *IEEE Trans. Smart Grid*, vol. 5, no. 4, pp. 1905–1919, 2014.

[11] F. Katiraei, R. Iravani, N. Hatziargyriou, and A. Dimeas, "Microgrids management," *IEEE Power Energy Mag.*, vol. 6, no. 3, pp. 54–65, May 2008.

[12] A. M. Bouzid, J. M. Guerrero, A. Cheriti, M. Bouhamida, P. Sicard, and M. Benghanem, "A survey on control of electric power distributed generation systems for microgrid applications," *Renew. Sustain. Energy Rev.*, vol. 44, pp. 751–766, Apr. 2015.

[13] B. Lasseter, "Microgrids [distributed power generation]," in *Proc. IEEE Power Engineering Society Winter Meeting*, 2001, vol. 1, pp. 146–149.

[14] R. H. Lasseter, “MicroGrids,” in *IEEE Power Engineering Society Winter Meeting*, 2002, vol. 1, pp. 305–308.

[15] N. Hatziargyriou, *Microgrids: Architectures and Control*. Chichester, UK: Wiley, 2014.

[16] N. Hatziargyriou, H. Asano, R. Iravani, and C. Marnay, “Microgrids,” *IEEE Power Energy Mag.*, vol. 5, no. 4, pp. 78–94, Jul. 2007.

[17] H. Laaksonen, “Technical Solutions for Low-Voltage Microgrid Concept,” Aalto University, 2011.

[18] B. Liu, F. Zhuo, Y. Zhu, and H. Yi, “System Operation and Energy Management of a Renewable Energy-Based DC Micro-Grid for High Penetration Depth Application,” *IEEE Trans. Smart Grid*, vol. 6, no. 3, pp. 1147–1155, May 2015.

[19] W. Su and J. Wang, “Energy Management Systems in Microgrid Operations,” *Electr. J.*, vol. 25, no. 8, pp. 45–60, Oct. 2012.

[20] M. Yazdanian and A. Mehrizi-Sani, “Distributed Control Techniques in Microgrids,” *IEEE Trans. Smart Grid*, vol. 5, no. 6, pp. 2901–2909, Nov. 2014.

[21] Q. Jiang, M. Xue, and G. Geng, “Energy Management of Microgrid in Grid-Connected and Stand-Alone Modes,” *IEEE Trans. Power Syst.*, vol. 28, no. 3, pp. 3380–3389, Aug. 2013.

[22] A. Tascikaraoglu, A. R. Boynuegri, and M. Uzunoglu, “A demand side management strategy based on forecasting of residential renewable sources: A smart home system in Turkey,” *Energy Build.*, vol. 80, pp. 309–320, 2014.

[23] Y.-H. Chen, S.-Y. Lu, Y.-R. Chang, T.-T. Lee, and M.-C. Hu, “Economic analysis and optimal energy management models for microgrid systems: A case study in Taiwan,” *Appl. Energy*, vol. 103, pp. 145–154, Mar. 2013.

[24] M. Marzband, A. Sumper, J. L. Domínguez-García, and R. Gumara-Ferret, “Experimental validation of a real time energy management system for microgrids in islanded mode using a local day-ahead electricity market and MINLP,” *Energy Convers. Manag.*, vol. 76, pp. 314–322, Dec. 2013.

[25] R. Palma-Behnke, C. Benavides, F. Lanas, B. Severino, L. Reyes, J. Llanos, and D. Saez, “A Microgrid Energy Management System Based on the Rolling Horizon Strategy,” *IEEE Trans. Smart Grid*, vol. 4, no. 2, pp. 996–1006, Jun. 2013.

[26] P. Malysz, S. Sirouspour, and A. Emadi, “An Optimal Energy Storage Control Strategy for Grid-connected Microgrids,” *IEEE Trans. Smart Grid*, vol. 5, no. 4, pp. 1785–1796, Jul. 2014.

[27] P. G. Arul, V. K. Ramachandaramurthy, and R. K. Rajkumar, “Control strategies for a hybrid renewable energy system: A review,” *Renew. Sustain. Energy Rev.*, vol. 42, pp. 597–608, Feb. 2015.

[28] J. M. Guerrero, J. C. Vasquez, J. Matas, L. G. de Vicuna, and M. Castilla, “Hierarchical Control of Droop-Controlled AC and DC Microgrids-A General Approach Toward Standardization,” *IEEE Trans. Ind. Electron.*, vol. 58, no. 1, pp. 158–172, Jan. 2011.

[29] O. Palizban, K. Kauhaniemi, and J. M. Guerrero, “Microgrids in active network management—Part I: Hierarchical control, energy storage, virtual power plants, and market participation,” *Renew. Sustain. Energy Rev.*, vol. 36, pp. 428–439, Aug. 2014.

[30] E. Unamuno and J. A. Barrena, “Hybrid ac/dc microgrids—Part II: Review and classification of control strategies,” *Renew. Sustain. Energy Rev.*, vol. 52, pp. 1123–1134, Dec. 2015.

[31] D. Tran and A. M. Khambadkone, “Energy Management for Lifetime Extension of Energy Storage System in Micro-Grid Applications,” *IEEE Trans. Smart Grid*, vol. 4, no. 3, pp. 1289–1296, Sep. 2013.

[32] M. Marinelli, F. Sossan, G. T. Costanzo, and H. W. Bindner, “Testing of a Predictive Control Strategy for Balancing Renewable Sources in a Microgrid,” *IEEE Trans. Sustain. Energy*, vol. 5, no. 4, pp. 1426–1433, Oct. 2014.

[33] A. Anvari-Moghaddam, H. Monsef, and A. Rahimi-Kian, “Optimal Smart Home Energy Management Considering Energy Saving and a Comfortable Lifestyle,” *IEEE Trans. Smart Grid*, vol. 6, no. 1, pp. 324–332, Jan. 2015.

[34] A. Anvari-Moghaddam, H. Monsef, A. Rahimi-Kian, J. M. Guerrero, and J. C. Vasquez, “Optimized energy management of a single-house residential micro-grid with automated demand response,” in *2015 IEEE Eindhoven PowerTech*, 2015, pp. 1–6.

[35] A. Anvari-Moghaddam, J. C. Vasquez, and J. M. Guerrero, “Load shifting control and management of domestic microgeneration systems for improved energy efficiency and comfort,” in *Proc. IECON 41st Annu. Conf. IEEE Ind. Electron. Soc.*, 2015, pp. 000096 – 000101.

[36] J. Pascual, P. Sanchis, and L. Marroyo, “Implementation and Control of a Residential Electrothermal Microgrid Based on Renewable Energies, a Hybrid Storage System and Demand Side Management,” *Energies*, vol. 7, no. 1, pp. 210–237, Jan. 2014.

[37] D. Wang, S. Ge, H. Jia, C. Wang, Y. Zhou, N. Lu, and X. Kong, “A Demand Response and Battery Storage Coordination Algorithm for Providing Microgrid Tie-Line Smoothing Services,” *IEEE Trans. Sustain. Energy*, vol. 5, no. 2, pp. 476–486, Apr. 2014.

[38] I. Prodan and E. Zio, “A model predictive control framework for reliable microgrid energy management,” *Int. J. Electr. Power Energy Syst.*, vol. 61, pp. 399–409, 2014.

[39] G. Bruni, S. Cordiner, V. Mulone, V. Rocco, and F. Spagnolo, “A study on the energy management in domestic micro-grids based on Model Predictive Control strategies,” *Energy Convers. Manag.*, vol. 102, pp. 50–58, 2015.

[40] P. García, J. P. Torreglosa, L. M. Fernández, and F. Jurado, “Optimal energy management system for stand-alone wind turbine/photovoltaic/hydrogen/battery hybrid system with supervisory control based on fuzzy logic,” *Int. J. Hydrogen Energy*, vol. 38, no. 33, pp. 14146–14158, Nov. 2013.

[41] J. Lagorse, M. G. Simoes, and A. Miraoui, “A Multiagent Fuzzy-Logic-Based Energy Management of Hybrid Systems,” *IEEE Trans. Ind. Appl.*, vol. 45, no. 6, pp. 2123–2129, 2009.

[42] G. Kyriakarakos, A. I. Dounis, K. G. Arvanitis, and G. Papadakis, “A fuzzy logic energy management system for polygeneration microgrids,” *Renew. Energy*, vol. 41, pp. 315–327, May 2012.

[43] Y.-K. Chen, Y.-C. Wu, C.-C. Song, and Y.-S. Chen, “Design and Implementation of Energy Management System With Fuzzy Control for DC Microgrid Systems,” *IEEE Trans. Power Electron.*, vol. 28, no. 4, pp. 1563–1570, Apr. 2013.

[44] L. Roine, K. Therani, Y. S. Manjili, and M. Jamshidi, “Microgrid energy management system using fuzzy logic control,” in *2014 World Automation Congress (WAC)*, 2014, pp. 462–467.

[45] R. G. C. Secretariat, “Grid connection code for renewable power plants (RPPs) connected to the Electricity Transmission System (TS) or the Distribution System (DS) in South Africa,” 2012.

[46] J. Pascual, “Estrategias avanzadas de gestión energética basadas en prediccion para microrredes electrotérmicas,” Universidad Pública de Navarra, Pamplona, España, 2015.

[47] W. A. Bisschoff and R. Gouws, “Energy management system for a residential grid-tied micro-grid,” in *2015 International Conference on the Domestic Use of Energy (DUE)*, 2015, pp. 85–91.

[48] R. Hanna, J. Kleissl, A. Nottrott, and M. Ferry, “Energy dispatch schedule optimization for demand charge reduction using a photovoltaic-battery storage system with solar forecasting,” *Sol. Energy*, vol. 103, pp. 269–287, May 2014.

[49] H. Zhou, T. Bhattacharya, D. Tran, T. S. T. Siew, and A. M. Khambadkone, “Composite Energy Storage System Involving Battery and Ultracapacitor With Dynamic Energy Management in Microgrid Applications,” *IEEE Trans. Power Electron.*, vol. 26, no. 3, pp. 923–930, Mar. 2011.

[50] J. Barricarte, “Integración en la red eléctrica de microrredes electrotérmicas: dimensionado, estrategias de gestión energética e implementación experimental,” Universidad Pública de Navarra, Pamplona, España, 2011.

[51] D. A. Aviles, F. Guinjoan, J. Barricarte, L. Marroyo, P. Sanchis, and H. Valderrama, “Battery management fuzzy control for a grid-tied microgrid with renewable generation,” in *Proc. IECON 38th Annu. Conf. IEEE Ind. Electron. Soc.*, 2012, pp. 5607–5612.

[52] D. Arcos-Aviles, N. Espinosa, F. Guinjoan, L. Marroyo, and P. Sanchis, “Improved Fuzzy Controller Design for Battery Energy Management in a Grid Connected Microgrid,” in *Proc. IECON 40th Annu. Conf. IEEE Ind. Electron. Soc.*, 2014, pp. 2128–2133.

[53] D. Arcos-Aviles, J. Pascual, L. Marroyo, P. Sanchis, F. Guinjoan, and M. P. Marietta, “Optimal Fuzzy Logic EMS design for residential grid-connected microgrid with hybrid renewable generation and storage,” in *Proc. IEEE 24th Int. Symp. Ind. Electron. (ISIE)*, 2015, pp. 742–747.

[54] D. Arcos-Aviles, J. Pascual, L. Marroyo, P. Sanchis, and F. Guinjoan, “Fuzzy Logic-Based Energy Management System Design for Residential Grid-Connected Microgrids,” *IEEE Trans. Smart Grid*, pp. 1–14, Apr. 2016.

[55] D. Arcos-Aviles, C. Vega, F. Guinjoan, L. Marroyo, and P. Sanchis, “Fuzzy logic controller design for battery energy management in a grid connected electro-thermal microgrid,” in *Proc. IEEE 23th Int. Symp. Ind. Electron. (ISIE)*, 2014, pp. 2014–2019.

[56] D. Arcos-Aviles, F. Guinjoan, and L. Marroyo, “Estrategia de gestión energética mediante controladores fuzzy logic para sistemas de almacenamiento de una microrred electro-térmica con conexión a red,” *Rev. Cienc.*, vol. 16, no. 2, pp. 193–207, Sep. 2014.

[57] J. Pascual, J. Barricarte, P. Sanchis, and L. Marroyo, “Energy management strategy for a renewable-based residential microgrid with generation and demand forecasting,” *Appl. Energy*, vol. 158, pp. 12–25, Nov. 2015.

[58] K. Passino and S. Yurkovich, *Fuzzy Control*. Menlo Park, CA: Addisson-Wesley, 1998.

[59] M. Serraji, J. Boumhidi, and E. H. Nfaoui, "MAS energy management of a microgrid based on fuzzy logic control," in *2015 Intelligent Systems and Computer Vision (ISCV)*, 2015, pp. 1–7.

[60] A. Mohamed and O. Mohammed, "Real-time energy management scheme for hybrid renewable energy systems in smart grid applications," *Electr. Power Syst. Res.*, vol. 96, pp. 133–143, Mar. 2013.

[61] J. P. Fossati, A. Galarza, A. Martín-Villate, J. M. Echeverría, and L. Fontán, "Optimal scheduling of a microgrid with a fuzzy logic controlled storage system," *Int. J. Electr. Power Energy Syst.*, vol. 68, pp. 61–70, Jun. 2015.

[62] D. Arcos-Aviles, F. Guinjoan, P. M. Marietta, J. Pascual, L. Marroyo, and P. Sanchis, "Energy management strategy for a grid-tied residential microgrid based on fuzzy logic and power forecasting," submitted paper, 2016.

[63] D. Arcos-Aviles, J. Pascual, L. Marroyo, P. Sanchis, and Francesc Guinjoan, "Fuzzy Logic Controller Design for Energy Management in a Grid Connected Residential Microgrid with Generation and Demand Forecasting," working paper, 2016.

[64] B. Solar, "BP585," 2002. [Online]. Available: http://www.comel.gr/pdf/bpsolar/BP585.pdf. [Accessed: 08-Mar-2016].

[65] Bornay, "Aerogenerador Bornay 6000," 2010. [Online]. Available: http://www.bornay.com/userfiles/descargas/bornay_6000_rev_6.pdf. [Accessed: 08-Mar-2016].

[66] AMETEK, "AMREL eLoad PLA Series," 2014. [Online]. Available: http://www.programmablepower.com/electronic-load/PLA/downloads/PLA_Datasheet.pdf. [Accessed: 08-Mar-2016].

[67] FIAMM, "SMG (OPzV)." [Online]. Available: http://www.interstatebatteries.com/powercare/stationary/pdf/SMG_OPzV_VRLA.pdf. [Accessed: 08-Mar-2016].

[68] Ingeteam Energy S.A., "Manual de Instalación Ingecon Hybrid MS," 2010. [Online]. Available: http://www.ingeteam.com/Portals/0/Catalogo/Producto/Documento/PRD_128_Archivo_ptd22-manual-de-instalacion-ingecon-hybrid-ms.pdf. [Accessed: 08-Mar-2016].

[69] National Instruments, "PXI Platform," 2016. [Online]. Available: http://www.ni.com/pxi/#. [Accessed: 08-Mar-2016].

[70] D. Rekioua and E. Matagne, *Optimization of Photovoltaic Power Systems*. London: Springer London, 2012.

[71] A. H. Fathima and K. Palanisamy, "Optimization in microgrids with hybrid energy systems – A review," *Renew. Sustain. Energy Rev.*, vol. 45, pp. 431–446, May 2015.

[72] B. Zhao, X. Zhang, J. Chen, C. Wang, and L. Guo, "Operation Optimization of Standalone Microgrids Considering Lifetime Characteristics of Battery Energy Storage System," *IEEE Trans. Sustain. Energy*, vol. 4, no. 4, pp. 934–943, Oct. 2013.

[73] J. Yoo, B. Park, K. An, E. A. Al-Ammar, Y. Khan, K. Hur, and J. H. Kim, "Look-Ahead Energy Management of a Grid-Connected Residential PV System with Energy Storage under Time-Based Rate Programs," *Energies*, vol. 5, no. 12, pp. 1116–1134, Apr. 2012.

[74] F. Bizzarri, M. Bongiorno, A. Brambilla, G. Gruosso, and G. S. Gajani, "Model of Photovoltaic Power Plants for Performance Analysis and Production Forecast," *IEEE Trans. Sustain. Energy*, vol. 4, no. 2, pp. 278–285, Apr. 2013.

[75] E. Lorenzo, "Energy Collected and Delivered by PV Modules," in *Handbook of Photovoltaic Science and Engineering*, A. Luque and S. Hegedus, Eds. Chichester, UK, UK: John Wiley & Sons, Ltd, 2011, pp. 984–1042.

[76] S. Mathew, "Wind energy : fundamentals, resource analysis and economics," Berlin: Springer, 2006, pp. 11–88.

[77] W. T. Chong, W. P. Hew, S. Y. Yip, A. Fazlizan, S. C. Poh, C. J. Tan, and H. C. Ong, "The experimental study on the wind turbine's guide-vanes and diffuser of an exhaust air energy recovery system integrated with the cooling tower," *Energy Convers. Manag.*, vol. 87, pp. 145–155, Nov. 2014.

[78] J. F. Manwell, J. G. McGowan, and A. L. Rogers, "Wind Energy Explained: Theory, Design and Application," Chichester, UK: John Wiley & Sons, Ltd, 2009, pp. 23–87.

[79] C. Ally, S. Bahadoorsingh, A. Singh, and C. Sharma, "A review and technical assessment integrating wind energy into an island power system," *Renew. Sustain. Energy Rev.*, vol. 51, pp. 863–874, Nov. 2015.

[80] Danish wind industry Association, "Wind Energy Reference Manual Part 1: Wind Energy Concepts." [Online]. Available: http://drømstørre.dk/wp-content/wind/miller/windpower web/en/stat/unitsw.htm#roughness.

[81] D. A. J. Rand and P. T. Moseley, "Energy Storage with Lead–Acid Batteries," in *Electrochemical Energy Storage for Renewable Sources and Grid Balancing*, P. T. Moseley and G. Jürgen, Eds. Kidlington: Elsevier, 2015, pp. 201–222.

[82] H. Tazvinga, B. Zhu, and X. Xia, "Optimal power flow management for distributed energy resources with batteries," *Energy Convers. Manag.*, vol. 102, pp. 104–110, Sep. 2015.

[83] J. P. Fossati, A. Galarza, A. Martín-Villate, and L. Fontán, "A method for optimal sizing energy storage systems for microgrids," *Renew. Energy*, vol. 77, pp. 539–549, 2015.

[84] F. Guo, H. Li, C. Yao, M. Alsolami, A. Lang, X. Lu, and J. Wang, "Residential usage profile optimization and experimental implementation of the retired HEV battery with a hybrid microgrid testbed," in *2014 IEEE Energy Conversion Congress and Exposition (ECCE)*, 2014, pp. 428–435.

[85] S. Anuphappharadorn, S. Sukchai, C. Sirisamphanwong, and N. Ketjoy, "Comparison the Economic Analysis of the Battery between Lithium-ion and Lead-acid in PV Stand-alone Application," *Energy Procedia*, vol. 56, pp. 352–358, 2014.

[86] J. A. Duffie and W. A. Beckman, *Solar Engineering of Thermal Processes*, 4th ed. Hoboken, NJ, EEUU: John Wiley & Sons, Inc., 2014.

[87] S. A. Kalogirou, *Solar Energy Engineering Processes and Systems*. Burlington, MA, EEUU: Elsevier, 2009.

[88] T. L. Bergman, A. S. Lavine, F. P. Incropera, and D. P. Dewitt, *Fundamentals of Heat and Mass Transfer*, 7th ed. Hoboken, NJ, USA: John Wiley & Sons, Inc., 2011.

[89] F. H. Fahmy, D. M. Atia, N. M. A. El-Rahman, and H. T. Dorrah, "Optimal sizing of solar water heating system based on genetic algorithm for aquaculture system," in *2010*

International Conference on Chemistry and Chemical Engineering, 2010, pp. 221–226.

[90] D. Wang and Y. Liu, "Study on Heat Storage Tank of Solar Heating System," in *2010 International Conference on Digital Manufacturing & Automation*, 2010, vol. 2, pp. 493–497.

[91] L. Zhang, N. Gari, and L. V. Hmurcik, "Energy management in a microgrid with distributed energy resources," *Energy Convers. Manag.*, vol. 78, pp. 297–305, Feb. 2014.

[92] Seul-Ki Kim, Jin-Hong Jeon, Chang-Hee Cho, Jong-Bo Ahn, and Sae-Hyuk Kwon, "Dynamic Modeling and Control of a Grid-Connected Hybrid Generation System With Versatile Power Transfer," *IEEE Trans. Ind. Electron.*, vol. 55, no. 4, pp. 1677–1688, Apr. 2008.

[93] J. Pascual, I. S. Martín, A. Ursúa, P. Sanchis, and L. Marroyo, "Implementation and control of a residential microgrid based on renewable energy sources , hybrid storage systems and thermal controllable loads," in *2013 IEEE Energy Conversion Congress and Exposition (ECCE)*, 2013, pp. 2304–2309.

[94] T. Butz, *Fourier Transformation for Pedestrians*, Second. Cham, Switzerland: Springer International Publishing, 2015.

[95] Kiam Heong Ang, G. Chong, and Yun Li, "PID control system analysis, design, and technology," *IEEE Trans. Control Syst. Technol.*, vol. 13, no. 4, pp. 559–576, Jul. 2005.

[96] J. Marcos, I. de la Parra, M. García, and L. Marroyo, "Control Strategies to Smooth Short-Term Power Fluctuations in Large Photovoltaic Plants Using Battery Storage Systems," *Energies*, vol. 7, no. 10, pp. 6593–6619, Oct. 2014.

[97] National Instruments, "Fuzzy System Designer," 2011. [Online]. Available: http://zone.ni.com/reference/en-XX/help/370401H-01/lvpid/fuzzy_system_designer_db/. [Accessed: 08-Mar-2016].

[98] Meteogalicia, "Servidor THREDDS de MeteoGalicia." [Online]. Available: http://www.meteogalicia.es/web/index.action. [Accessed: 10-Mar-2016].

[99] A. M. Foley, P. G. Leahy, A. Marvuglia, and E. J. McKeogh, "Current methods and advances in forecasting of wind power generation," *Renew. Energy*, vol. 37, no. 1, pp. 1–8, Jan. 2012.

[100] C. Yang, A. A. Thatte, and L. Xie, "Multitime-Scale Data-Driven Spatio-Temporal Forecast of Photovoltaic Generation," *IEEE Trans. Sustain. Energy*, vol. 6, no. 1, pp. 104–112, Jan. 2015.

[101] X. Lü, T. Lu, C. J. Kibert, and M. Viljanen, "A novel dynamic modeling approach for predicting building energy performance," *Appl. Energy*, vol. 114, pp. 91–103, Feb. 2014.

[102] H. Madsen, P. Pinson, G. Kariniotakis, H. A. Nielsen, and T. Nielsen, "Standardizing the Performance Evaluation of ShortTerm Wind Power Prediction Models," *Wind Eng.*, vol. 29, no. 6, pp. 475–489, Dec. 2005.

[103] C. Vamos and M. Craciun, "Noise Smoothing," in *Automatic Trend Estimation*, C. Vamos and M. Craciun, Eds. Dordrecht: Springer Netherlands, 2012, pp. 43–59.